High Power Led-Based Light Engine with Double Linear Fresnel Lenses for Solar Simulators

by

Ali FAGHIH

THESIS PRESENTED TO ÉCOLE DE TECHNOLOGIE SUPÉRIEURE
IN PARTIAL FULFILLMENT FOR A MASTER'S DEGREE
WITH THESIS IN ELECTRICAL ENGINEERING
M.A.Sc.

MONTRÉAL, OCTOBER 21, 2021

ÉCOLE DE TECHNOLOGIE SUPÉRIEURE
UNIVERSITÉ DU QUÉBEC

BOARD OF EXAMINERS

THIS THESIS HAS BEEN EVALUATED

BY THE FOLLOWING BOARD OF EXAMINERS

Mr. Ricardo Izquierdo, Thesis Supervisor
Department of Electrical Engineering, École de technologie supérieure

Mr. Bora Ung, President of the Board of Examiners
Department of Electrical Engineering, École de technologie supérieure

Mr. François Blanchard, Member of the jury
Department of Electrical Engineering, École de technologie supérieure

THIS THESIS WAS PRESENTED AND DEFENDED

IN THE PRESENCE OF A BOARD OF EXAMINERS AND PUBLIC

SEPTEMBER 20, 2021

AT ÉCOLE DE TECHNOLOGIE SUPÉRIEURE

ACKNOWLEDGMENT

Foremost, my completion of this project could not have been accomplished without the support of my sweetheart wife Maryam, the most caring, loving, patient, and supportive companion, and my little son Houman, who never disrupt me while working from home. To Maryam and Houman thank you for allowing me time away from you to research and write, even on weekends and lockdown caused by COVID19, you always had me just physically at dwelling.

I would like to express my deep and sincere gratitude to my research supervisor Professor Ricardo Izquierdo for giving me the opportunity to do research and providing invaluable guidance throughout this research. I am always impressed by his manners, patience, and knowledge. Dear Professor, the day I met you in your office was a turning point for a new chapter in my life in Canada.

High Power Led-Based Light Engine with Double Linear Fresnel Lenses for Solar Simulators

Ali FAGHIH

RÉSUMÉ

Alors que l'utilisation de l'énergie solaire se développe, les tests de performance sont devenus l'un des thèmes principaux pour garantir la sécurité des instruments photovoltaïques. Les sources lumineuses sont les composants les plus critiques des simulateurs solaires utilisés pour les expériences avec les cellules solaires. Les développements rapides des diodes électroluminescentes (LED) ont fourni des outils suffisants pour concevoir des simulations solaires à LED pour imiter le soleil avec précision. Les LED présentent de nombreux avantages par rapport à la technologie à base de lampes actuellement utilisée. Mais ces avantages n'ont pas été exploités en raison des normes de correspondance de spectre spécifiques, de la stabilité temporelle et de la lumière de sortie uniforme sur une zone de test. Des optiques secondaires sont utilisées pour collimater les rayons lumineux en un faisceau contrôlé qui apportera cette pleine intensité à la zone requise.

L'objectif principal de cette étude est de concevoir et de fabriquer un module d'éclairage haute puissance pour simulateurs solaires basé sur des LED intégrées avec un concentrateur de lumière utilisant des lentilles de Fresnel pour atteindre plus d'un rayonnement solaire. Pour atteindre cet objectif, la partie principale de la recherche s'est concentrée sur la sélection de LED Cheap On Board (COB) haute puissance appropriées avec l'utilisation d'une plus faible quantité de sources de lumière tout en respectant les spécifications des normes de l'American Society for Testing Materials (ASTM). L'autre composant important considéré pour fabriquer le dispositif était la lentille de Fresnel pour correspondre aux COB et aux autres dimensions des composants. Les résultats expérimentaux ont été obtenus et présentés dans un chapitre séparé. L'objectif global de la recherche est de concevoir et de fabriquer un moteur d'éclairage haute puissance à base de LED pour simulateurs solaires atteint avec près de 5 rayons solaires. Le moteur d'éclairage réalisé pourrait être utilisé pour construire un simulateur solaire à haut flux dans le futur.

Mots-clés: énergie solaire, diode électroluminescente, pas cher à bord, effets photovoltaïques, simulation, moteur lumineux, lentille de Fresnel.

High Power Led-Based Light Engine with Double Linear Fresnel Lenses for Solar Simulators

Ali FAGHIH

ABSTRACT

As the use of solar power is growing, performance testing has become one of the main themes to guarantee the safety of photovoltaic instruments. Light sources are the most critical components of sun simulators used for experiments with solar cells. Rapid developments in light-emitting diodes (LEDs) have provided sufficient tools for designing LED solar simulations to imitate the sun accurately. LEDs have many benefits over presently used lamps-based technology. But these advantages were not harnessed due to the specific spectrum matching standards, Temporal instability, and uniform output light on a test area. Secondary optics are used to collimate the light rays into a controlled beam that will bring that full intensity to the needed area.

The main purpose of this study is to design and fabricate a high-power light engine for solar simulators based on LED integrated with a light concentrator using Fresnel lenses to reach more than one sun output. To aim, this objective main part of the research focused on selecting appropriate high-power Cheap On Board (COB) LED with the utilization of lower quantity of light sources while the specification of American Society for Testing Materials (ASTM) standards meets. The other important component considered to fabricate the device was the Fresnel lens to match with COBs and other component dimensions. The experimental results have been obtained and presented in a separate chapter. The overall objective of the research is to design and fabricate a LED-Based high-power light engine for solar simulators achieved with almost 5 sunlight output. The performed light engine could be used to construct a high-flux solar simulator in the future.

Keywords: Solar energy, light-emitting diode, cheap on board, photovoltaic effects, simulation, light engine, Fresnel lens.

TABLE OF CONTENTS

Page

XII

LIST OF TABLES

LIST OF FIGURES

Page

XVIII

LIST OF ABREVIATIONS

GHG	Green House Gasses
PVMA	Photovoltaic Market Alliance
HCPV	High-Concentration Photovoltaic
PV	Photo Voltaic
STC	Standard Test Condition
LED	Light Emitting Diodes
COB	Cheap on Board
UV	Ultraviolet
IR	Infrared
SS	Solar Simulator
HFSS	High Flux Solar Simulator
CSI	Compact Source Iodide
ASTM	American Society for Testing and Materials
IEC	International Electrotechnical Commission
SMD	Surface Mounted Device
DIP	Dual In-line Package
CPC	Compound Parabolic Concentrator
CPV	Concentrator Photovoltaic
CSP	Concentrated Solar Power
2-D	Two-Dimensional
3-D	Three-Dimensional
NIR	Near InfraRed

PWM	Pulse Width Modulation
PCB	Printed Circuit Boards
MCPCB	Metal-Core Printed Circuit Boards
USB	Universal Serial Bus
JIS	Japanese Industrial Standards
STI	Short-Term Instability
LTI	Long-Term Instability
CCT	Correlated Color Temperature
CRI	Color Rendering Index
PMMA	Polymethyl methacrylate
DPST	Double Pole Single Throw Switch
NREL	National Renewable Energy Laboratory
a-Si	Amorphous Silicon
CIGS	Copper Indium Gallium Selenide
mono-Si	Monocrystalline
OPV	Organic Photovoltaic
SMU	Source Measure Unit

INTRODUCTION

People on the earth are facing two major problems for leaving on the planet: lack of energy and greenhouse gases (GHG) emission due to increased production of energy (Sellami & Mallick, 2013). The increasing demands of energy for industrial production and urban facilities ask for new strategies for energy sources (Ucal & Xydis, 2020). Based on existing economic growth estimates, world energy demand is forecast to increase 19% by 2040. (*Our Energy Needs: World Energy Consumption & Demand | CAPP*, 2020)
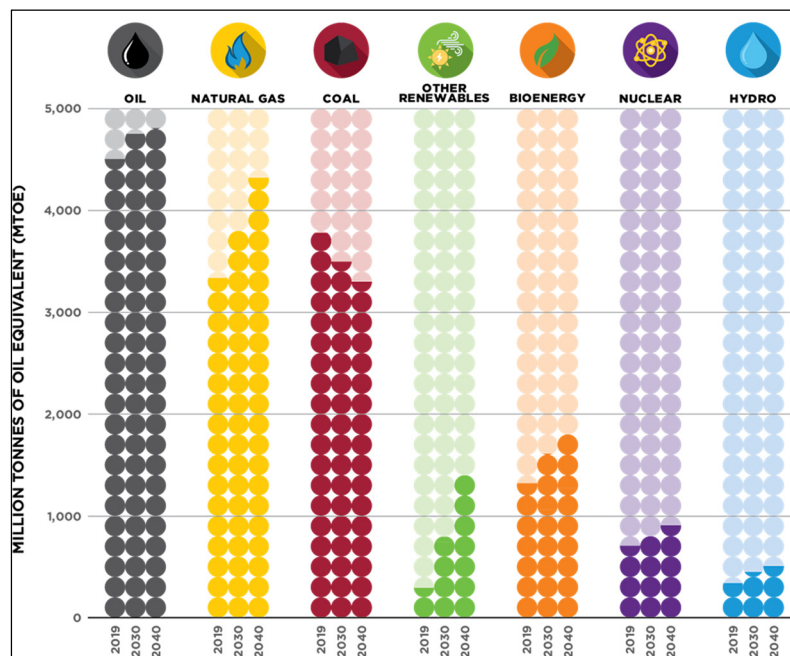
Figure 1.1 World Energy Outlook
Taken from International Energy Agency (2020)

These two mentioned problems are linked to fulfilling the energy needs of the population. Green energy, like renewable and clean energy, is the most relevant solution for explained issues. A large amount of this energy needs to be produced by sources that are environmentally sustainable and renewable. Among these new sources of energy, solar power is one of the most important sources of alternative energies and became in more attention by researchers

worldwide (Jinglong Du, Xiang Huang, 2013). According to PV Market Alliance (PVMA) market value will grow by 19.4% from 2017 to 2023, and in 2023 will reach $39512 million. Solar Panels are one of the largest green energy producers (Ajayan et al., 2020). However, the efficiency of these cells during their operations also needs some improvement and optimization. The development and research on photovoltaic systems, especially solar cells, is one of the most important issues in the energy field today. To have a fast learning curve in terms of improving and characterization of high-concentration photovoltaic (HCPV) production lines, using an in-line proper test device is needed (Dominguez et al., 2008). Mainstream technologies illustrate up to 20% performance and that is while record performance has reached 40% demonstrating the ability for more technical development and performance growth (Tito-haykestep et al., 2020). As a result of this growing usage of solar cells over the world, it is critical and more important than it has ever been to provide a high-quality characterization of photovoltaic (PV) modules to have a reliable power rating and accurate estimation of energy yield measurements.

Through a diverse background, one of the most important solar cell characterization parameters is its energy conversion. The incoming energy to a solar cell is the energy that exists in the irradiance of light. When a solar cell is in the direction parallel to incoming photons, it absorbs 95% of the incoming optical energy (*Solar Energy Conversion: The Solar Cell - R.C. Neville - Google Books*, n.d.). Nevertheless, I-V curve tracers are the main performance assessment of operating PV models and Engineers usually use this as a classification of different PV cells in the market (Sarikh et al., 2020). Current-voltage characteristics of photovoltaic cells and modules can be assessed in many different situations but for researching purposes and accurate data collection, it should determine under specific conditions so-called Standard Test Condition (STC) (IEC 60904-9, 2006). Manufacturers report their PV module power output at STC, which is correlated with 1000 W/m2 at 25 $^{\circ C}$ with air mass 1.5 (*ASTM E892 - 87(1992) Tables for Terrestrial Solar Spectral Irradiance at Air Mass 1.5 for a 37-Deg Tilted Surface (Withdrawn 1999)*, n.d.). Figure 1.2 shows the reference solar spectral irradiance distribution from the ASTM G173 standard.
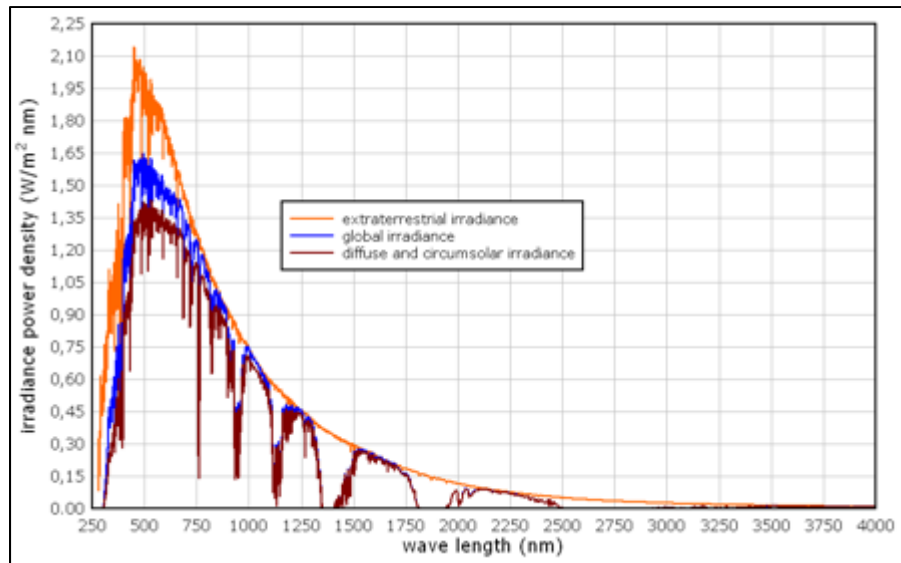
Figure 1.2 Reference Solar Spectrum Irradiance distribution
Taken from ASTM (2013, p. 3)

As such, variable weather, and test condition outside the laboratory in some areas, such as Montreal and cities with cloud climates most of the year, have turned the testing and characterization process of PV devices into a time-consuming procedure. In fact, there is not enough sunlight to test the specimen in question, for testing under the so-called Standard Test Conditions (STC) requires a simulator that can handle conditions similar to the actual conditions of sunlight To the surface of the cell to provide the sun indoors (Kohraku & Kurokawa, 2006).

A solar simulator (also artificial sun) is a device that provides illumination approximating natural sunlight. The purpose of the solar simulator is to provide a controllable indoor test facility under laboratory conditions, used for the testing of solar cells, sunscreen, plastics, and other materials and devices (ASTM-E927-05, 2005). Where there is not enough natural sunlight or where it is not feasible, solar simulators played an important role in testing and developing the productions. Solar simulators can be used for various in-laboratory tests, a long-term research study of solar photovoltaic, awnings, plastics, polymers, and other products that use sunlight sensitive materials (Tavakoli et al., 2020)

The most essential part of solar simulators in PV device studies is the light sources that they use. Sun simulators of the first generation were usually based on and their variations of halogen, xenon, or tungsten light sources. Complex optical systems had to be installed to achieve homogeneous light intensity. Optical components such as filters, reflectors, diffusers, etc. were required to acquire the desired spectral composition. In the 1990s, new types of sun simulator's light source appeared with the accelerated growth of semiconductor technologies. They experimented with an alternative to previously described light sources that was cheaper, more lightweight, and more energy-efficient (Bodnár et al., 2020). The use of light-emitting diodes (LED) has been considered, which has lower consumption, higher acetyl, and higher efficiency than low-density xenon and halogen lamps. It also has a better life expectancy than previous light sources, which greatly reduces device maintenance costs in the future (Linden et al., 2014). The LED-based solar simulator also has consequences for the possible use in a commercial environment, which enables the purchasers to imitate natural light with LEDs (Schembri, n.d.).

Reviewing former works reveals that only a few research have been done using high power chips onboard LEDs and non of them were conducted on high flux solar simulators. Thus, the main goal of this thesis is to design and build a high-power LED-based light engine with more than one sun output for solar simulators. Therefore, the following specific objectives have been proposed:

- A comprehensive review of the PV solar simulator literature.
- Explanation of the information and background information about solar energy and solar panels.
- The design, simulation, and fabrication of a Cheap On Board (COB) LED-based light engine for solar simulators, to create a large area solar simulator using two linear Fresnel lenses.
- Describing some problems and issues during the design, manufacture, and experimental process.
- Presenting the conclusion of this thesis project and outlook, including information about potential future works (the information can be used by others).

CHAPTER 1

STATE OF THE ART LITERATURE REVIEW

With the advancement of science and the addition of various equipment to human life, the need for energy is felt more and more, and renewable energies, including the energy of the sun, are highly welcomed. Therefore, the equipment related to the energy utilization of the sun also needs development. Hence, laboratory equipment has a special place to test and develop such instruments, such as the sun ray simulator equipment, which is due to the limitations of test outside the laboratory and the absence of uniform conditions in most of the cases and instability, we need to have a solar simulator with conditions under control so that we can perform different tests and conditions on the produced samples and try to improve their performance and function.

A solar simulator (also artificial sun) is a device that provides illumination approximating natural sunlight. The purpose of the solar simulator is to provide a controllable indoor test facility under laboratory conditions, used for the testing of solar cells, sunscreen, plastics, and other materials and devices (ASTM-E927-05, 2005). Where there is not enough natural sunlight or where it is not feasible, solar simulators played an important role in testing and developing the productions.

1.1   Main Component of solar simulators

Solar simulators may also be advantageous over outdoor testing, since solar simulators are controllable, unlike natural conditions. A solar simulator usually consists of three major components: a light source(s) and associated power supply, any optics and filters used to modify the output beam to meet the requirements, and necessary controls to operate the simulator. Each part is selected to obtain a controlled output conforming to specific requirements. The current work focuses on the selection of a suitable light source and optics,

which is critical to ensure simulated solar radiation quality and reliability (*Artificial Light Source for Solar Simulation (Conference) | ETDEWEB*, n.d.)

1.1.1 The light source of solar simulators for photovoltaic device

Light source selection is the most important part of solar simulator design for the simulation of sunlight and its intensity, and spectral properties of the light source, illumination pattern, collimation, light flow stability, and light range should be taken into account for the selection. This light source is required to meet several criteria: spectral quality, illumination uniformity, collimation, flux stability, and a range of obtainable flux (Krusi & Schmid, 1983b). Figure 1.1 shows the light source classification of solar simulators.
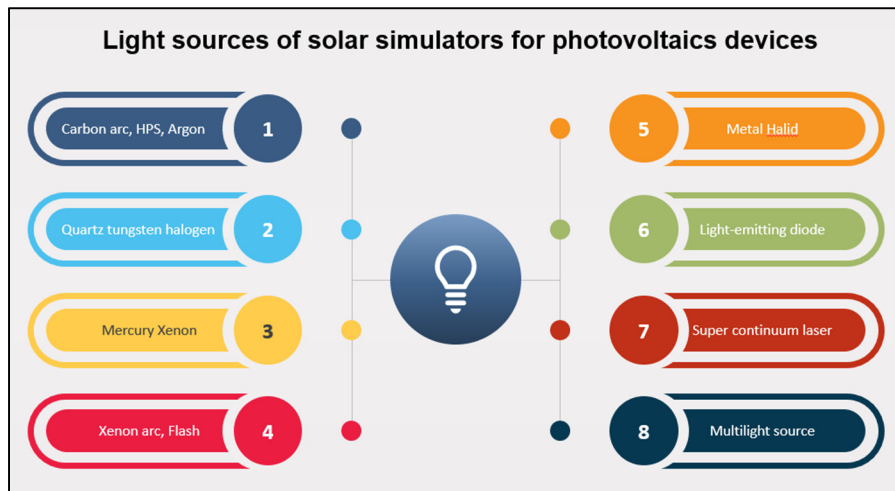
Figure 1.1 Light sources of solar simulators for photovoltaic devices

1.1.1.1 Carbon arc, high-pressure sodium vapor, and argon lamp

As the spectral structure of carbon arc light is compatible with AM0, these are used instead for the terrestrial photovoltaic panel tests as a light source for space solar simulators and multi-junction solar cell optimization (Multijunction & Cells, 2000). Based on (Kockott & Schoenlein, n.d.) carbon arc lamps in comparison to xenon lamps have a weaker wavelength.

Other carbon arc light drawbacks may be defined as operating limited time, unstable operation, and extreme blue arc radiation (Bickler, 1962). Carbon arc lamps could be a good solar simulator however, a solution to the instability problem should be found (Ross B, 1963). The report by Mirtich states that the carbon arc lamp spectrum that he used in his solar simulator was fully compatible with the Johnston curve (MIRTICH, 1976). Figure 1.2 shows the lighting box with a carbon arc lamp fabricated in (Multijunction & Cells, 2000).
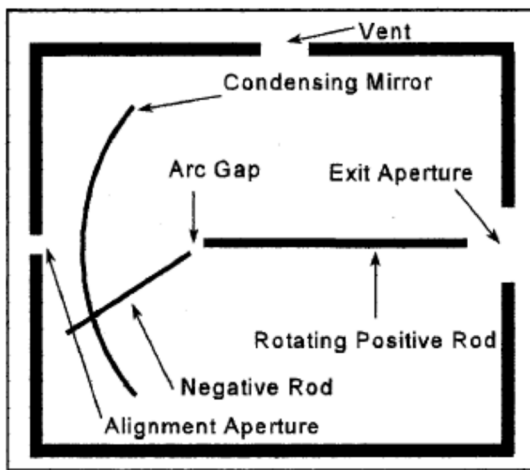
Figure 1.2 Diagram of carbon arc lamp housing
Taken from Xu et al. (2000, p. 1325)

The first High-pressure sodium (HPS) lamp was developed in 1966 (*US3248590A - High Pressure Sodium Vapor Lamp - Google Patents*, n.d.). The spectral range of HPS is between 250 to 2500 nm and its widely used in solar simulators as a light source. High efficiency and long-life cycle are the other advantages of HPS to be used. Their spectral radiance is around the visible yellow region (Girish, 2006). This yellow light is named D-line and is approximately 586 nm (van Vliet & de Groot, 1981). Same as carbon arc lamps HPS lamps are expensive and to control the lamp power during its operation it is needed to use an extra electronic device called ballast. Figure 1.3 illustrates a typical high-pressure sodium lamp.
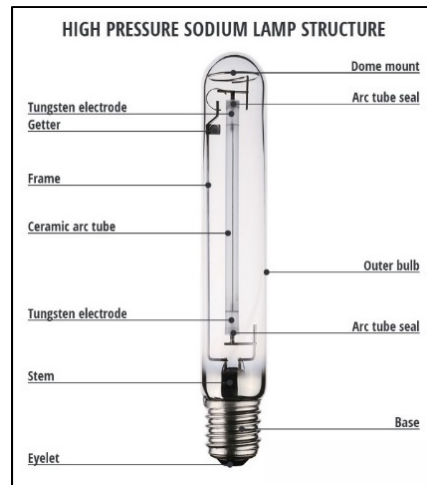
Figure 1.3 High-pressure Sodium Lamp
Taken from HTPC (2018, p. 1)

Argon arc lamps are used in the solar simulator as well. Some research stated that it is an appropriate light source for solar simulators that provide a competent uniformity besides stable irradiance however, the lifetime of this kind of lamp needs to be improved (DECKER & POLLACK, 1972).

The visible color of argon arc lamps is in the white region and the black body color temperature is about 6500K between 275nm to 1525 nm spectrum range. Hirsch et al demonstrate a high flux solar simulator with a 75 kW high-pressure argon lamp (Hirsch et al., 2003).
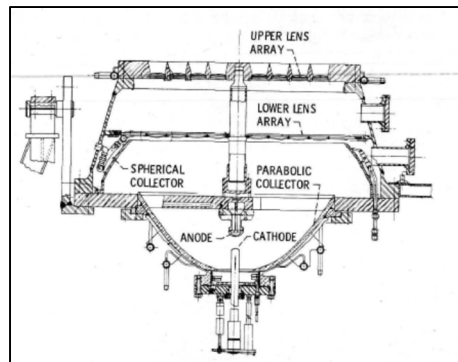
Figure 1.4 Sketch of argon arc lamp
Taken from Decker et al. (1972, p. 17)

Normally, the arc lamps produce visible wavelengths beside infrared and ultraviolet spectrum but for adjusting the spectrum to match the AM0 and AM1.5 some advanced optical filters are needed (Petrasch et al., 2007a). Figure 1.5 shows a high-flux solar simulator with 10 arc lamps in the Paul Scherrer Institute.

Figure 1.5 The high-flux solar simulator at Paul Scherrer Institute
Taken from Petrasch et al. (2007, p. 410)

1.1.1.2   Quartz tungsten halogen lamp

Tungsten-Halogen lamps were first developed in the early 1960s by replacing the traditional glass bulb with a higher performance quartz envelope that was no longer spherical, but in tubular shape (Burgin & Edwards, 1970). This kind of lamp is preferred to use in solar simulators due to its high light output intensity, low cost, and wide spectral wavelength that is near natural sunlight (Irwan et al., 2015). Figure 1.6 shows two typical tungsten halogen lamps, linear double-ended lamps, and cap-type tungsten halogen lamps.
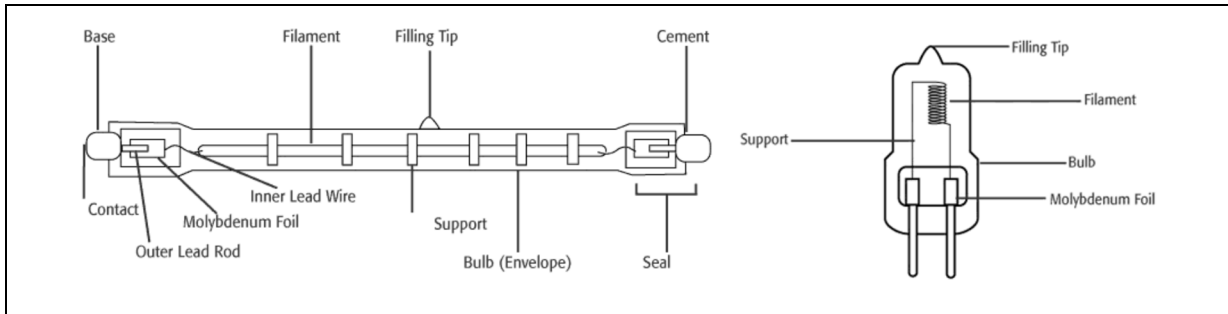
Figure 1.6 Linear double-ended and R7S cap base tungsten lamp
Taken from Cobotex (2020, p. 2)

In research, for the improvement of a four-piston Stirling engine, they use four 1000 W halogen lamps as a light source for the solar simulator. The increased light intensity also increased the motor performance, which the solar simulator provided the desired efficiency (Kongtragool & Wongwises, 2008). In some designs, they added a blue filter to the light source to reach 5400K instead of 3400 K color temperature which is the yellowish color of the tungsten halogen lamps. Figure 1.7 shows the setup configuration used to correct the Tungsten lamp spectrum (Landrock et al., 2011).
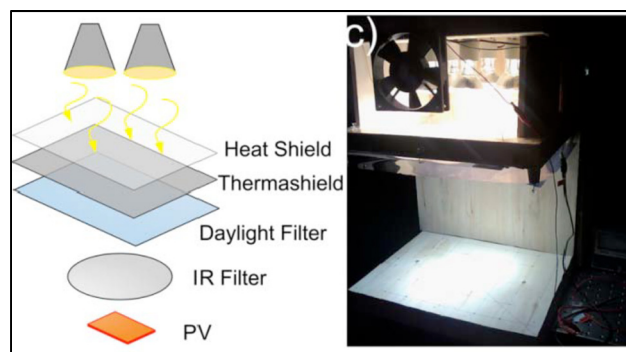
Figure 1.7 Configuration setup used for spectrum correction of a tungsten lamp
Taken from Landrock et al. (2011, p. 157)

A low-cost solar simulator fabricated by Hussain et al. used a halogen lamp as a light source shown in figure 1.8 (Hussain et al., 2011)

Figure 1.8 Halogen lamp light source solar simulator
Drawn from Hussain et al. (2011, p. 5)

1.1.1.3   Mercury xenon lamp

Mercury xenon lamps (Hg-Xe) have the features of xenon arc lamps and high-pressure mercury lamps. They combine the ultraviolet (UV) spectrum of mercury vapor lamps and the infrared (IR) spectrum of xenon lamps (Giller H. F., 2000). Although mercury xenon lamps are used as a light source in specific applications (Ivo Alxneit, 2011), series of security problems were reported: Ozone creation, lamp explosion, and mercury vapor from the lamp (Goranson, 1965). Figure 1.9 shows a typical mercury xenon lamp.

Figure 1.9 500 W Mercury Xenon arc lamp
Taken from Newport (2020, p. 66142)

1.1.1.4 Xenon arc lamp and flash lamp

Xenon arc lamps are the most used light source in solar simulators especially the high flux solar simulators (HFSS). However, in the IR region between 800 nm and 1000 nm, they have an intensity peak. This problem can be filtered by a glass filter (Bickler, 1962). Xenon short-arc lamps proposition a decent point light with high intensity and a close match to the natural sun spectrum, suitable for air mass 1.5 (Wang et al., 2014). Figure 1.10 illustrates the schematic of a commercial xenon lamp and the comparison with natural solar irradiation.
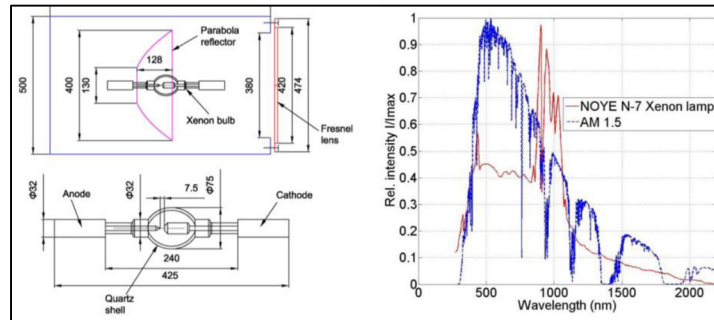
Figure 1.10 Schematic of the NOYE xenon lamp and comparison of its spectral distribution
with natural solar irradiation
Taken from ASTM International (1998, p. 10)

One of the most disadvantages of xenon arc lamps is the high operation pressure, which could escalate to a danger of explosion besides an expensive power supply and a low lifetime of about 600 hours (Gallo et al., 2017). Xenon arc lamps are used with ellipsoidal reflectors as they have a point source light (Petrasch et al., 2007b). Figure 1.11 shows a 10 kW xenon lamp.

Figure 1.11 A 10 kW xenon lamp showing the cathode and anode
Taken from Thomas et al. (2011, p. 4)

In most of the studies that they used a xenon arc lamp as a light source for their solar simulators, SS light output matched Class A at standard test conditions. Figure 1.12 represents a commercial solar simulator that uses a xenon arc lamp as a light source.
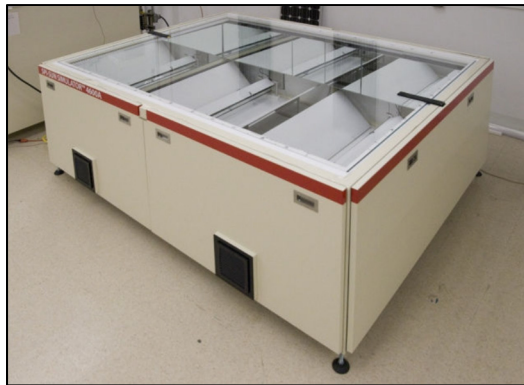
Figure 1.12 Xenon arc light source Solar Simulator
Taken from Serreze et al. (2012, p. 460)

1.1.1.5   Metal halide arc lamp and Compact source iodide lamps

This kind of light source is replaced by many solar simulators as Metal halide lamps and their proper ballasts are the most cost-effective per-watt in comparison to xenon arc lamps. However, the unfiltered emission spectrum does not match the spectrum of sunlight (Codd et al., 2010). When compact source iodide (CSI) was developed, Metal halide arc lamps were

introduced as a high light efficiency of over 90 lm/W and a long lifetime of over 1000 hours (Beeson, 1978). CSI lamps are weak at the UV part while they emit a lot of IR energy (Krusi & Schmid, 1983a). in research by Gevorgyan et al. metal halide lamps were used for Atlas 1200 solar (Gevorgyan et al., 2013). In 2011 a large-scale multiple-lamp solar simulator was designed and constructed to provide a test platform for the simulation of solar radiation at the earth's surface. They used 188 metal halide lamps and conform to Class B of the ASTM (American Society for Testing and Materials) and IEC (International Electrotechnical Commission) standard (Meng et al., 2011). Figure 1.13 illustrated metal halide lamp source solar simulator made by Meng et al.

Figure 1.13 Multiple lamp solar simulator
Taken from Meng et al. (2011, p. 1760)

Figure 1.14 demonstrates a solar simulator with 35 metal halide lamps placed in an aluminum box (a) and an Osram HMP 575 W metal halide lamp (b) (Zacharopoulos et al., 2009)
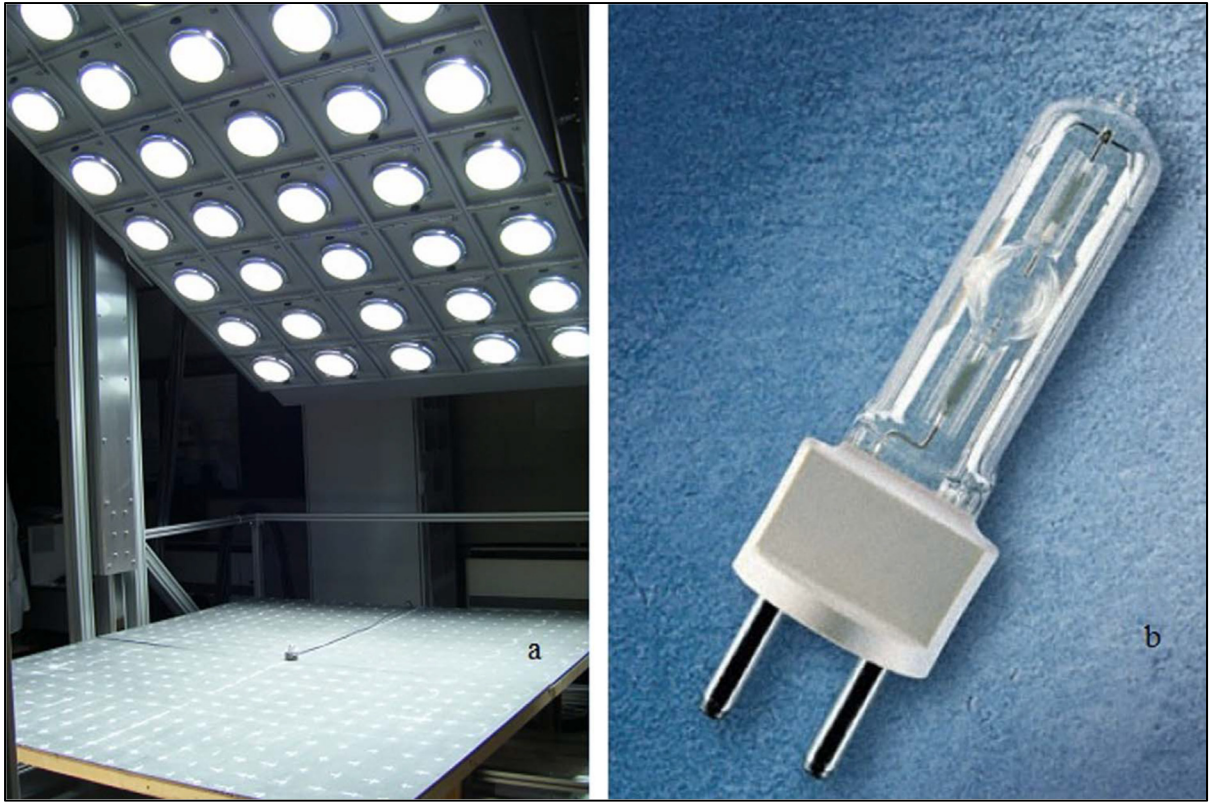
Figure 1.14 (A) Metal halide light sourced solar simulation example
(B) metal halide lamp
Taken from Zacharopoulos et al. (2009, p. 856)

1.1.1.6   Light-emitting diode (LED)

In energy-efficient lighting, LED is the new technology. LED stands for "light-emitting diode" and it is a semiconductor light source based on the electroluminescence phenomenon, that converts forwarded electricity on a p-n junction, into the narrow-spectrum light. Figure 1.15 shows schematic diagrams of Light Emitting Diodes. Neither a filament lamp nor an arc light is close to the LED's emission process.
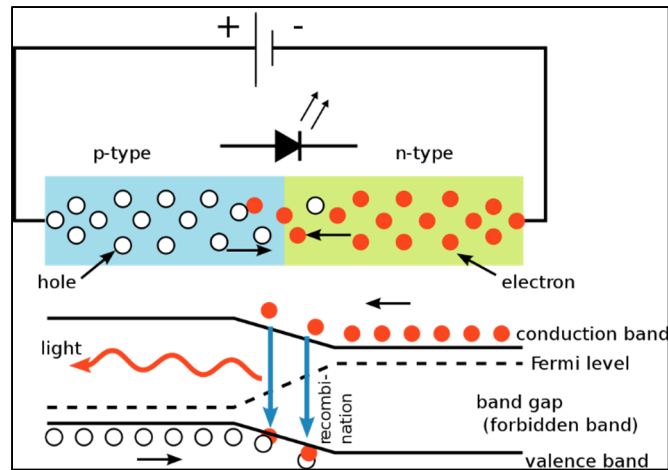
Figure 1.15 Schematic diagrams of Light Emitting Diodes (LED)
Taken from Wikimedia (2020)

In the beginning, LEDs is used mainly for their low light level markers and signals. LEDs were introduced as a new light source for many purposes as like solar simulator design in the early 2000s after a massive development of high-power LED technology (Bliss et al., 2008). Figure 1.16 illustrates the evolution of LED package technology from the 1960s to date.
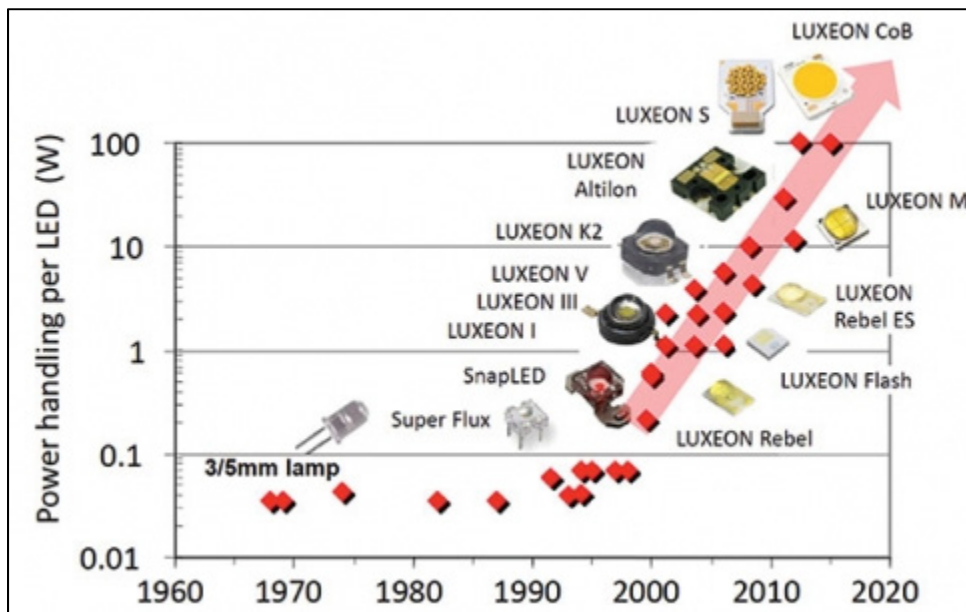
Figure 1.16 Evolution of LED package technology
Taken from Compound Semiconductor (2015, p. 2)

LEDs have many benefits over traditional light sources in solar simulators due to their special characteristics (Kohraku & Kurokawa, 2006), (Bliss et al., 2008), (Bazzi et al., 2012):

I. LEDs can be controlled very fast within microseconds or operated stably at the same amount of intensity continuously for a long time. As shown in Figure 1.17 a research on using LED as a flashlight for a small camera, compared to a Xenon lamp in terms of response and shape of intensity pulse. Apart from a special integrated driver for LED that makes a distinctive pulse shape (blue line) this plot demonstrates LED fast response.
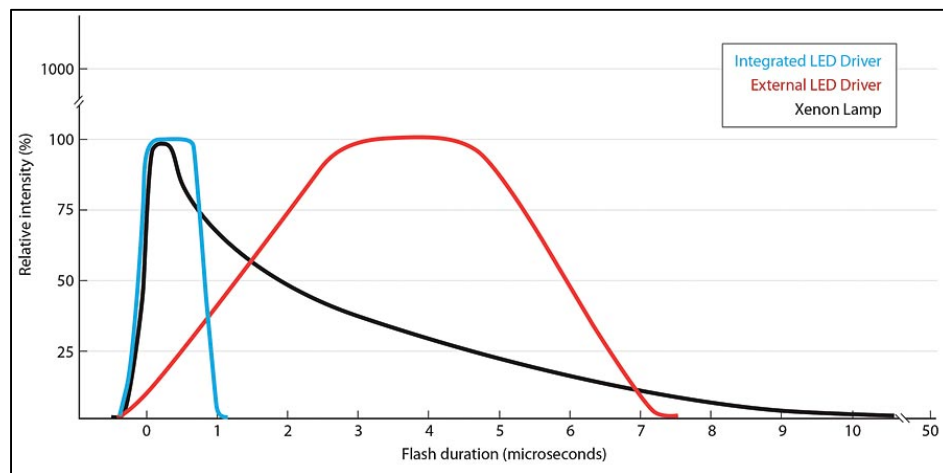
Figure 1.17 Comparative Pulse Widths for Machine Vision Light Sources
Taken from Kinney (2020, p. 5)

Contrast the performance of these sources with the controlled pulse shape from LED designs, integrate driver and controller allows the LED to achieve full power in the 300 to 500 nanosecond time frame and deliver repeatable, high-intensity pulses with duration in the microsecond range (*LED Light Pulses Enter the Nano Realm to Keep Pace with High-Speed Imaging - ProQuest*, n.d.).

Fast controlling and operated continuously, make it possible to combine a steady-state solar simulator and flash solar simulator together with additional functions such as variable flash frequencies and flash shape.

II. LEDs have a relatively narrow monochromatic output spectrum (except white LEDs) and are available in a wide variety of colors and wavelengths, which means combining several required colors LEDs can obtain a close-matched AM0, AM1.5, AM2, or another special application spectrum.

A MATLAB software program simulates the different LED spectral based on the mathematical model of LED. Figure 1.18 gives the output spectral of each LED and the total output spectral (Tito-haykestep et al., 2020).
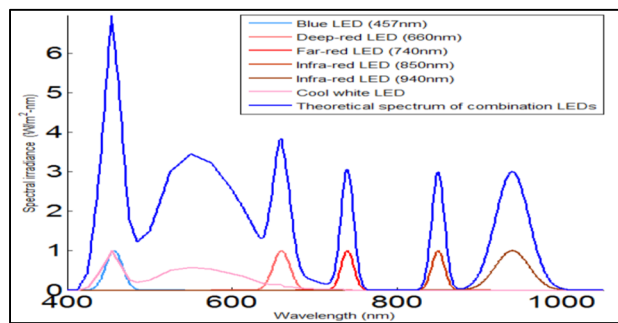
Figure 1.18 Simulation of sample various kinds of LEDs
Taken from Tito-haykestep et al. (2020, p. 70)

A single LED can not fulfill the Solar Simulation Spectral Standard needs (IEC, 2008), however, combining various colors and wavelengths of LED gives the opportunity to build a close matched AM1.5G spectrum which is prescribed for calibration of photovoltaic devices.
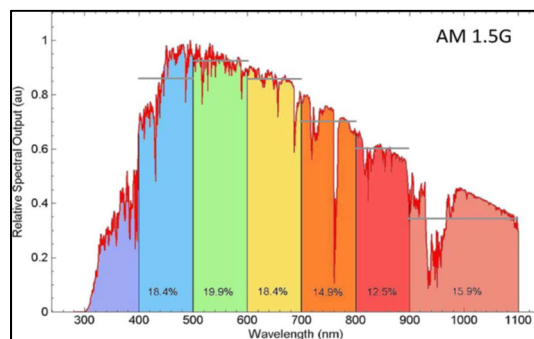
Figure 1.19 IEC 60904-9 reference solar spectral irradiance distribution
Taken from Grandi et al. (2014, p. 3056)

This advantage also gives the ability to build a device not only for solar cell testing but for various test and research purposes like sun protection factor (SPF) (Bacardit & Cartoixà, 2020), human lenses (Duarte et al., 2019), automotive industry (Öztürk, Emre; Aktaş, Mehmet; Şenyüz, 2020), sunlight exposure testing and of colorfastness and material stability for textile, plastics, and paints (Kejlová et al., 2020)
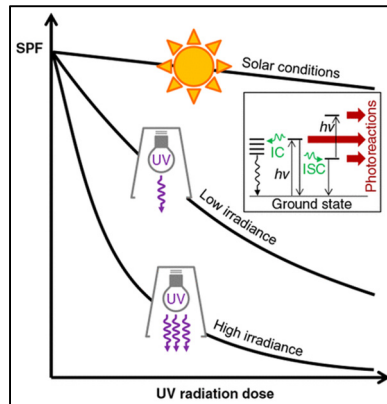
Figure 1.20 Solar simulated conditions typically used in SPF determination tests
Taken from Bacardit et al. (2020, p. 1209)

III. With the development of high-power LEDs, 1000W/m2 level light intensity LEDs are available, higher intensity LEDs are expected in the future. A multi-chip LED package with a chip-on-board structure (COB) and laser-driven white illumination were developed to achieve the desired lumen output (Li et al., 2019). COB LEDs have several advantages over past LED technologies, such as Surface Mounted Device (SMD) LEDs or Dual In-line Package (DIP) LEDs. Figure 9 shows a comparison of a square array on a small area (10mm x 10mm) between DIP, SMD, and COB technology.
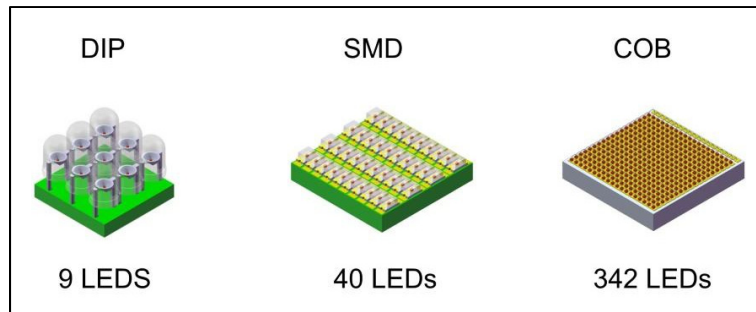
Figure 1.21 Comparison of LED Array Packing Density (10mm x 10mm)
Taken from Kinney (2020, p. 7)

As illustrated in the picture above different array packing results in 38 times more LEDs compared to DIP LED technology and 8.5 times more LEDs compared to SMD LED technology. This ability and achieved technology results in increased light intensity and uniformity (*What Are "COB" LEDs and Why Do They Matter?*, n.d.)

IV. LEDs have a very long lifetime up to 50,000 to 100,000 hours in general, which means that they not only compensate for a higher cost per light intensity but also reduce the maintenance cost to a minimum.
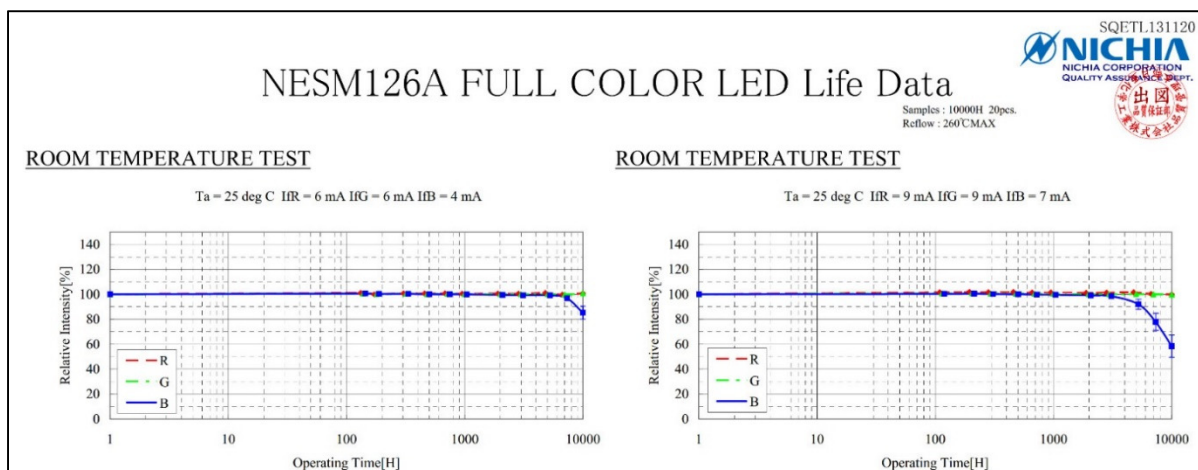
Figure 1.22 Nichia real-life data up to 100,000 hours
Taken from QST Education (2017, p. 2)

Nichia, recognized as the top LED brand in the world--and associated with 2014 Nobel Prize recipient and "Father of the blue LED," Dr. Shuji Nakamura reports real-life data of their LED (Figure 1.22).

V. More compact and energy saving. In contrast to Xenon lamp type solar simulators with large size, LED solar simulators can be designed very compact due to the higher efficiency light source, fewer electronic devices, and without large size concentrator.

Figure 1.23 Size comparison of Xenon and LED solar simulator
Taken from Newport (2020)

Figure 1.23 compares two Solar simulators with a Xenon lamp at the left and an LED light source at the right, from Newport. Xenon lamp Solar simulator dimensions is about 90cm x 50cm x 41cm (*94063A Solar Simulator*, n.d.) in compare of LED lamp source solar simulator with 10cm x 20cm x 18cm (*Class ABA LED Solar Simulator*, n.d.).

1.1.1.7   Supercontinuum laser

Nowadays, the most used light source in solar simulators is xenon arc lamps and lighting emitted diodes. This kind of lamp source has a wide spectral spectrum range and for some purposes that need more focused spectral area, it is hard to use them (Dennis, 2014). Supercontinuum lasers radiate to a smaller angle area than LEDs. But in the ultraviolet (UV)

and infrared (IR) wavelengths they are incomplete (Behrang H. Hamadani et al., 2013). It is easy to focus the lasers besides they are very powerful. However, they have a very narrow spectrum (Dennis et al., 2016). The latest achievements show that laser technology will improve in the near future and it will be used in researches with small region lighting areas (Mundus et al., 2015), (Dennis et al., 2015).

1.1.2 Concentrator

As discussed in 1.1.1 most of the light sources for solar simulators are approximately point sources or line sources, therefore, to have a specific required light level on the testing area, an optical system should apply. For-solar simulator system, particularly for a solar high flow simulator, the optical concentrator is a key optical component. Its principal functions are 1) to collect light radiation in different directions by the light source and project in accordance with the appropriate direction; 2) to increase the light stream power density to satisfy these requirements. Figure 1.24 illustrates a schematic diagram of a concentrator. The surfaces of input and output can be faced in any direction, and it is presumed that the 'A' opening is simply wide enough to allow the occurrence of all the rays passing through the internal optics within a specified collecting angle (Winston et al., 2005).
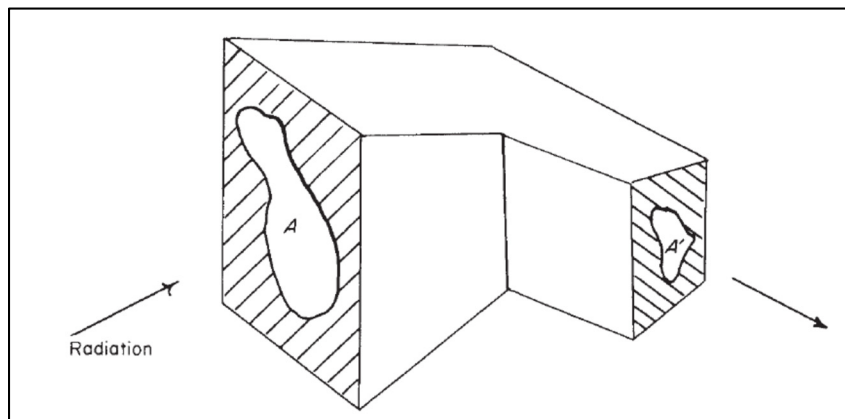
Figure 1.24 Schematic diagram of a concentrator
Taken from Winston et al. (2005, p. 3)

By reviewing the works on solar simulators and their optical design these various concentrators have been used: the ellipsoidal reflector, compound parabolic concentrator (CPC), light cone, hyperboloid concentrator, parabolic dish concentrator, and Fresnel lens.

1.1.2.1   Ellipsoidal concentrator

An ellipsoidal concentrator is defined that all rays originating at one of its foci must pass through the other after a single specular reflection (Petrasch & Steinfeld, 2005). Figure 1.25 demonstrates two focuses of the ellipsoids reflector. When a light is placed at one of them, its beams are first reflected on the other one. Ellipsoidal concentrators are commonly used in systems that require not only the aggregation of emitted light but also an increase in light intensity since they can satisfy each of these criteria without any external optical components. This can make optical systems more compact and efficient.
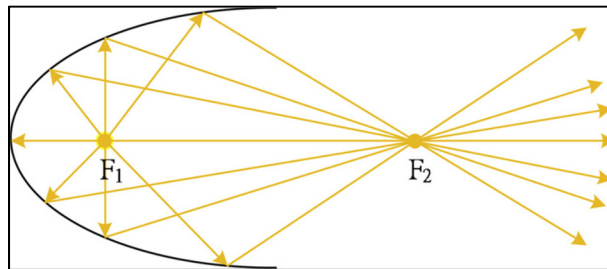
Figure 1.25 Schematic of optical-geometrical characteristics of an ellipsoid reflector
Taken from Ma et al. (2019, p. 92)

High flux solar simulators for solar point focus system simulation like a solar dish or solar power tower system, the optical characteristic becomes more important and more additional optical component means more operation failure risk and more expenses on the cooling system for optical material (I Alxneit et al., n.d.). In addition, some errors may accrue during the installation of the optical systems. To date, most of the HFSS used ellipsoidal concentrators in their optical systems (Kuhn & Hunt, 1991).

1.1.2.2   Parabolic dish concentrator

In 2003 the very first concentrator photovoltaic (CPV) solar simulator was presented by IES-UPM. The concept of a solar simulator is based on collimation through a parabolic reflector (Antón et al., 2005). The parabola is the mathematical figure that shows that every ray coming from its focus is reflected parallel to its axis. Figure 1.26 by Mark Fedkin illustrates the geometry of a parabolic reflector. All rays parallel to the parabola axis are reflected through the focal point.
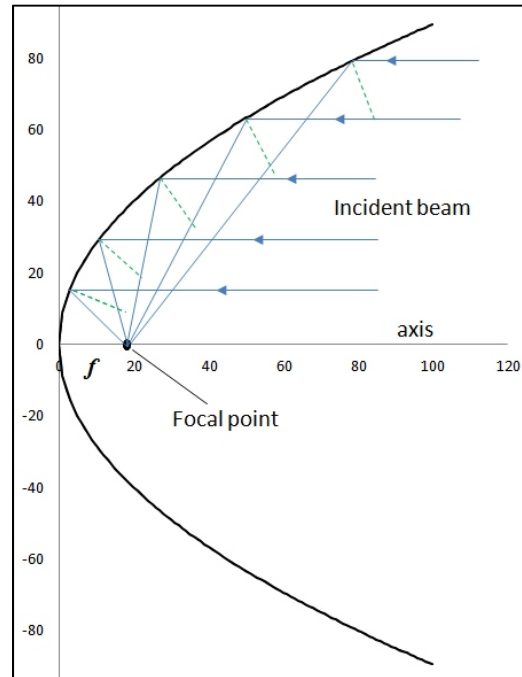
Figure 1.26 Geometry of a parabolic reflector
Taken from Fedkin et al. (2013, p. 3)

Therefore, if a parabolic reflector or mirror is illuminated with a small point source lamp, it could regenerate a collimated light on a certain surface equal to the same reflector size. Due to the characterization of parabolic dish concentrators that can concentrate parallel light on its focal spot, they are widely used in concentrated solar power (CSP) (Pernpeintner et al., 2015). In solar simulators also this characterization is a good ability to collect all the light outputs from a light source and concentrate them on to test area (Ekman et al., 2015). In addition, some

research demonstrates that if the light is already collimated, a parabolic dish can also be used as the concentrator for HFSS (Domínguez et al., 2008).

Figure 1.27 Collimator mirror manufactured at JUPASA
Taken from Research gate (2020)

1.1.2.3   Compound parabolic concentrator (CPC)

The basic shape of the compound parabolic concentrator is illustrated in figure 1.28. The name is derived from the fact that the CPC consists of two parabolic mirror parts with different focal points as defined. A (F_A) lies on parabola B whereas the focal point of parabola B (F_B) lies on parabola A. Winston et al. discuss the concentration ratio and the geometry parameters in (Winston et al., 2005). In the low concentration ratio CSP system and CPV system, the CPC concentrator was shown as an optical concentrator. There are only a few researches that use CPC on their solar simulator's designs.
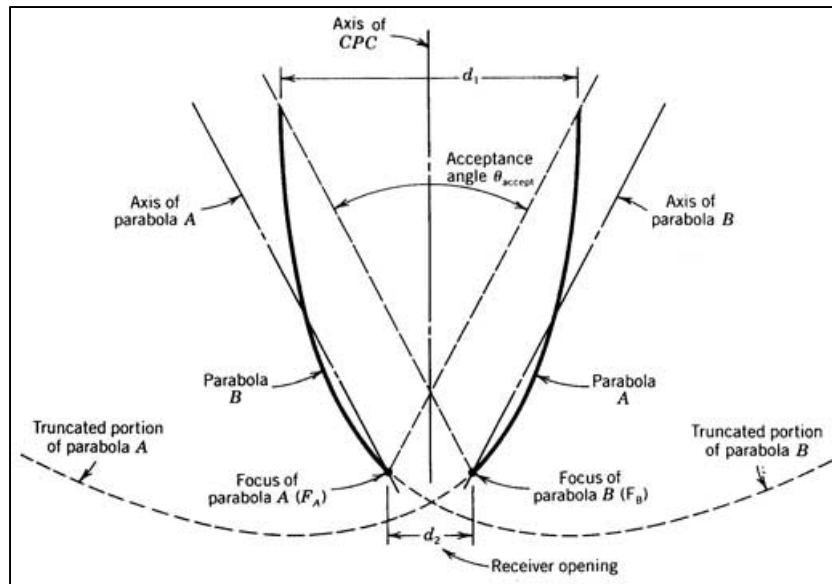
Figure 1.28 The compound parabolic concentrator (CPC)
Taken from William et al. (2001, p. 51)

1.1.2.4 Hyperboloid concentrator

A hyperboloid concentrator uses the geometry characterization of a hyperboloid to concentrate the light rays to the receiver area that can be a test plane (Sellami, 2013). Figure 1.29 (A) demonstrates a two-dimensional (2-D) of a flow-line concentrator which is concentrated by a truncated hyperboloid and light cone. Figure 1.29 (B) shows a three-dimensional (3-D) elliptical hyperboloid concentrator designed by Imhamed M. et al.
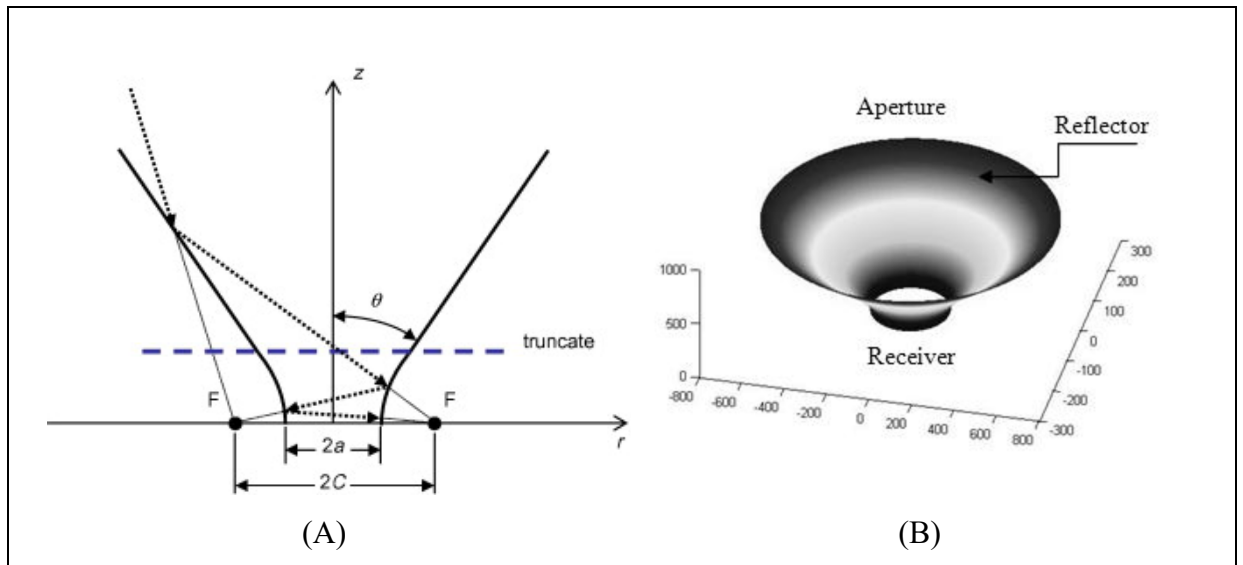
Figure 1.29 (A) 2-D hyperboloid concentrator
Taken from Codd et al. (2010, p. 2206
(B) 3-D elliptical hyperboloid concentrator
Taken from Imhamed et al. (2010, p. 2)

1.1.2.5   Light cone

The light cone is a basic type of concentrator and has been used for many years (Holter et al., 1962). Figure 1.30 shows a schematic of a light cone.
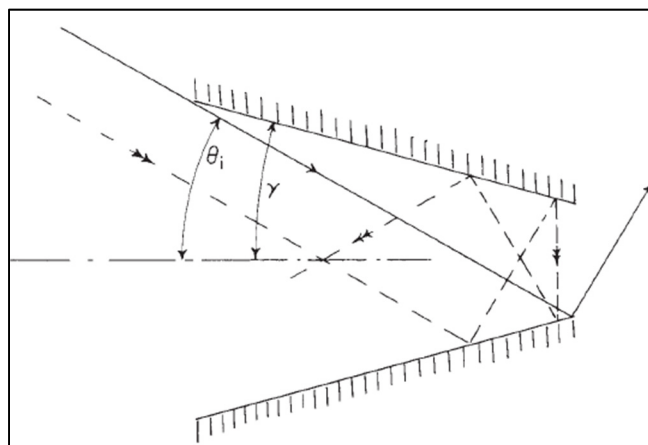
Figure 1.30 The cone concentrator
Taken from Winston et al. (2005, p. 553)

Since the design and fabrication of the light cone are easy, it is still used in some designs for solar cookers and solar simulators combine with other optic materials (Codd et al., 2010). Figure 1.31 shows a low-cost solar simulator with the use of a secondary cone concentrator designed by Codd et al.
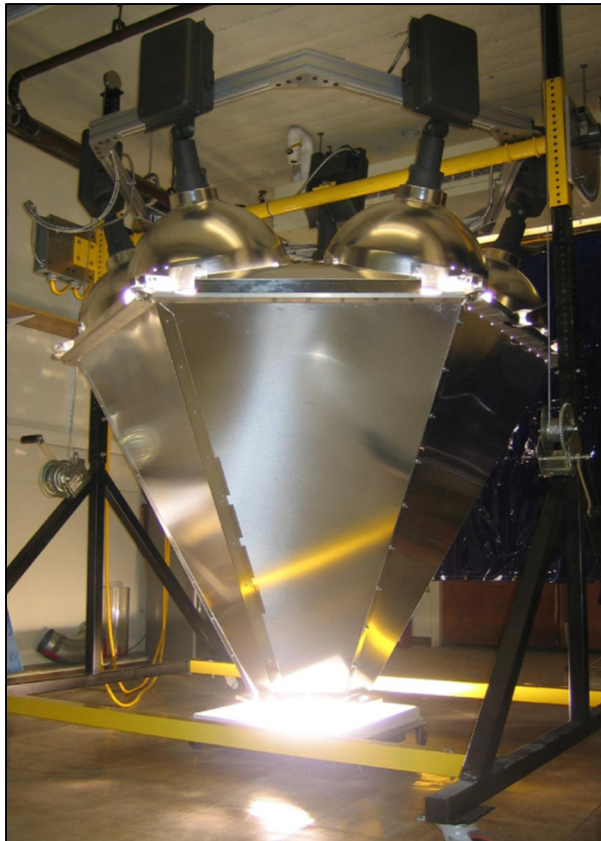
Figure 1.31 Secondary concentrator structure
Taken from Codd et al. (2010, p. 2207)

1.1.2.6   Fresnel lens

A Fresnel lens is a unique type of lens that operates differently than typical spherical or even aspheric lenses. Essentially a chain of prisms which each prism represents the slope of the lens surface, but without the material of the full body of the conventional singlet. Figure 1.32 shows the fresnel lens design steps and how they cut a typical convex shape (1) lens edges and placed the curve segments (2) onto a plane (3).
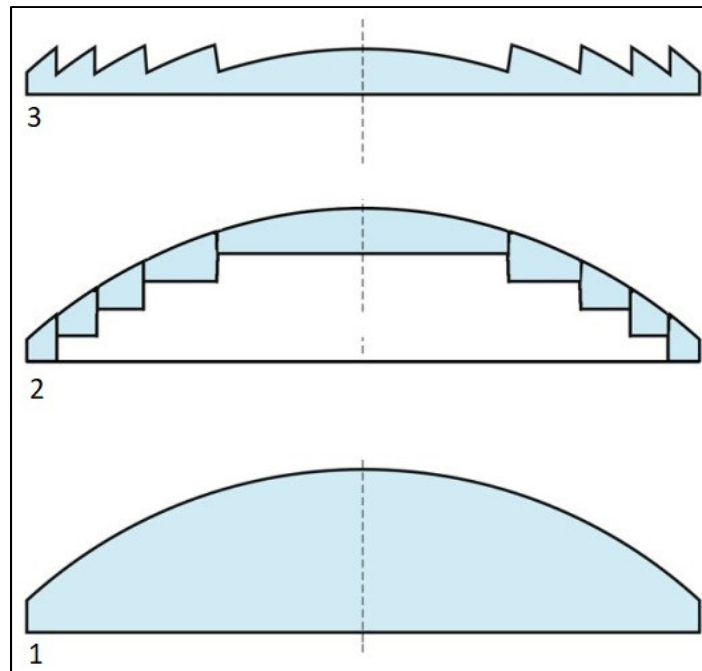
Figure 1.32 Fresnel lens design
Taken from Jarphys (2015)

These concentric grooves that etched into one side of a sheet of plastic fresnel lenses act as individual refracting surfaces that bend parallel rays in a similar fashion to a conventional lens and thus have similarly specified focal lengths. However, Fresnel lenses have a lighter and thinner design, far less absorption due to the smaller thickness and a larger variety of size options (Davis, 2011). Fresnel lenses have a variety of applications but are not appropriate in all-optical systems (Xie et al., 2011). The drawbacks of these lenses include chromatic aberration when used with broadband sources, distortion to any images formed, and poor image quality when used in imaging systems. Though still not recommended, higher groove densities do provide slightly better image formation (Davis et al., 2001).

One common application of Fresnel lenses is the solar collection. Due to the availability of Fresnel lenses in large sizes, they are the ideal choice for focusing sunlight to heat a sample placed at the focal point of the lens (Ren et al., 2007). They are also commonly used to collect light for solar cell heat collectors. Aspheric Fresnel lenses will provide better light-concentrating ability than a conventional spherical Fresnel lens. Smaller Fresnel lenses can

accomplish the same focusing abilities as in a solar collection setup but on a smaller scale (Han et al., 2007). They can collimate light emitted from LEDs or other light sources or can be used to focus light into sensors in a non-imaging setup. Fresnel lenses are also common in illumination systems since they are very useful for providing even illumination from non-uniform light sources (Vu et al., 2020). Collimated light occurs when light rays are traveling parallel to each other, as opposed to converging to a focus or diverging away from the center. Essentially, it can be considered that collimated light focused on infinity. Figure 1.33 (A) illustrates a positive focal length Fresnel lens used as a collimator.

(A)   (B)
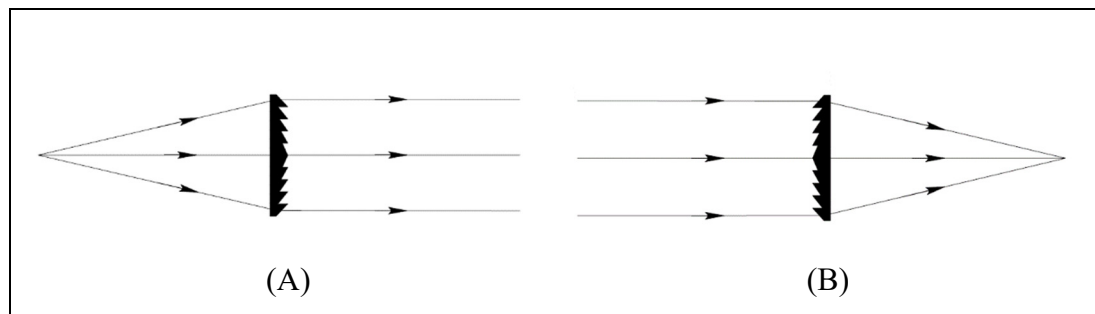
Figure 1.33 (A) Light Collimation of a Point Source with a Positive Focal Fresnel Lens.
(B) Light Collection to a Point with a Positive Fresnel Lens
Taken from Fresnel technologies (2014, p.1)

To collimate a diverging light source with a lens, we can place the lens a distance away from the source, equal to the focal length of the lens. Alternatively, if collimated light enters a lens, it focuses on a distance equal to one focal length. We can assume that light is collimated or coming from infinity if the light source is greater than a distance equal to 10x the focal length of the lens away (Allil et al., 2018). Figure 1.33 (B) shows a positive focal length Fresnel lens used as a collimator. The AM2 solar simulator developed by Lewis Research Center is one of the earliest solar simulators which used plastic Fresnel lenses as the main concentrators for the lamps (Yass & Curtis, n.d.). In many other solar simulators, Fresnel lenses were used as the concentrator (Humphries, 1978).

1.2 Evaluation and Comparison of Different Designs with LEDs

Researchers have tried to design an effective solar simulator with low-cost production needs and more efficient output. They have dealt with multiple types of light sources to reach the standard criteria with a certain light level and uniformity. One of the earliest works that have been done on LED-based solar simulators was in 2003 by Kohraku and Kurokawa. They focused on light unevenness and absolute spectral response in their experiments and measurements. As they did their research before the publication of ASTM standards for solar simulators, this solar simulator was not classified. They assumed that the unevenness is a function of the distance between the light source and test area and also the number of LEDs. The result for spectral response illustrated that the photocurrent of solar cells is estimated with a bright-line spectrum (Kohraku & Kurokawa, 2003). This paper demonstrated the potential of LED technology as a light source for solar simulators, however, leaves many questions unanswered. Figure 1.34 shows a low-cost, hybrid LED-Halogen solar simulator light source fabrication. The choice of Halogen lamps was due to cover the range of near-infrared (NIR). This configuration showed they reached Class B of spectral matching with better than 5% spatial nonuniformity over a 10x10 cm^2 test area (Grandi et al., 2014).
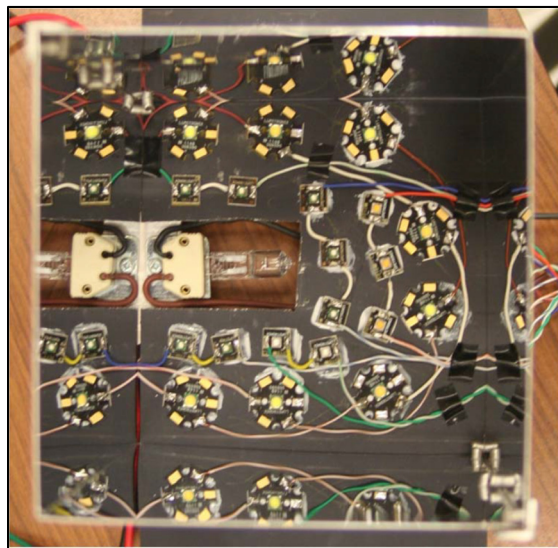
Figure 1.34 Hybrid LED-Halogen solar simulator light source
Taken from Grandi et al. (2014, p. 3059)

Class A spectral match in the visible region of the spectrum and class B in the overall spectral match was obtained by (Mohan et al., 2014). They have controlled the intensity of LEDs with separated pulse width modulation (PWM) drivers. The use of a Halogen lamp beside the LEDs accrued poor IR spectrum which made the overall spectrum match in class B. In a Led-based solar simulator that was fabricated by Bliss et al. an array of 376 LEDs in 8 different colors was used and covered the light spectrum from UV to red. They also used halogen lamps to cover the IR range (Bliss et al., 2014). Figure 1.36 shows an LED array prototype with halogen lamps that Bliss et al. fabricated. They designed the solar simulator light sources for future replacement of the halogen lamps with LEDs. They have reached an AAB class with 1.9% uniformity over a target area of 4.5x4.5 cm^2 and Class B in the spectral match due to lack of light emission in the 700 to 800 nm range. The total irradiance has been measured in 2009 by Bliss et al. to illustrate that due to spectral match they achieved AM1.5G spectral match and a maximum irradiance to 1.2 Suns with LED light sources and 590W/m^2 can be reached.
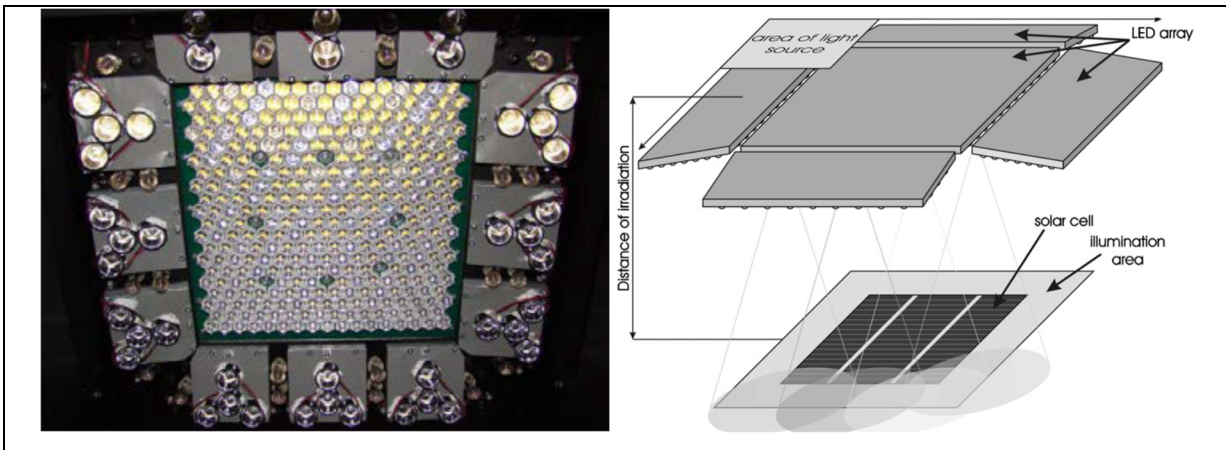
Figure 1.35 The LED array of the solar simulator
Drawn from Bliss et al. (2014, p. 3) (2009, 827)

In a solar simulator that fabricated by (Jang & Shin, 2010), a 96 LED package with a power of 1.5W per LED was installed on an aluminum plate as a heatsink. The light emitted by LEDs went through a collimated lens with a transmittance of a 99% air mass filter (AM1.5D). A full LED-based solar simulator designed and tested by Kolberg et al. demonstrated that with SMD LEDs and customized driver with linear regulators as current sinks companied with a multi-

channel digital-to-analog converter (DAC) with software control, they could achieve a very close match to AM1.5G with full-intensity, full-spectrum lighting solar simulator, nevertheless, their high-power LED sources not yet achieved the desired homogeneity demands (Kolberg et al., 2011). Figure 1.37 shows an optical mirror used for this solar simulator which needs some improvement to reach the desired uniformity.
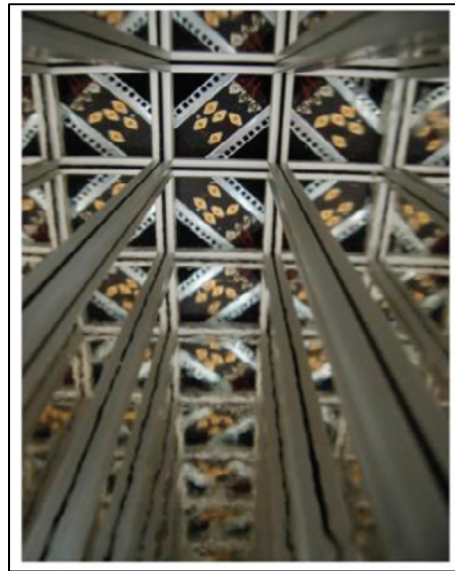
Figure 1.36 Upside-down view into SMD solar simulator
Taken from Kolberg et al. (2011, p. 104)

One of the biggest optic solutions represented in (B. H. Hamadani et al., 2012) used a three-meter-long tapered light guide. Spatial nonuniformity of 10% with 1 sun intensity delivered on a 27x27 cm^2 test plane, thus qualified it as a Class C solar simulator. As shown in figure 1.40 a matrix of 34 high-power LED from 395nm to 970nm was designed and a computer-controlled LED driver was connected to adjust the current and subsequently the total output spectrum.
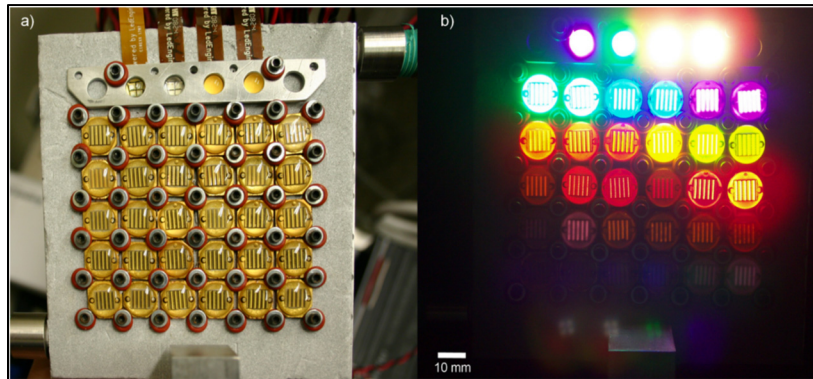
Figure 1.37 LED matrix heat sink/mount with built-in water circulating channels
Taken from Hamadani et al. (2013, p. 73)

Gonzalez (González, 2017) looked at the design of an LED solar simulator specifically for use in student labs. The prototype is seen in Figure 41. Since the requirements are relatively non-stringent for student labs, halogen lamps often suffice as the source. However, Gonzalez (2017) suggests a cost-effective LED-based solar simulator by comparing LED to sunlight and halogen using the following parameters: irradiance and uniformity. The halogen produced higher irradiance than the LED for a given distance due to higher power consumption. As expected, the LED showed good uniformity for all distances while the halogen showed good uniformity at large distances. The characteristic curves of a student PV module were measured. At a given irradiance level, the PV module output was similar for LED and the sun, while the halogen performed poorly due to its richness in high wavelength, low energy photons.

Figure 1.38 Prototype of the LED solar simulator
Taken from González (2017, p. 2)

In the solar simulator which was made for light soaking and current-voltage measurement of amorphous silicon solar cells, 11 different LED types were used and installed on 16 identical printed circuit boards (PCBs) with separated power supplies. They have reached class A AM1.5G spectrum between 400 to 750 nm. Reflecting foils are used as the only optic consideration to prevent intensity losses. All LEDs were controlled via 192 channels (12 channels for 16 PCBs) to reach the spectrum and homogeneity (Stuckelberger et al., 2014). Class A spectrum was also achieved for an area 6x6 cm^2 by using 19 high-power emitters in Novickovas et al's research. Six types of LED with different wavelengths from 400 to 1100nm were used. LEDs were mounted on individual hexagonal star-type metal-core printed circuit boards (MCPCB). To ensure optimal flux homogeneity a honeycomb-like installation was defined and an aluminum-coated polycarbonate reflector with a 32-degree viewing angle was used. Class C in uniformity achieved due to overlap of LED beams were class A in spectral matched represented (Novickovas et al., 2015). In research done by Alessandro et al, 4 identical high-power LEDs were installed on a 26x26 cm^2. They have reached 95% uniformity at a distance of 160mm on a 200cm^2 test area (Alessandro et al., 2020). Experimental results done by (Tavakoli et al., 2020) demonstrate that a class AAA solar simulator achieved in a 2.3x2.3 cm^2 area at a distance of 8.7 cm. Figure 1.38 demonstrate possible improvement for a larger test area by using several LED configuration were designed by them, and tilting the LEDs close to each other.

Figure 1.39 LED arrangement and possible method to the sizeable solar simulator
Taken from Tavakoli et al. (2020, p. 3)

Tito-haykestep et al. designed and fabricated a solar simulator with 19 LEDs installed on an MCPCB arranged in the form of a honeycomb cluster which resulted in a 20mm distance between LEDs (figure 1.39). This included 6 cool white, 1 blue, 6 IR, 3 deeps red, and 3 far-red LEDs. Due to the weakness in the infra-red range especially from 800nm to 1100nm, some changes in LED's arrangement should be made and no result on uniformity was reported.

Figure 1.40 The distribution structure of LEDs for the solar simulator
Taken from Tito-haykestep et al. (2020, p. 75)

Bodnar et al designed a solar simulator for their laboratory with an area of 15x15 cm^2 and 4 LED blocks of different colors besides a halogen lamp. Figure 1.35 illustrates the LED block and simulated structure for the designed solar simulator (Bodnár et al., 2020). Four different

color LEDs, neutral white, red, green, and blue were used in each block. Their design consists of a combination of 36 pieces of colored, 3 W LED lights and 8 pieces of 50 W halogen lamps which indicate a 508W in total. A 9.96% of non-uniformity with 951W/m^2 light intensity was achieved, which is a good approximation of average light intensity on a clear day as they said.

Figure 1.41 Simulated solar simulator and an LED block light source
Taken from Bodnár et al. (2020, p. 177)

1.3   Conclusions and perspectives

As observed, from (Kohraku & Kurokawa, 2003) to (Bodnár et al., 2020) there have been many significant developments in LED technology and the use of them as light sources in solar simulators. Researchers focus on developing different factors and parameters relevant to the solar simulators especially in light source and optics to perfecting the overall performance. They indicated that where LED is used as a light source, very precise spectral matching can be done. Moreover, the cost of the solar simulator is much less than an equivalent simulator with a Xenon arc lamp or other light sources. In general, every design has contributed by adding new useful knowledge to the creation of this technology and it is possible to learn from their mistakes and achievements to develop a LED-based solar simulator.

CHAPTER 2

THEORETICAL BACKGROUND

2.1   Introduction to Solar Energy

The theoretical potential for supplying most of the energy needs of our planet (about 15 TW) is from four sources: solar, wind, geothermal, and ocean waves. Sunlight really does have the greatest theoretical capacity for clean energy supplies in the world. The solar constant which is a flux density measuring on a surface perpendicular to the solar rays is 1.37 kW/m². The time-and-space-averaged solar flux striking the outer atmosphere of the earth is (1.37 kW/m²)/ 4 = 342.5 W/m². (Tsao et al., n.d.)
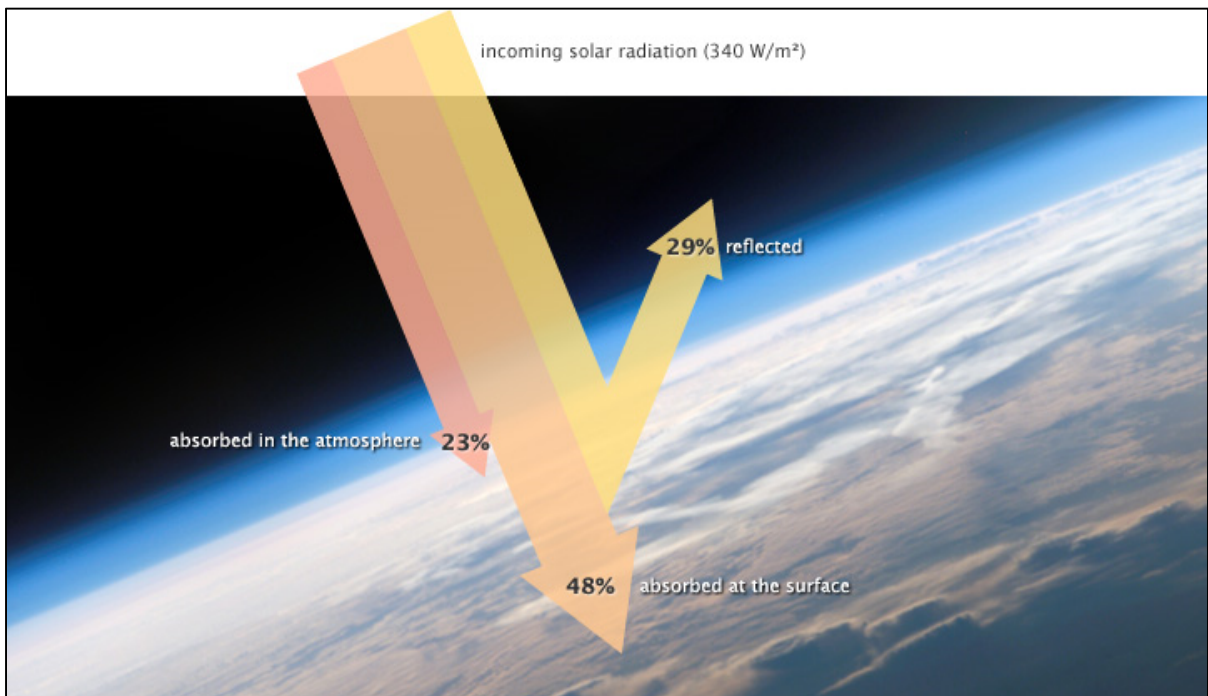
Figure 2.1 NASA illustration by Robert Simmon. Astronaut photograph ISS013-E-8948
Taken from Lindsey (2009, p. 5)

As illustrated in figure 2.1 about 29 percent of the solar radiation which reaches the top of the atmosphere is mirrored back into space by clouds, atmospheric objects, or bright earth surfaces

such as ocean ice and snow. About 23 percent of incoming solar energy is absorbed in the atmosphere by water vapor, dust, and ozone, and 48 percent passes through the atmosphere and is absorbed by the surface. In total, about 71 percent of incoming solar energy is absorbed by the earth system. (Trenberth et al., 2009). These particles are sufficient for generating annual solar energy and meet global energy requirements. Solar energy is obviously the most feasible energy fuel for the future. Another way has been mentioned that enough solar power falls into the planet in 1 hour from what we as societies absorb in one year (Lewis & Francisco, 2007). This resource surplus aims to minimize climate change and emissions while at the same time preserving our existing technical convenience.

2.1.1   The technology of solar energy

Examples of utilizing the sun's resources last thousands of years, and several related technologies are still in high demand; human beings used several solar instruments to capture energy from the sun for heating the water, dry foods, etc. Since the late 1800s that Augustin Mouchot invented his first solar-powered engine, and Abel Pifre who developed the first solar power printing press (figure 2.2), development in technology nowadays could supply adequate electricity from the sun to fulfill our current energy demands.
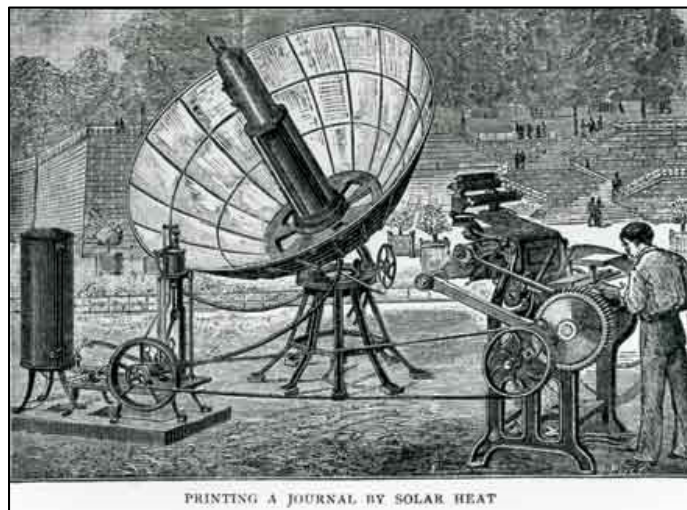
Figure 2.2 Abel Pifre, Solar Power printer
Taken from Abbot (1929, p. 197)

There are two main types of solar energy technologies, photovoltaics (PV), and concentrating solar power (CSP). CSP is also known as concentrated solar thermal, this systems use mirrors to reflect and concentrate sunlight onto receivers that collect solar energy and convert it to heat, which can then be used to produce electricity or stored for later use. In PV solar technology, which is utilized in solar panels, energy from the sunlight is absorbed by the PV cells in the panel. This energy creates electrical charges that move in response to an internal electric field in the cell, causing electricity to flow.

2.2   Photovoltaic (PV) Solar Cells

Most of the PV cells which use the p-n junction generate the electric current when absorbed light creates a free electron and a hole, and if a wire is connected to the junction, the electron will flow through the wire, creating a flow of electric current. According to the report done by (Green, 2009) from the first solar cell which is reported in 1941 with 1% energy conversion efficiency compared to the 25% efficiency which is reported by them, there has been a 57% improvement. In an analysis done by Nushra et al., their proposed models of future solar cells have the ability to reach 85% to 95% overall efficiency (Nushra Oishi et al., 2020).

Solar cells are divided into three generations that signify how essential each one has become. Research is currently being performed by all three generations, with first-generation technologies comprising 89.6 percent of production in 2007 being the most commonly represented in industrial production (William P. Hirshman, Garret Hering, 2008). First-generation cells are large-scale, high-quality, and single-joint devices and theoretically have the limitation of 33 percent efficiency. The second generation was developed to reduce the cost of production (Green, 2002) this generation is thin films that include amorphous silicon, cadmium telluride, or copper indium gallium selenide (Gangopadhyay et al., 2013). Third-generation technologies seek to increase second-generation electrical efficiency (thin-film technologies) while retaining relatively low production costs. There are a few methods to reach this high efficiency: multijunction photovoltaic cell, modifying incident spectrum, use of excess thermal generation (caused by UV light) to enhance voltages or carrier collection, use

of infrared spectrum to produce electricity at night. Third-generation technologies include silicon nanostructures, up/down converters, hot-carrier cells, thermoelectric cells (Conibeer, 2007). PV development was closely monitored by the National Renewable Energy Lab (NREL) and illustrated in figure 2.3.
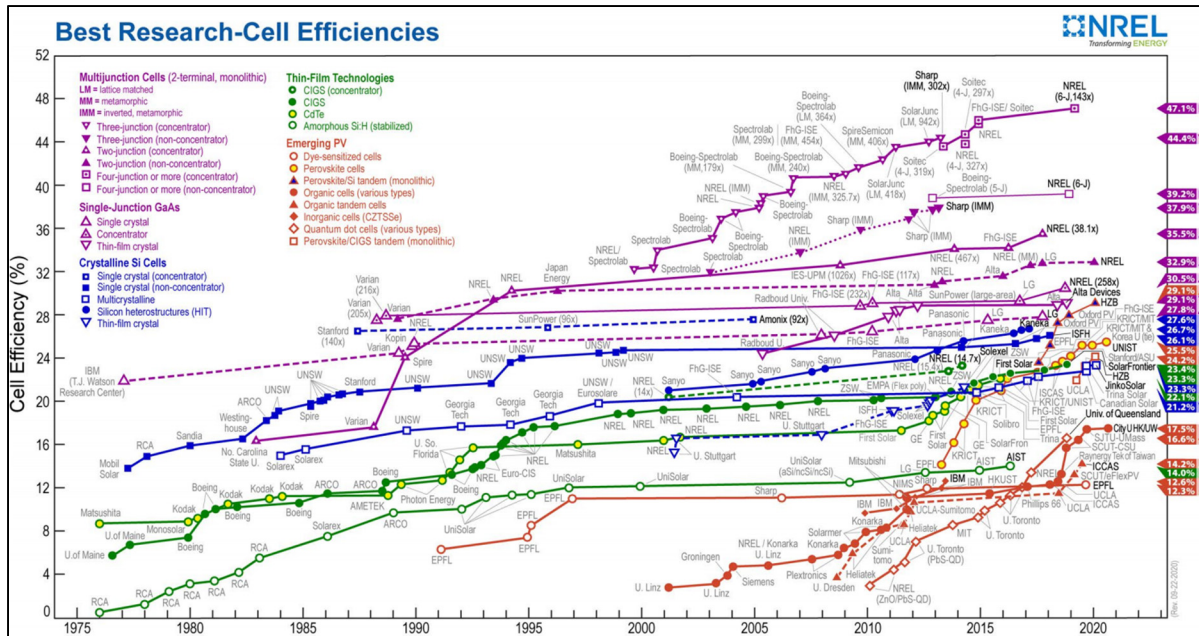
Figure 2.3 Record Solar-Cell Efficiency
Taken from Nrel (2020)

PV research is currently increasingly expanding and diversifying to enhance photovoltaic cell efficiency, content, and cost reduction. At the same time, these advances need modern, more dynamic PV cell characterization instrumentation.

2.3   Solar simulators

Each of the technologies described in the previous section besides all other materials and devices that work with solar powers requires a device to mimic the sun, this device is called a solar simulator. The purpose of the solar simulator is to provide an indoor testing facility for the testing of solar technology under laboratory conditions with artificial light sources, hence

international standard committees provide a series of guidelines for specify the requirement for better performance and classify the solar simulators.

2.3.1 Modes of operation

Solar simulators can be divided into three main types in terms of mode of operation: Continuous, Flash, and Pulse. The biggest distinction is between pulsed and continuous simulators. Pulsed solar simulators produce a light pulse of much less than one-second length, whereas continuous solar simulators have steady light for several hours (Kalogirou, 2014a). Continuous solar simulators are mostly used for the electrical characterization of solar cells and low-intensity testing, ranging from below one sun to several suns (Kalogirou, 2014b). Flash solar simulators are ideal for PV cells and panel testing. Assessment with this solar simulator is immediate and lasts nearly as long as a shutter flash (several milliseconds). Up to several thousand suns are possible with this type of solar simulator. In pulsed solar simulators, solar cells are not heated during the test and special techniques are required to quantify slow response cells (Lisbona, 2013).

2.3.2 Solar simulators classification standards

Three different international institutes provide standards to quantifying the performance of solar simulators: the International Electrotechnical Commission (IEC) 60904-9 Edition 2 (2007) Photovoltaic Devices – Part 9: Solar Simulator Performance Requirements; the Japanese Industrial Standards (JIS) C 8912-1998, Solar Simulators for Crystalline Solar Cells and Modules; and the ASTM E 927-05 (2005) Specification for Solar Simulation for Terrestrial PV Testing (Manke, 2010). In all these three standards the method of characterization of a solar simulator is defined in three classes (A, B, or C) for spectral match, spatial non-uniformity, and Temporal instability.

The tables below illustrated the criteria for each of these three standards. Notice that although expectations are broadly identical, the main variations remain. IEC offers short- and long-term

instability (STI and LTI respectively) whereas ASTM differentiates simulator classifications for different illumination areas and JIS demands lower Temporal instability for Class A than the ASTM and IEC.

Table 2.1 ASTM Solar Simulator Class Specifications

Classification	Spectral Match (each interval)	Irradiance Spatial Non-Uniformity	Temporal Instability
Class A	0.75-1.25	2%	2%
Class B	0.6-1.4	5%	5%
Class C	0.4-2.0	10%	10%

Table 2.2 IEC Solar Simulator Class Specifications

Classification	Spectral Match (each interval)	Irradiance Spatial Non-Uniformity	Short-term Temporal Instability	Long-term Temporal Instability
Class A	0.75-1.25	2%	0.5%	2%
Class B	0.6-1.4	5%	2%	5%
Class C	0.4-2.0	10%	10%	10%

Table 2.3 JIS Solar Simulator Class Specifications

Classification	Spectral Match (each interval)	Irradiance Spatial Non-Uniformity	Temporal Instability
Class A	0.75-1.25	2%	1%
Class B	0.6-1.4	3%	3%
Class C	0.4-2.0	10%	10%

2.3.3   Spectral match

As the light of the sun passes through the atmosphere, its power is reduced by air and dust. Air Mass (AM) quantifies this reduction. Air mass is a coefficient that defines the optical path length which light takes through the earth's atmosphere, normalized to the shortest possible path, that is the overhead sun:

$$Air\ Mass = \frac{1}{\cos\theta} \qquad (2.1)$$

Θ is the angle of the light path from the vertical which is known as the zenith angle. So, when the sun is directly overhead and sunlight has the shortest possible path AM is 1 (AM1). AM0 is the irradiance outside of the Earth's atmosphere (zero atmospheres), and AM1.5 corresponds to a standard at a zenith angle of 48.19°. Figure 2.4 illustrate AM1 and AM1.5 condition.

The spectrum of the sun varies on location and time on the earth, but standard committees provided three spectra standards as a reference which could be used to match the irradiance spectrum of solar simulators. Extraterrestrial, terrestrial direct, and terrestrial global solar irradiance spectra conditions named AM0, AM1.5D, and AM1.5G, respectively (*Designation: E490 − 00a Standard Solar Constant and Zero Air Mass Solar Spectral Irradiance Tables 1*, n.d.).
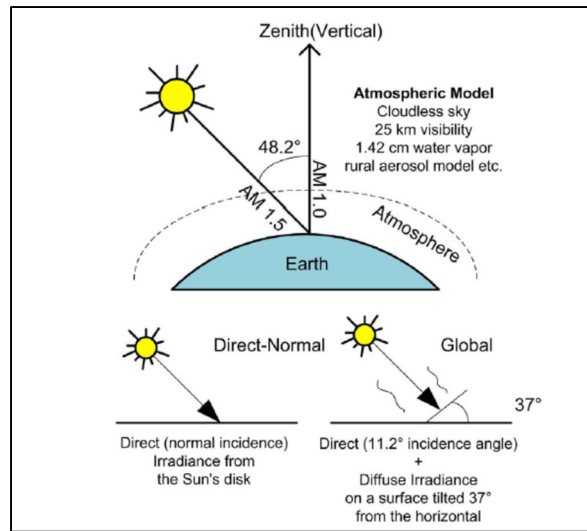
Figure 2.4 Schematic of AM1.5 reference spectral condition
Taken from Esen et al. (2017, p. 1241)

Figure 2.5 shows two different air masses compare to the black body radiation source at $5250^{\circ C}$ modeled in black. The yellow curve represents the AM0 which rises at about 250 nm and extends beyond 2500 nm, while the spectrum in red defines AM1.5D which is measured at the earth's surface (sea level). AM1.5G has more energy than direct (AM1.5D) and it is because of extra diffuse radiation. AM1.5 was used to characterize and standardize PV cells testing with one sun irradiance of 1000 W/m^2.
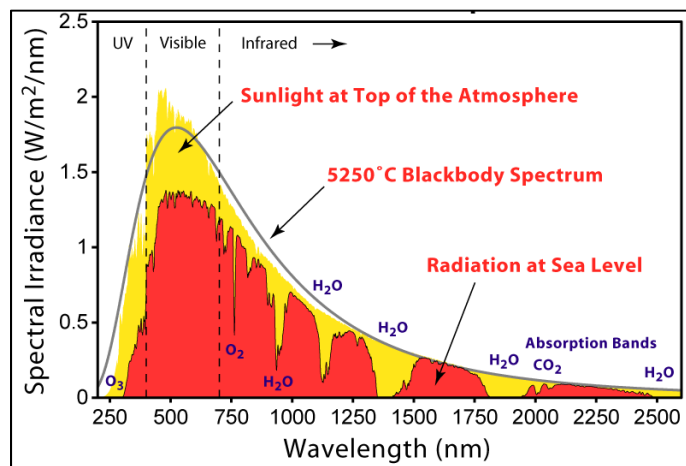
Figure 2.5 Solar Radiation Spectrum
Taken from Wikimedia (2020)

Spectral match refers to the distribution of intensity across the wavelength emission spectrum of the solar simulator. Solar simulator spectrum is compared to the reference spectrum by calculating irradiance spread as a percentage of overall irradiance across specific standard-defined wavebands. The spectral match test for a solar simulator measures the simulator output spectrum and compared it to the reference spectrum is by measuring the distribution of irradiance as a percentage of the total irradiance across specific wavebands defined by the standard. Table 2.4 shows the irradiance requirements defined by ASTM.

Table 2.4 ASTM Spectral Distribution of Irradiance Performance Requirements
Standard reference spectra
Adapted from ASTM E927-05 (2005, p. 3)

Wavelength Interval [nm]	AM1.5D	AM1.5G	AM0
300–400	no spec	no spec	8.0%
400–500	16.9%	18.4%	16.4%
500–600	19.7%	19.9%	16.3%
600–700	18.5%	18.4%	13.9%
700–800	15.2%	14.9%	11.2%
800–900	12.9%	12.5%	9.0%
900–1100	16.8%	15.9%	13.1%
1100–1400	no spec	no spec	12.2%

As specified in Table 2.4 and based on ASTM standard (Table 2.1), spectrum comparison with each solar spectrum interval shall indicate the spectral match classification as per the following:

Class A: Spectral match within 0.75-1.25 for each wavelength interval

Class B: Spectral match within 0.60-1.40 for each wavelength interval

Class C: Spectral match within 0.40-2.00 for each wavelength interval

2.3.4 Spatial non-uniformity

The other specification of solar simulators is irradiance inhomogeneity on the selected test area. Spatial non-uniformity refers to the degree of inconsistency as one moves along the length and width of the entire test region at an instant in time. To grade the solar simulator in terms of spatial uniformity, the test area should divide into a grid of measurement positions using equation 2.2 to determine the non-uniformity across the entire test area in comparison with tables 2.1 to 2.3.

$$Non-uniformity\ (\%) = \left[\frac{Max\ irradiance - Min\ irradiance}{Max\ irradiance + Min\ irradiance}\right] \times 100\ \% \qquad (2.2)$$

The number of measuring depends upon the size of the selected test area and used standard. ASTM divide the defined test area into at least 36 equally sized (by area) test positions (ASTM-E927-05, 2005) while IEC considered 64 equally sized test blocks as a minimum test position (IEC 60904-9, 2006) and the JIS proposed a lower sample measurement grids about 17 positions (JIS C 8912, 1998).

In all three standards, the +/- 2 percent gauge is the same, hence the method of measuring and grade the proper class is different.

2.3.5 Temporal instability

The next criterion for solar simulator characterization is Temporal instability; this is defined by two parameters: short-term instability (STI), long-term instability (LTI). STI relates to the data sampling time of a data set during an I-V measurement and may be different between data sets. LTI is related to the time period of interest. In all standards, the general approach for calculating temporal instability is the measuring over a given time span of irradiation of the solar simulator beam and calculate the instability with this equation:

$$Temporal\ instability\ (\%) = \left[\frac{E\ Max - E\ Min}{E\ Max + E\ Min}\right] \times 100\ \% \qquad (2.3)$$

Where E is the irradiance of the light source and the maximum and minimum irradiance depend on the application of the solar simulator. If the solar simulator is used for endurance irradiation tests, temporal instability is defined by the maximum and minimum irradiance measured with a detector at any point on the test plane during the time of exposure.

CHAPTER 3

METHODOLOGY

3.1   Introduction

The methods for the design and installation of the solar simulator are discussed in this chapter. The aim is to design a 30cm x 30cm measurement area device with a high flux LED-based light engine. Data collection methods, components, and materials which utilized, and other steps were taken to fabricate the LED-Based solar simulator will be explained in more depth here. The solar simulator proposed in this work is fabricated with off-shelf components where has been accurately selected and considered.

Figure 3.1 demonstrates the flow chart of the methodology which is chosen for this project. As seen in this flow chart there are four key steps: planning, design, implementation, and analysis.

Figure 3.1 Methodology Flow Chart

Each of these steps has some subsections which will discuss below.

3.2   Planning

The project approach requires preparation and planning process since it eliminates any future obstacles and risks. Planning also can make the project more cost-effective and more efficient. In this project planning phase based on the optical part the solar simulator cover LEDs, Drivers, Lenses, reflectors, and the structure. In the following paragraphs, further discussion of these issues is given.

3.2.1   Data Collection

A literature review is the first component of the data collection, which has been conducted using secondary sources to obtain information on the topic of study. Scientific journals on the related topic like LEDs Magazine, IEEE Solar Journal, Journal of Solar Panels, Journal of Renewable Energy, etc. are some examples of these secondary sources. Beyond literature review which has the evaluation of past designs, testing, failures, and successes an assessment on various related hardware were performed.

3.2.2   Hardware Requirements

Following a comprehensive literature analysis, informed decisions on the hardware specifications for the solar simulator were taken. The main goal among all parts of a solar simulator in this project is to design and fabricate a high-power LED-based light engine for solar simulators. To fabricate a light engine even it is for a general lighting purpose or for a specific illumination like simulating a sun in a targeted test area three important parts should be considered as depicted in figure 3.2. Housing system (HS), Electrical system (ES), and Optical system (OS). Each main part has its subpart. The housing system includes structure and heatsinks plus materials for isolating, Optical system includes light sources like LEDs, lenses, reflectors, and if needed diffusers, etc. Finally, the Electrical system involves drivers and controls beside all wiring and electrical connections. These parts of each hardware system are presented below.
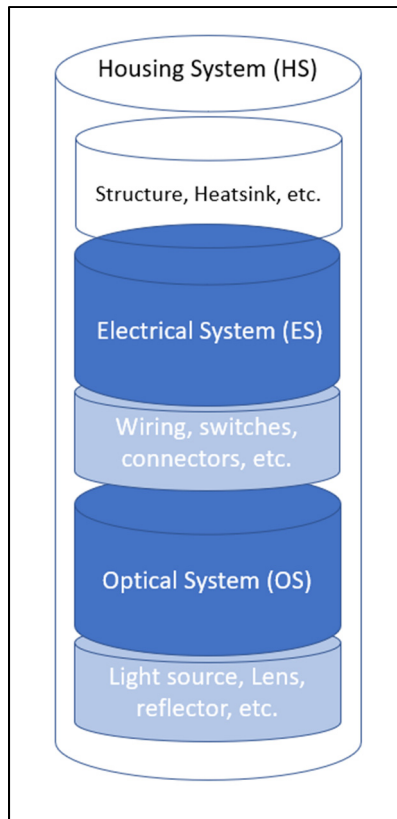
Figure 3.2 Three main parts of the solar simulator light engine - HS, ES, OS

1) LEDs and Selection

When solar radiation infiltrates the earth's atmosphere only a portion of sunlight reaches the earth's surface. Figure 3.3 shows the wavelength distribution of solar light at the outside of the atmosphere and the sea level. 52 to 55 percent of whole solar energy is infrared (above 700 nm), 42 to 43 percent visible (400 to 700 nm), while only 3 to 5 percent is ultraviolet (below 400 nm). As indicated in the literature review chapter, numbers of solar simulator designs use LEDs for the visible portion of the light, mentioned that UV and IR parts of the wavelength are not absorbed by P-type and n-type semiconductors (Kim et al., 2014), (Reynolds, 2015), thus researcher contented using visible wavelength ranges of available LEDs, however few of them use some halogen lamps to cover these two ranges.
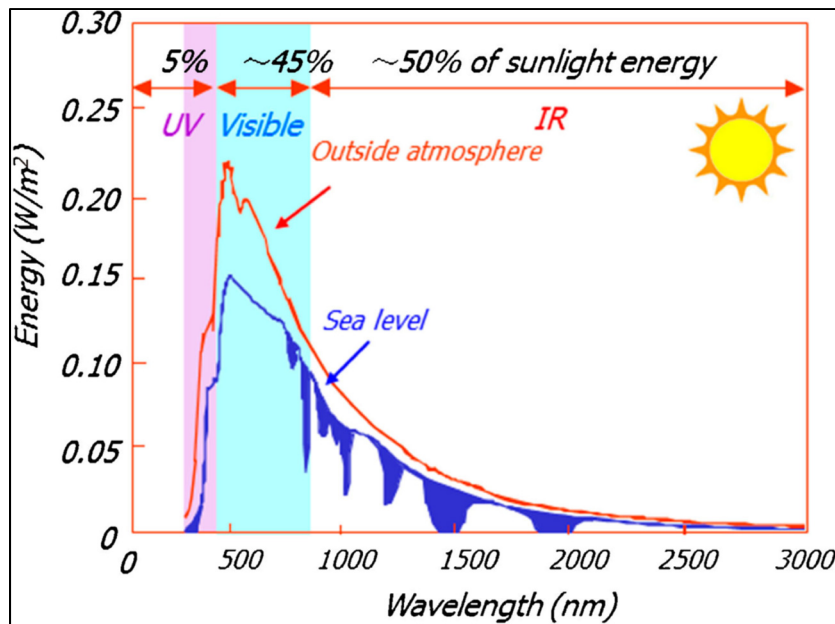
Figure 3.3 Distribution of solar light
Taken from Yin (2015, p. 823)

The first approach for fabricating a LED-based light engine was using the SMDs. Variety in wavelength production lines and easier implementation especially in terms of cooling the chips were good enough to conduct research on them for forming a light engine. Based on research and communication with manufacturers, and project supervisor requests which is a high lumen output light engine this approach terminated, and research on high power LEDs began.

As described in 1.1.1.6 light-emitting diodes have various packages and the kind of packaging represents their limitation of power. With new design and technology manufacturers of COB LEDs could install more chips on the same board thus we have more power in one piece. Since the world's first COB development and launched by CITIZEN Electronic Co. (*History | CITIZEN ELECTRONICS CO.,LTD.*, n.d.) this technology improved dramatically, and in the time that this project is done there are various LED COBs in almost all ranges of wavelengths. As considered a high lumen output LED usage our research resulted in some high-power LEDs as listed in Table 3.1, however, the lake of off-shelf COB LEDs in UV ranges ended up with this decision.

Table 3.1 COB LEDs specifications

Item	Power (Watt)	Wavelength (nm)	Chip brand	Voltage (V)	Current (mA)
1	500 – 600	440 – 780 *	YUJILEDS	35 - 42	12000-15000
2	100	850	Epistar	16 - 18	3500
3	100	940	Epistar	14 - 16	3500
4	100	390	OUMURUI	32 - 35	3500

*With correlated color temperature (CCT) of 5600K and Color rendering index (CRI) of 95 they covered a full visible spectrum near the sun.

Figure 3.4 shows the physical layout of operational COBs were chosen to use in the light engine with their dimensions in the caption. These high-power COBs have to install on proper heatsinks to prevent thermal damages.

(A) (B) (C)
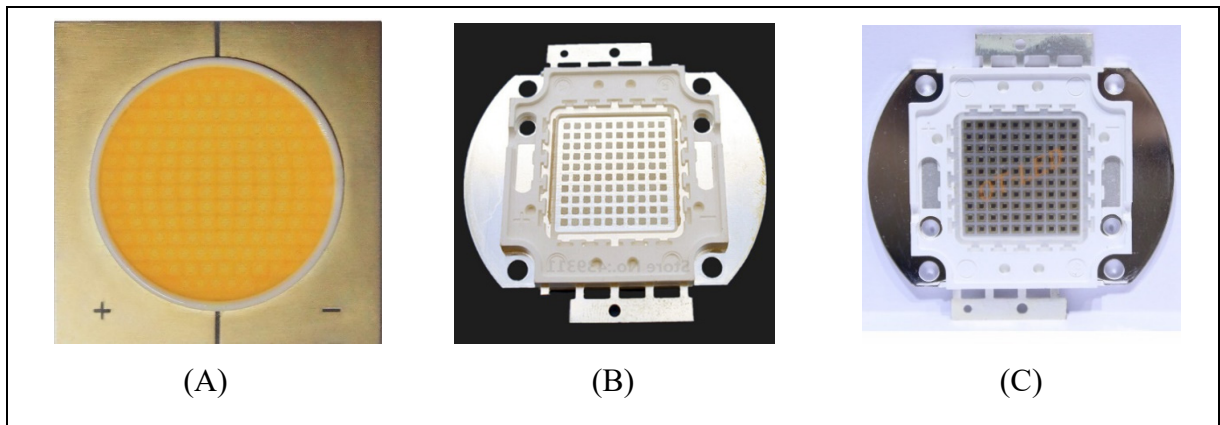
Figure 3.4 (A) 500W COB 27mmx27mmx0.5mm (B) 100W IR COB 45mmx45mm (C) 100W UV COB 45mmx45mm COB

In the time that this project was conducted two ranges of IR high-power COBs and one range of UV high-power COB were available off-the-shelf and used as stated in Table 3.1.

Table 3.2 summarized the information about standard wavelengths which solar cells received based on NREL and ASTM standards in comparison to available high-power COBs that were chosen and used in this solar simulator. Based on this table which clearly shows the standard

wavelength of the solar spectrum in three regions, used COBs covered most of the effective light wavelength ranges to simulate the solar wavelength.

Table 3.2 On earth solar radiation in comparison to used COB

Type of light	Wavelength range	Percentage of sunlight	COB's wavelength used
Ultraviolet	10 – 400 nm	3 – 5 %	390 nm
Visible light	400 – 700 nm	42 – 43 %	440 – 780 nm
Infrared	700 – 1,000,000 nm	52 – 55 %	850 nm, 940 nm

2) LEDs Driver

In LED technology, drivers could be a frustrating part. There are so many various forms and combinations that may also feel confusing. An LED driver is an electrical device that regulates power to an LED or a string of LEDs. It is vital to an LED circuit, and working without it would result in device failure as the forward voltage (V_f) of a high-power LED changes with temperature. If the temperature rises, the LED's forward voltage falls, allowing the LED to pull more current. Choosing a good quality LED driver to prevent thermal runaway as the constant current LED driver makes up for shifts in forwarding voltage when supplying constant LED current.

One of the best options for driving a high-power LED was MEANWELL Enterprises Co. Dual constant current and constant voltage mode metal housing drivers with over 50000 hours of a lifetime and more than 5 years warranty bring them at the top of driver chose. Thanks to the high efficiency of up to 96%, with the fan-less design, the entire selected series is able to

operate for -40$^{\circ C}$ to +90$^{\circ C}$ case temperature under free air convection. Table 3.3 define the specification of 2 chosen driver for COBs.

Table 3.3 Standard Constant Current LED Power Drivers

Item	Model	Power (Watt)	Output Voltage (VDC)	Output Current (A)
1	HLG-600H-42A	600	42	14.3
2	ELG-150-42A-3Y	150	42	3.57

The schematic of the LED drivers is seen in Figure 3.5, for more specifications and features of these products refer to Appendix I.

(A) (B)

Figure 3.5 High-power used drivers (A) HLG-600H (B) ELG-150
Taken from Meanwell

3) Reflectors

In this project, the light concentrator was designed and constructed to ensure parallel rays reached to desired lenses and prevent light tress pass to unwanted surfaces. Hence, a rectangular reflector box was considered as a light cone for this purpose. There are a lot of materials which are suitable for this purpose as a former experience like Aluminum anodized

with almost 98% reflection factor and white papers with high reflection index, to enhance the project in a short time an off-shelf high-quality reflector used in this project. The length of the reflector box was chosen 60cm and due to the simulation illustrated in figure 3.6, the uniformity underneath reached almost 0.92 to 0.96.
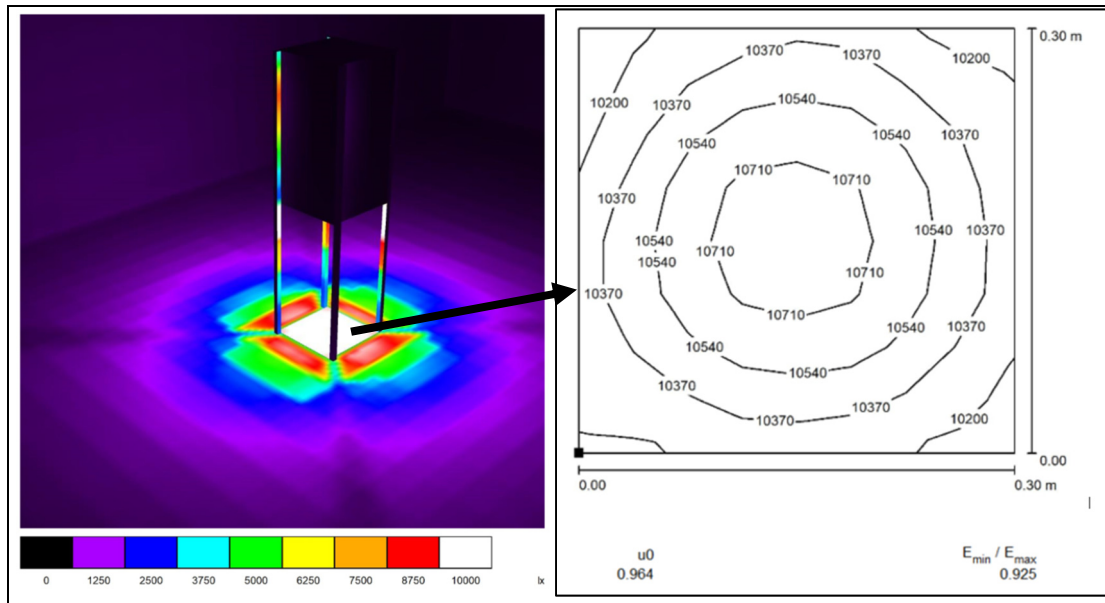
Figure 3.6 Reflector box simulation and reported uniformity calculation

4) Lenses

Clear plastic acrylic material especially PMMA plastic Fresnel lenses are the best choice for integrated with a large area reflector box and finalize the light engine. For this design, two flat linear Fresnel lenses with positive focal length are desired to focus the output lights of LEDs into the test area. The focal length of selected lenses is in front of the pitches which means that parallel rays will concentrate when goes through a positive focal length in the pitch side of the lens. There is no more information about the exact material specification and PMMA airmass used in the production line, from the manufacturer. This kind of Fresnel lens is usually used for solar energy collection applications.

Due to this fact, three arrangements of lenses were proposed and simulated to use on the fabricated solar simulator:

1- **PD:** One lens with the pitch oriented downward

2- **PD-PERP-PD:** Two lenses on top of each other with downward pitches perpendicular to each other

3- **PU-PAR-PD:** Two lenses on top of each other while pitches of the one on the top are toward up and pitches of below lens are downward.

These configurations of two lenses and one lens demonstrate in Figure 3.7.
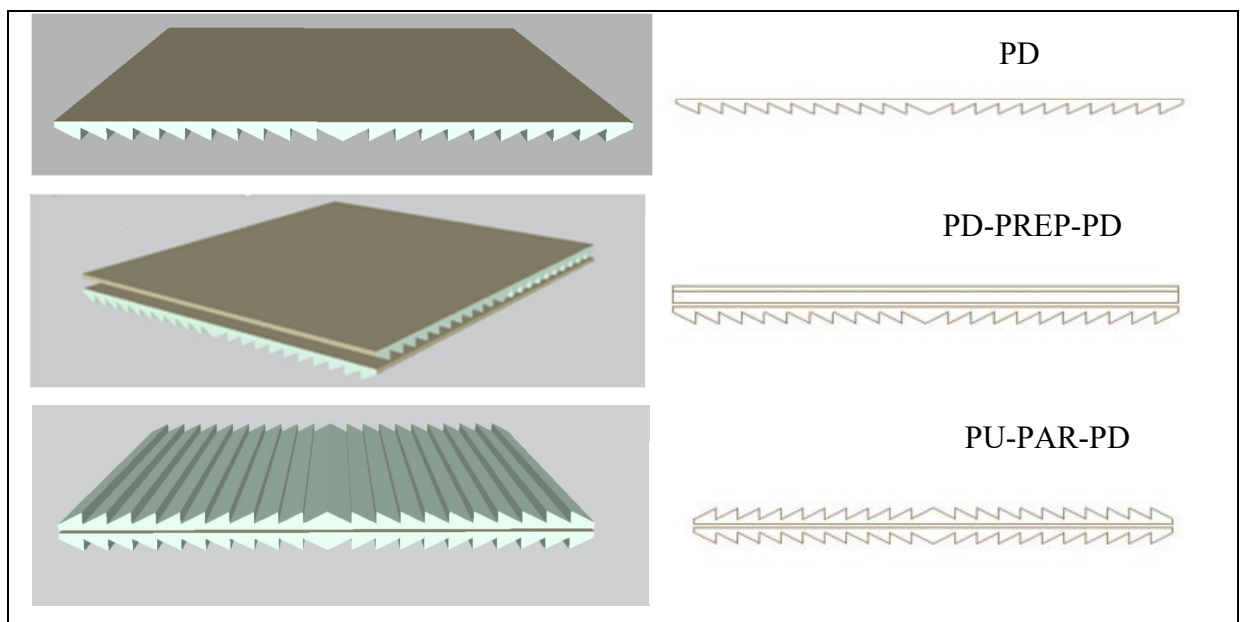
Figure 3.7 3D simulation for 3 different configurations of Fresnel lenses

The first configuration (PD) acts like a normally expected lens to concentrate the parallel so-called artificial sun to the focal area that would be a line here. The second configuration (PD-PERP-PD) desired to concentrate all direction rays to a high-intensity square on target. And the third Configuration (PU-PAR-PD) is set with this default that there are more non-parallel rays in the reflector box and made them parallel for the second lens. Finally, Figure 3.8 shows the simulation of PD-PREP-PD configuration which results in a high-intensity square on the test plane. Each of these three configurations of lenses has it is own output pattern and will report in the result chapter.
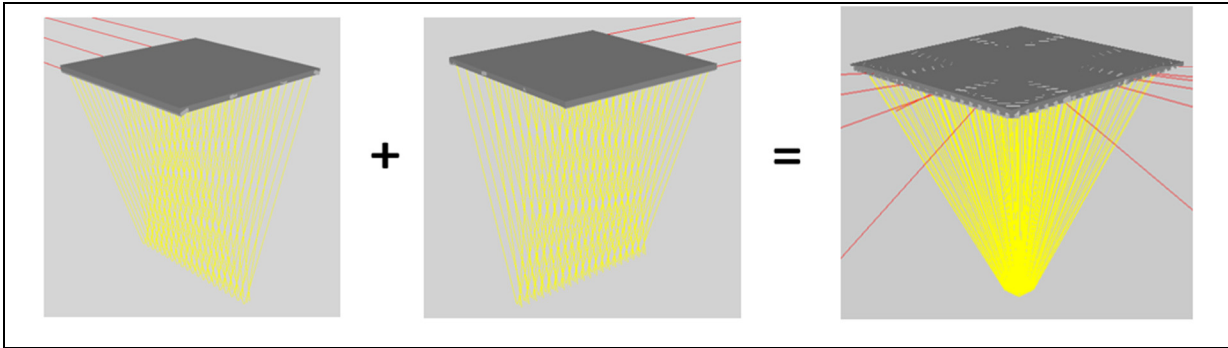
Figure 3.8 Simulation of double linear Fresnel lens arrangement (PD-PREP-PD)

3.3   Design and Implementation

The implementation is the next important step in methodology. The purpose of this phase of the project is to layout the entire project, to check the design and the equipment, and to tune the design. Firstly, the designed structure brings the ability to adjust and replace any part of the fabricated light engine in any step e.g., changing the lens arrangement and adjust the test plane height. Then, as mentioned before the main purpose of this project is to design and demonstrate the ability of High-power COB LEDs and fabricate a light engine for the solar simulator, thus there is no complicated electrical circuit for the electrical system of this lighting engine. This part could be part of future research work and recommended toward developing a controllable high-power LED-based solar simulator. However, highly accurate LED installation was considered to save the LED's life as much as possible. The schematic illustration of the LED solar simulator is shown in Figure 3.12. Each main part of the device will describe in the next sections.
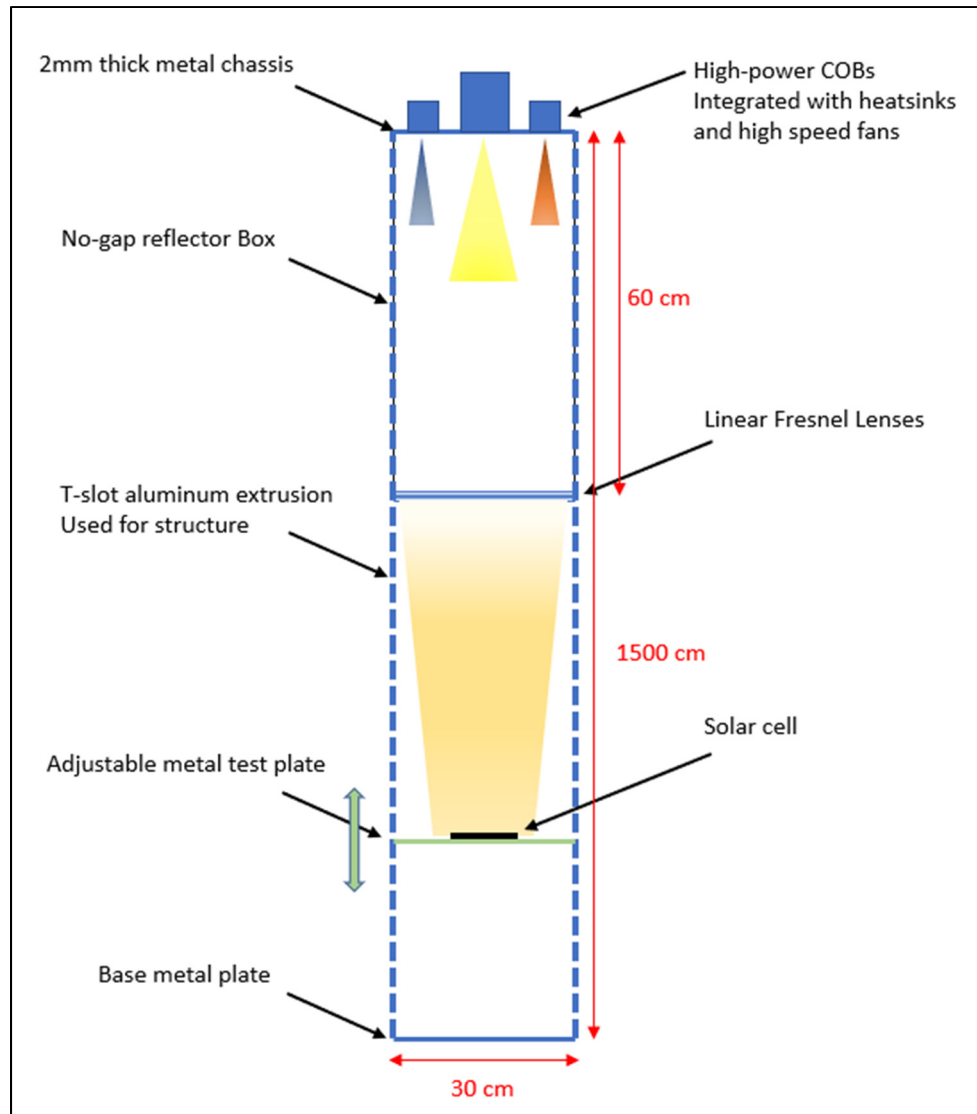
Figure 3.9 Schematic of the fabricated LED solar simulator

3.3.1 Structure and reflector box

In the final design process, the lighting box structure was designed to be modular and adjustable. One of the important prospects was to create a structure with no dark spot in the reflector box. Figure 3.13 illustrates a plan view of aluminum rods used to eliminate the gaps and Figure 3.14 shows a photo of inside the fabricated lightbox.
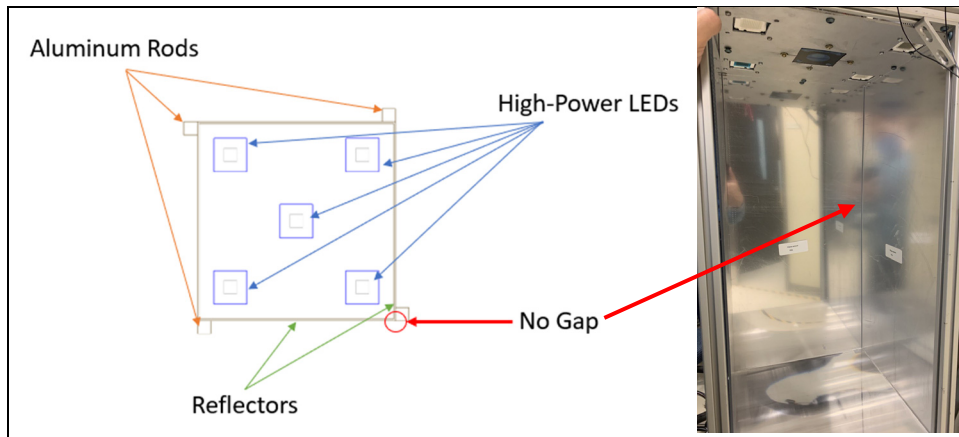
Figure 3.10 Inside lightbox with no gaps between reflectors

This reflector box could be considered as a light concentrator that conducts parallel light rays to Fresnel lenses and increases the reflection of lights with a dimension of 30cm × 30cm with 60cm height. To arrange a mixed light output of these 4 types of COBs asymmetric distribution is proposed.
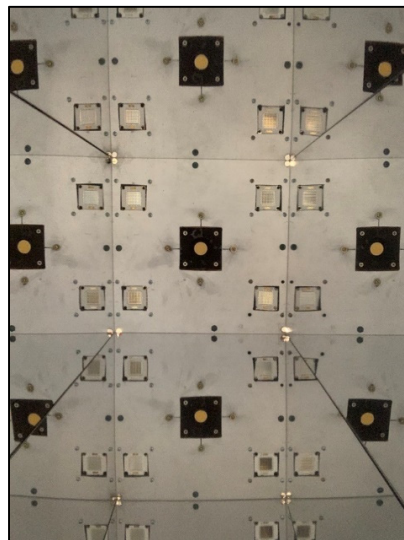
Figure 3.11 Upside-down inside reflector box showing no gap in corners between reflectors

3.3.2   COBs and Heatsinks

Heat sinks are used on LEDs with high heat dissipation capability due to the extreme heat produced by LEDs. The heat sink is circulating in the passive or active air to cool it. Too much heat can damage LED phosphor, resulting in low light output, changes in color, and decreasing life. To avoid these thermal issues, we used two different types of active heatsinks as showed in Figure 3.15. For installing COBs on the mentioned heatsinks sufficient thermal paste was used between COBs and heatsinks and thermal resistance fisher papers to isolate the COBs from metal installation plate to prevent presumptive short circuits.

(A)   (B)
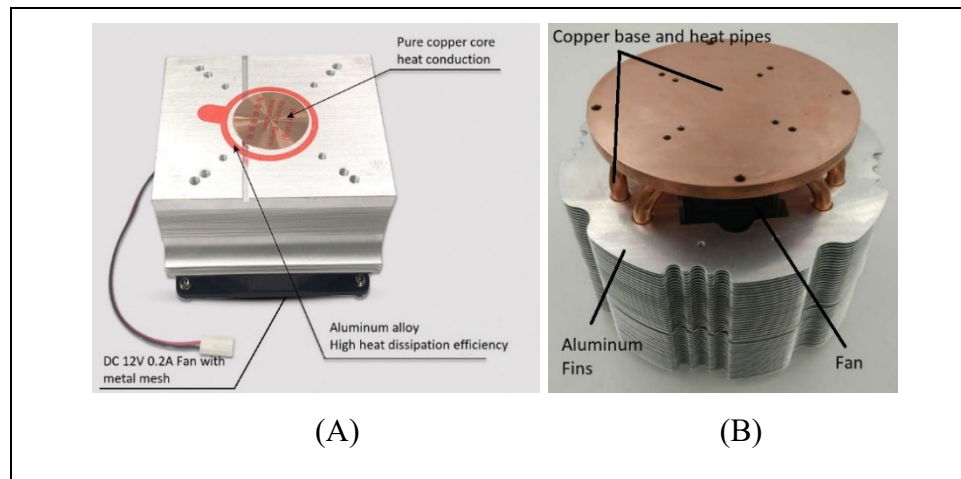
Figure 3.12 Two types of used heatsinks (A) Active Copper core heatsink
(B) Copper base Active heatsink with heat pipes

All COBs are installed on proper heatsinks with adequate thermal past to protect them against thermal damages then they are installed on a 2mm thick metal sheet to bear the weight of all LEDs and their heatsinks. Heat resistance and non-conductive paper were used between COBs and the metal sheet to prevent electrical shocks. In addition to all these heatsinks and their fan, two extra fans were used to add more safety against thermal damage during a long period of work. All these parts could be seen in Figure 3.16.
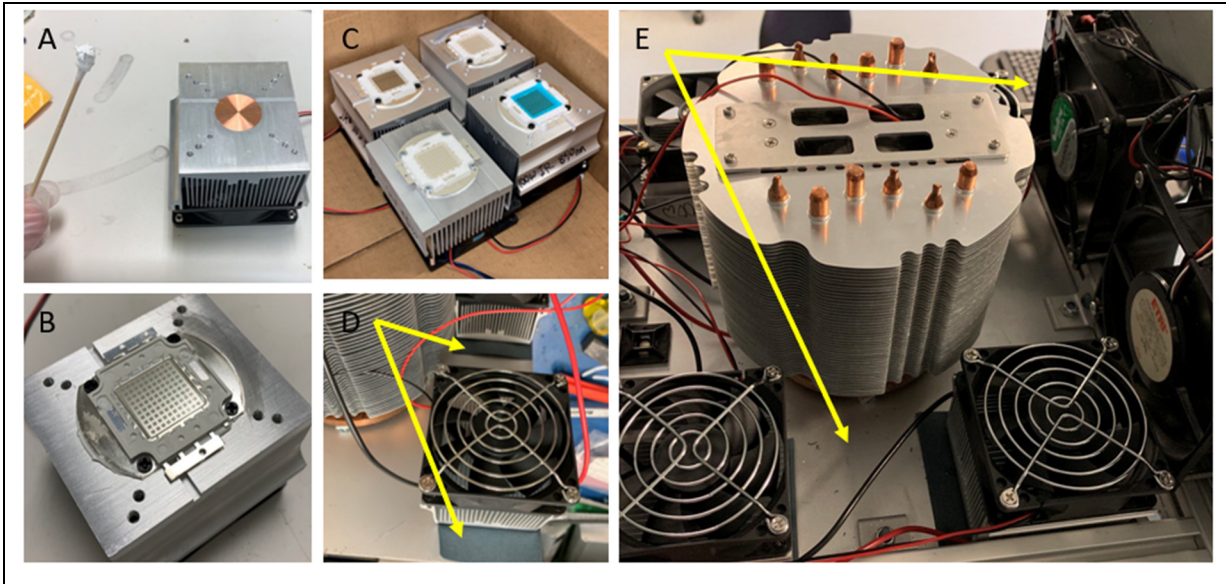
Figure 3.13 COB installation on metal sheet and heat management
(A) Using thermal paste on cooper core aluminum heatsink (B) screwed COB on the heatsink
(C) Prepared COBs installed on heatsinks (D) Fisher papers
(E) Two extra fans and base metal sheet

3.3.3 Control Panel

As described, design a complicated electrical power control is not a part of this project, however as shown in Figure 3.17 different Double Pole Single Throw (DPST) switches were considered to loop in each COB separately with a simultaneous ignition of related heatsink fans.
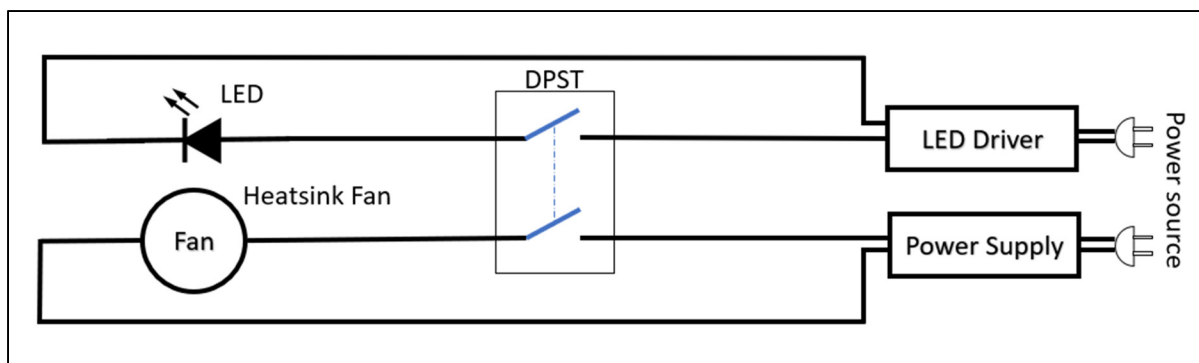
Figure 3.14 Electrical circuit schematic for the simultaneous start of LED and Fan

To cover safety for solar simulator users two indicator lamps were used for two UV LEDs to show when they are on/off. Figure 3.18 illustrates the final control panel of the solar simulator.

Figure 3.15 Control panel for LEDs and Heatsinks Fans

3.4 Light output measurement

The measuring of output light was conducted with 3 different devices described below. Each device has its own specification and output. The tools and software are provided by *École de Technologie Supérieure* (ETS) university of Quebec in Montreal to quantify as accurately as possible the wavelength and intensity of the lights. However, some limitation was noticed for each device in terms of their ability to measure the amount of light level or wavelength of visible light.

3.4.1 Ocean optic High-Resolution Fiber Optic Spectrometers

The HR4000 High-Resolution Miniature Fiber Optic Spectrometer provides optical resolution as good as 0.025 nm. The HR4000 is responsive from 200-1100 nm. The values from the

spectrometer are read by operating software that is installed on a computer. As shown in figure 3.9 the HR4000 Spectrometer connects to a notebook or desktop computer via USB port and draws power from a host computer, this ability eliminating the need for an external power supply.
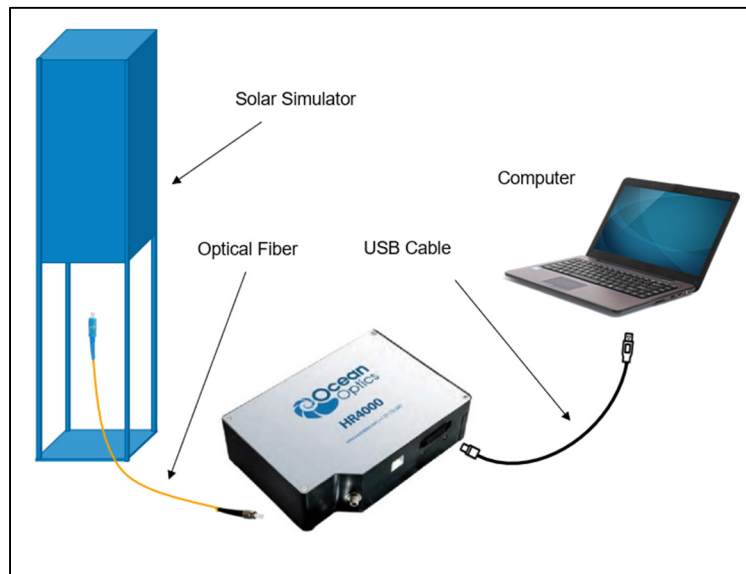
Figure 3.16 Ocean Optics HR4000 High-Resolution Fiber Optic Spectrometer

3.4.2 Photo Research SpectraScan® Spectroradiometer

The other instrument used for spectral measurements was a Photo Research Spectroradiometer Model PR-670 Spectra Scan, which measures radiation from 380 nm to 780 nm in the increment of 2 nm with a bandwidth of 8 nm. This device gives us primary color coordinates to compare with LEDs specifications in datasheets. This device has the ability to store the measuring data and store up to 80000 measurements on a 512 MB SD card. Measurements stored on the SD card can be viewed on the instrument or using the optional SpectraWin® 2 Windows software.

Figure 3.10 illustrates the implementation diagram using the Photo research PR670 SpectraScan device.
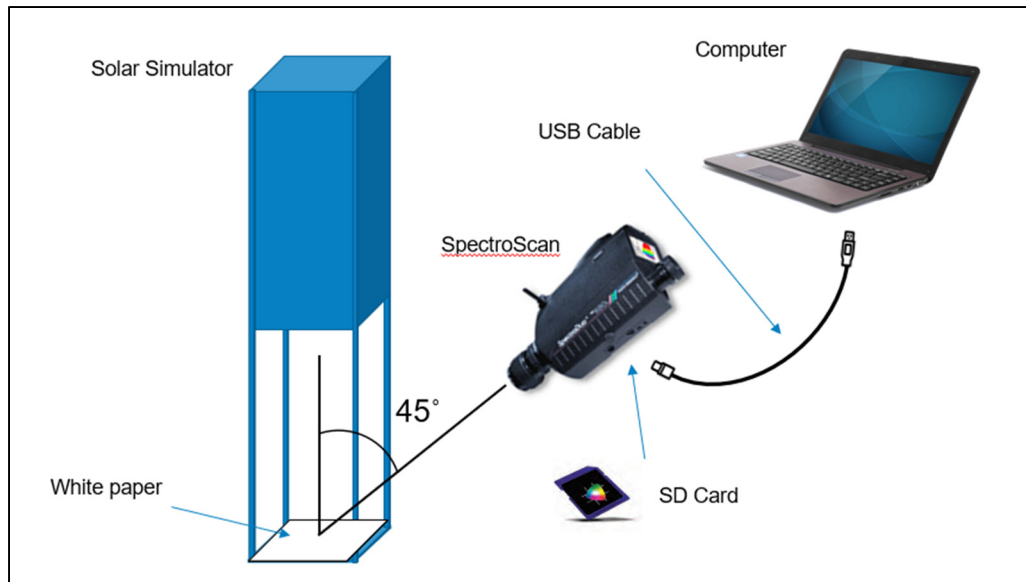
Figure 3.17 Photo Research PR670 spectroradiometer

3.4.3 THORLABS photodiode power optical measurements

A C-Series Photodiode Power Meter Sensor with a handheld digital power meter console of THORLabs© was used to measure the power and energy of the solar simulator output. These series of sensors cover a wide power and wavelength range. The S130C photodiode power meter sensors feature enhanced shielding to avoid electromagnetic interference as well as an over-temperature alert sensor to warn against damage and measurement errors due to overheating of the sensor. This sensor can measure a wavelength between $400 - 1100 \; nm$ from $500 \; pW$ Up to $500 \; mW$ power range. Figure 3.11 shows the power meter console and sensor.

68
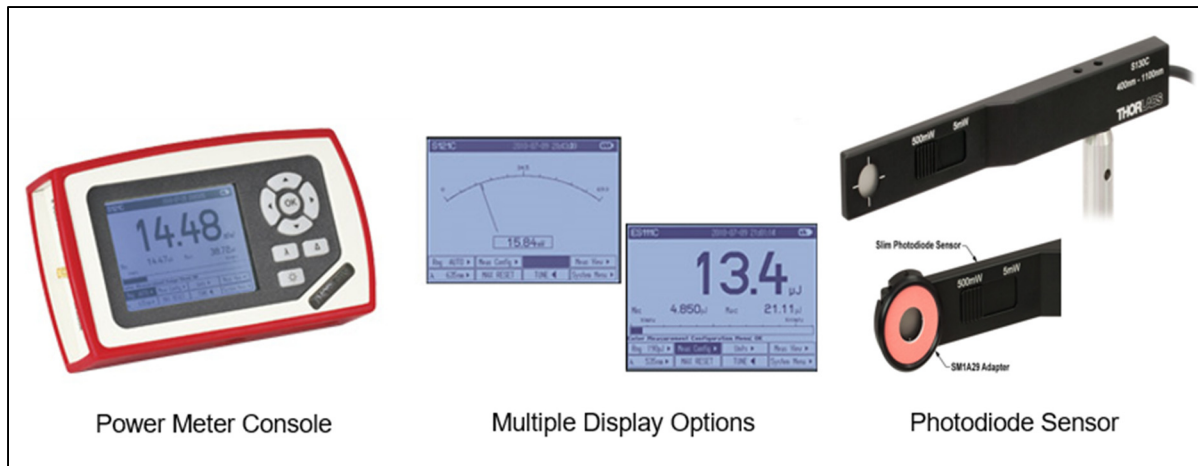
Figure 3.18 THORLABS Power and Energy Meter Console and Sensor
Taken from THORLABS

3.5 Conclusion remarks

All in all, the methodology for any project is an essential phase that could lead to success in the project. Different assessment methodologies could be more applicable, based on the main priorities and constraints in terms of expenditure, time, and other available tools. For fabrication described light engine for the solar simulator in Figure 3.2 methodology divided into four main parts. Planning, which contains data collection and literature review; Design which is based on our goals and former works on related topics, also data collection from different sources aligns with the research topic. Implementation containing hardware requirement and project layout, and in analysis part available tools investigated and used to classified and analyzed the output of the light engine.

CHAPTER 4

RESULTS AND DISCUSSION

4.1   Introduction

This chapter contains a collection of test results of the outlined experiments. The objective is to build a standard Class AAA LED-based solar simulator with a large test area of 30cm x 30cm and a high flux output of more than 5 suns on the illuminated test area. Each letter in this classification represents one feature of the simulator. The first letter stands for Spectral performance, the second letter Uniformity of Irradiance, and the third letter representing Temporal instability. Six tests were applied to classify the solar simulator based on standards: 1) Intensity, 2) Color temperature, 3) Spectral match, 4) Spatial non-uniformity, 5) Temporal instability, and 6) I-V curve measurement. Results of Test 1 show the optical power output of the solar simulator in different lens configurations and indicate in which distance away from lenses achieves the highest light level, Test 2 studied to compare the color temperature of the LED light engine with the sun as proof of chosen COB. Results of Tests 3-5 are compared with the ASTM standards that are depicted in Table 2.1 to characterized the simulator based on the standard. Finally, Test 6 was conducted to indicate the performance of the used light engine via measuring the efficiency of solar cells under the fabricated device in comparison to a standard LED-based solar simulator.

Test 1 - Intensity: Intensity measurements were evaluated with a ThorLab photodiode from the Photonic innovation lab (phi-lab) in École de Technologie Supérieure. The result is shown in graphs as a function of distance from the lenses in different lens configurations. The aim of this test was to find the focal length for different lens configurations then fixing the test plane at a measured distance from lenses for the next tests and studies.

Test 2 - Color temperature: The color temperature of the visible light source was measured with a Photo research SpectraScan as proof of spec sheet specification of the main COB LED.

Test 3 - Spectral match: It is well known that all the energy from the sun that reaches the earth arrives as solar radiation. This radiation is part of a large so-called electromagnetic radiation

spectrum collection which includes visible light, ultraviolet light, infrared, radio waves, X-rays, and gamma rays. Shorter waves move faster and have more energy, and longer waves travel more slowly and have less energy. For instance, visible light or UV light has a shorter wavelength, and has more energy, while infrared with a longer wavelength has less energy. The spectral match test defined the proportional variation in the weighting of the light sources from the global AM1.5G range for different wavelength bands. The spectrum was measured with an Ocean Optic HR4000 spectrometer for each type of light source (broadband and narrow bands) and the results were superimposed on the normalized reference solar AM1.5G irradiance.

Test 4 - Spatial non-uniformity: A spatial non-uniformity evaluation was conducted on two different zones on the test plane. A 30cm x 30cm zone and a smaller 6cm x 6cm zone in the center of the test plane were used. This feature was studied for 3 lens configurations as mentioned in the methodology, and for 2 different distances from the lenses to indicate the best configuration and distance from the lenses.

Test 5 - Temporal instability: The temporal instability test calculated the instability of irradiance at specific points on the test plane during certain time intervals of data acquisition.

Test 6 - I-V curve measurement: I-V curve measurement comparisons for different types of solar cells were performed under the fabricated solar simulator and a standard LED-based solar simulator in UQAM university to determine the efficiency of the built solar simulator. Further explanation of the results is given in the following sections.

There is a limited set of high-power COB wavelengths that exist especially in the invisible range of the spectrum. It is, therefore, a significant prerequisite for a viable combination of the wavelength and a range of LEDs to exist in order to achieve maximum efficiency in a limited budget. Not only are the multiple LEDs important for the precise regulation of device architecture but high-quality Fresnel lenses and reflectors often need to be combined with those light sources to build a light engine for the solar simulator. In addition, if the system was not optimally planned, costs may be overrun by deployment. Furthermore, the proposed approach takes into account the initial costs as well as the lifetime costs.

4.2   Intensity

One of the main goals of this study is to obtain a high-flux solar simulator using high-power cheap-on-board LEDs combined with a reflector box and linear Fresnel lenses to concentrate the output light on the test plane. For the first evaluation of the fabricated device, the intensity was measured using a ThorLab Optical Power and Energy Meter. This measurement was repeated with different lens configurations and variable test plane distances from the lenses to determine the highest intensity output of the different configurations.

Due to the modular design of the device structure, different lens configuration setups could be fixed on the reflector box. In addition, the test plane has the ability to move vertically and adjust the distance from the lenses. As described in Chapter 3, the three lens configurations are: 1) One lens with its pitches aimed downward (PD), 2) Two lenses perpendicular pattern to each other with downward pitches (PD-PERP-PD), 3) Two lenses with parallel pattern while one of them has the pitches aimed upward and the other is downward (PU-PAR-PD). Table 4.1 presents the various lenses configurations and their symbols.

Table 4.1 Lenses configurations and their symbols
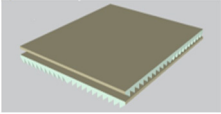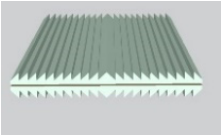
Lenses Configuration	3D simulated view	Symbol
PD		
PD-PERP-PD		
PU-PAR-PD		

Figure 4.1 shows the test setup for PD-PERP-PD lenses configuration. Measurements were done by fixing the photodiode in the center of the test plane.
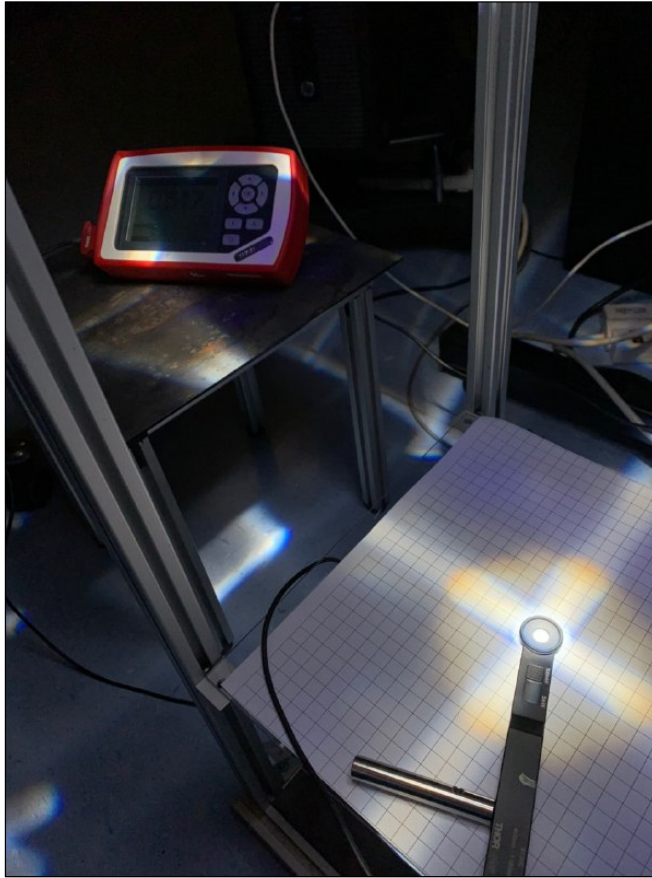
Figure 4.1 Intensity measurement setup

The structure of the device allows the test plane to move from the lenses to a distance of 80cm in the vertical direction. The intensity test in the center of the test plane was performed from a 10cm to 80cm distance from the lenses. Figure 4.2 shows the result of the intensity measurement of solar simulator output light as a function of the distance from the lenses on the test plane for each lens configuration. Since the light output for the PD-PERP-PD lenses configuration is very high the results are shown in a separate graph.
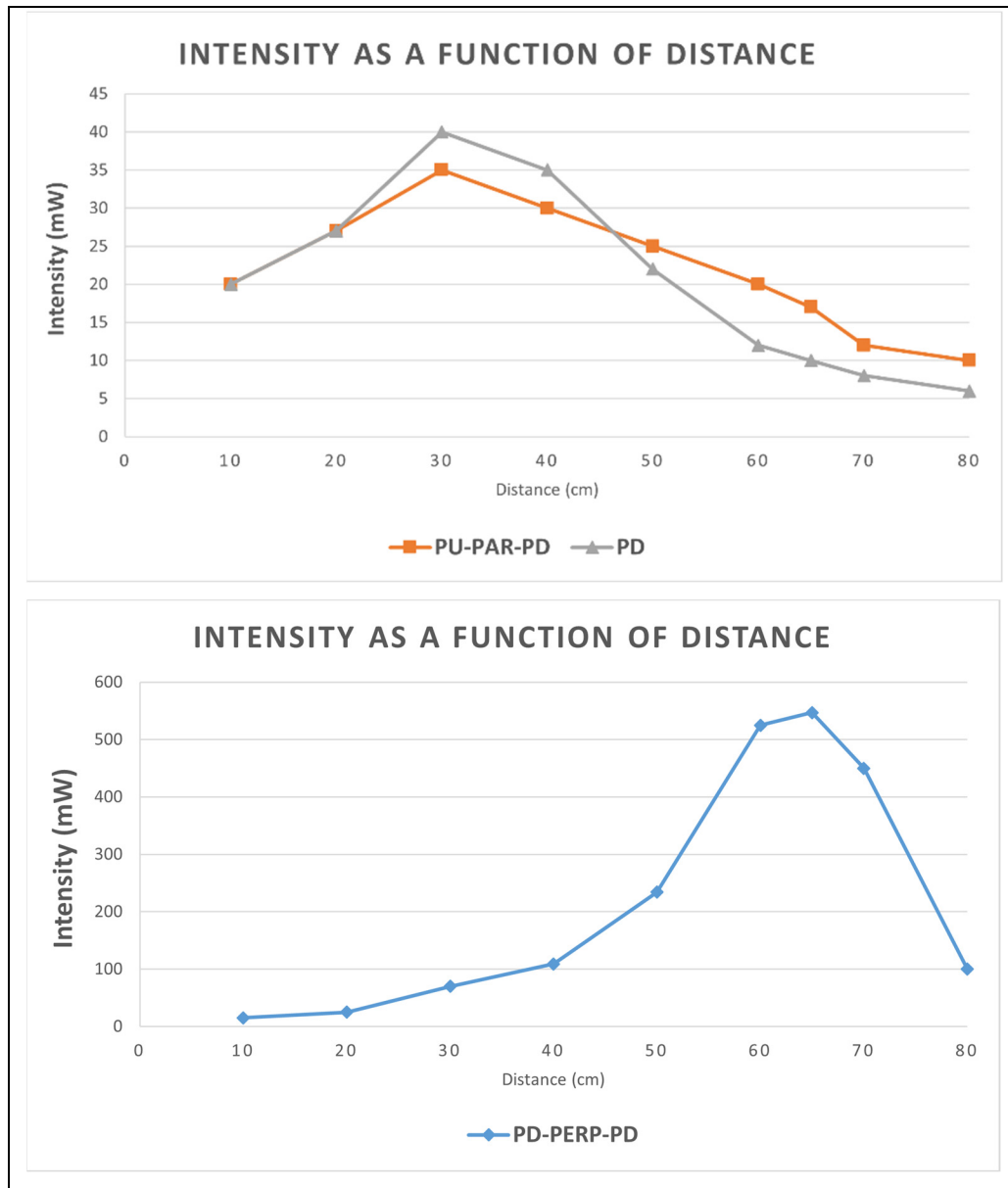
Figure 4.2 Light intensity and Distance from lens

As seen in the results graphs there are two different distances that the light output reached the maximum on the test plane, which indicates the focal lengths of each configuration. Due to the main goal of having a high flux simulator, in each configuration of the lenses, the maximum intensity focal length was chosen to fix the test plane for other experiments. For PD and PU-PAR-PD the focal length is 30cm, and for PD-PERP-PD configuration the focal length is 65cm. The maximum intensity achieved for PD-PERP-PD is 547 milliwatt (mW), which was

measured with a Thorlabs photodiode power meter. To calculate the output light in Sun power it should be converted to 1000 W/m2, which is the irradiance equal to 1 Sun. For this objective, we need to divide the light power value by the sensor's active area which is indicated in the photodiode spec sheet. Equation 4.1 is used to calculate and convert measured intensity to Sun power unit.

$$Sun\ Power\ (1000^{w}/m^{2}) = \frac{\text{Measured value by Power Meter } (mW)}{\text{Photodiode Active Detector Area } (mm^{2})} \times 10^{-2} \qquad (4.1)$$

The outcome of fabricated solar simulator light, which is the measured light powers converted to Sun power based on equation 4.1 and the Detector Area dimension from the spec-sheets of Power meter, is shown in table 4.2.

Table 4.2 Sun Power output of the solar simulator

Lenses Configuration	Symbol	Maximum Light Power (mW)	Calculated Sun Power of solar simulator (Sun)
PD		40	0.4
PD-PERP-PD		547	5.47
PU-PAR-PD		35	0.35

4.3   Color temperature

The effective color temperature of sunlight inside the atmosphere is 5772 Kelvin, as reported by NASA (*Sun Fact Sheet*, 2018). A simulated sun with an artificial light source should therefore have the same light color as the Sun. As proof of concept, the Color temperature

measurement was done with a Photo research Spectra Scan to demonstrate the accuracy of the light source. Unfortunately, the licensed software for the computer was not available at the time that this research was conducted to have the report on file, albeit the result could be read and reported by using a small built-in screen on the device. Figure 4.3 shows a photo of the test setup for this device (A) as well as the screen which demonstrates the output while the lenses were in the PD-PERP-PD configuration and the test plane was at a 65cm distance from the lenses.
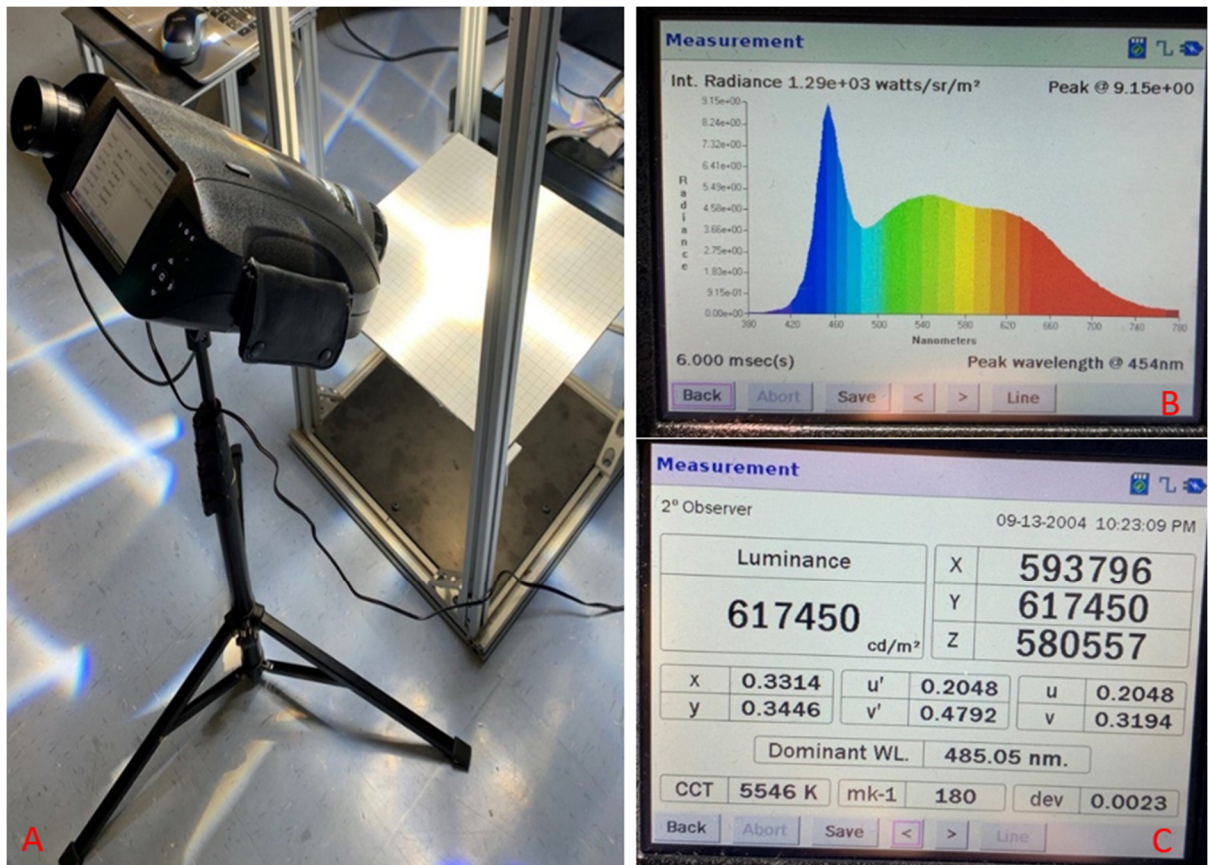
Figure 4.3 A) Photoresearch SpectraScan setup
B) Measured spectrum C) CCT measurement

This measurement displayed the full spectrum of the visible light source and the 5546 Kelvin color temperature which was noted in the used COB specification. The resulted color temperature is near to the effective color temperature of sunlight.

4.4   Spectral match

The very fine variability of the output spectrum was described as a major advantage when using LEDs as the main light source. As described in the LED selection part of Chapter 3, the off-the-shelf high-power COBs have a limited wavelength width, especially in UV and IR ranges. Nevertheless, there are still specific ways to improve these limitations, which can be incorporated into the device as future work. Three different 100W COBs were chosen to cover the UV and IR spectrum region: two UV COB with 390nm wavelength, one IR COB with 850nm, and one IR COB with 940nm wavelength. The main 600W COB covers the full spectrum in the visible range and it is expected that the combination of these COBs will result in a proper light engine spectrum close to the predefined AM1.5G standard spectrum. Hence, the spectral match test was conducted in two steps to measure the spectral mismatch within the wavelength of the fabricated light engine. Figure 4.4 demonstrates the test setup using a High-Resolution Spectrometer (Ocean Optic HR4000) that measures the spectrum length from 200 to 1100 nm. Using a USB cable, the Ocean Optic HR4000 spectrometer is connected to a computer running OceanView software. An optical fiber connected to the Optic HR4000 was used to that transfer the light to the spectrometer.
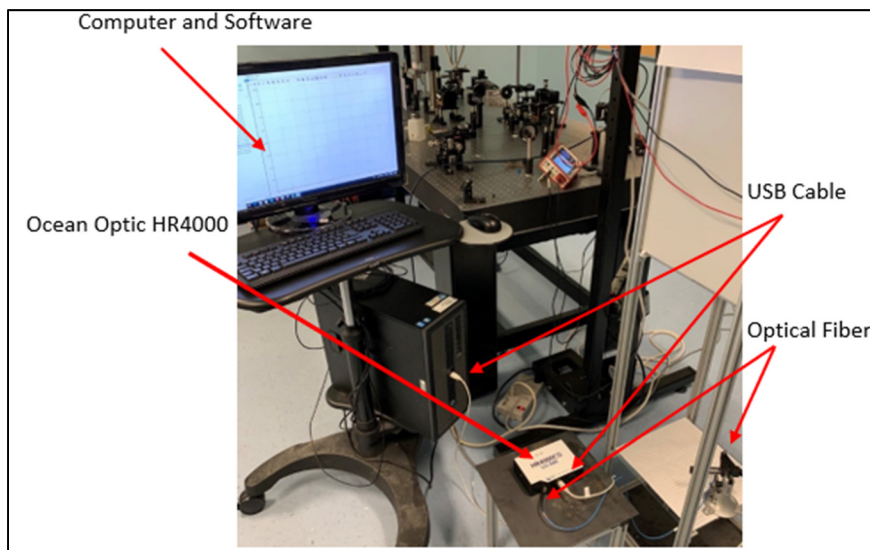
Figure 4.4 Spectrometry setup with Ocean Optic HR4000

In the first step of this test, the spectral irradiance of each COB was measured individually. Figure 4.5 shows the normalized spectral profiles of four different COBs namely: UV light sources, Visible light source, and IR light sources superimposed on the normalized solar AM1.5G irradiance that has been used in our fabricated light engine.
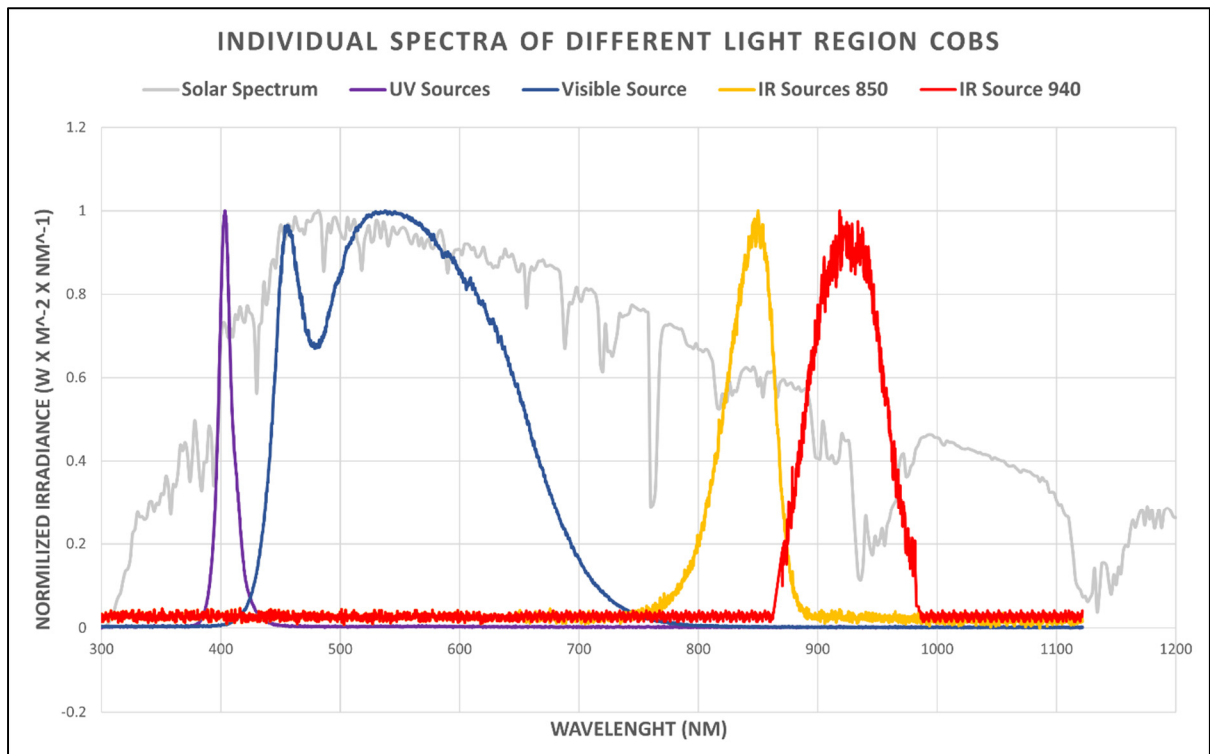
Figure 4.5 Normalized spectra of different COBs

Each COB has its own wavelength characteristics. Due to the spectrum measurement for each COB, it can clearly be seen the UV spectrum (purple graph) has a peak of 403nm which is slightly more than what the manufacturer of the COB said in their catalog. In the visible range between 400 nm to 700 nm, the blue line shows that the main COB obtained full coverage with a peak of 537 nanometers, however between 600nm to 700nm the irradiance dropped in comparison to the standard graph (in gray color) because of the lack of red color in the light source. In the infrared range, the orange line shows the result of the IR850nm COB with a peak

of 849nm and the red line represents the outcome of the IR940nm COB with an irradiance peak at 920nm which is marginally less than the specification in spec sheets.

In the next step, all the COB light sources were switched on and the test was performed again to measure the mixed output light spectrum of all COBs as a single LED-based light engine. Figure 4.6 shows the final normalized spectrum result of the LED-based light engine for the fabricated solar simulator alongside the AM1.5G spectrum defined by ATSM G173 (ASTM, 2013) for comparison.
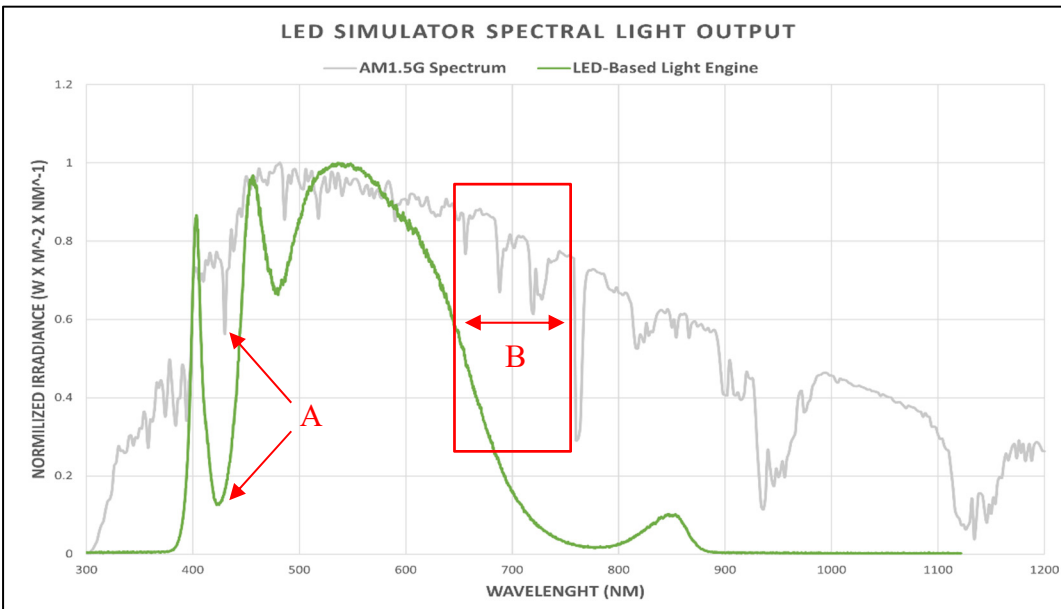
Figure 4.6 LED-Based Simulator Spectral light output

As can be seen, due to the limited spectrum range of COBs, the spectrum does not perfectly match with AM1.5G. However, the advantage of using the high color rendering index (≥ 95) COB in the visible range of the spectrum is that it could almost match the solar spectrum as a class A. Starting with lower spectrum wavelengths of the resulted graph shows a peak at 390nm but right after that, we have a fall that is indicated as "A" in figure 4.6. This drop is following the reference graph but with lower irradiance and lack of blue light in the visible COB spectrum, between 400nm to 430nm. In the B area, there is a dramatic fall in the spectrum irradiance which shows the need for reddish visible light between 630nm to 700nm and more power and spectrum on the IR region (≥ 700nm) of the spectrum. Therefore, if a visible light

with warmer color light and lower Kelvin temperature were added to the light engine, the spectrum would match the reference graph and obtained Class A in the visible region. In the IR region, the lower irradiance of IR COBs and limited spectrum wavelength widths ends up with a depreciation of the AM1.5G reference graph.

As described in Chapter 2, to classify the spectrum of solar simulator each interval indicated in ASTM standard should compare to the intervals in Table 2.4 and the spectrum distribution should meet the limitation for each class of spectral match. Based on that information fabricated solar simulator could not be classified. However, in the visible range of the spectrum, it can be considered as a Class C spectral match, as we have 26, 39, and 26 percent for the first three intervals and they are beyond the limits of Class C. In this simulator as the light engine is easy to access and the COBs are replaceable, adding a lower color temperature COB in the visible range with an IR COB that has more power in the 780nm to 1100nm range could level up the curve in that wavelength band and make it much more similar to the desired AM1.5G spectrum and may yield better outcomes.

4.5   Spatial Non-Uniformity

The next evaluation for the fabricated solar simulator is to measure spatial non-uniformity and specify how uniform the light output is on the test plane. Firstly, based on the standards described in section 2.3.4, the target test area should be divided into 36 equal-size squares. Therefore, the whole area of the test plane with 30cm x 30cm dimensions is divided into 36 equal-size squares and named Zone 1. Secondly, based on visual experiment, since the uniformity is shown to have a better pattern in the center of the test plane, we decided to subdivide the center of the test plane to an area named Zone 2 with 6cm x 6cm dimensions and mark 36 equal-size squares in this area for to test the intensity and calculate the uniformity in this area as well. This division's grid of test areas can be seen in Figure 4.7.
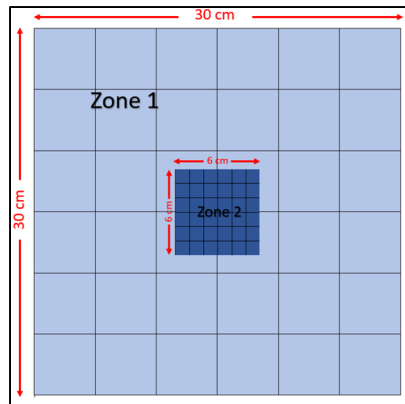
Figure 4.7 Test grid zones and dimensions

A THORLAB photodiode power meter was used to measure the light intensity over the two Zones for each fixed test plate. Figure 4.8 illustrates the measurement setup and the test area division in a closer look.
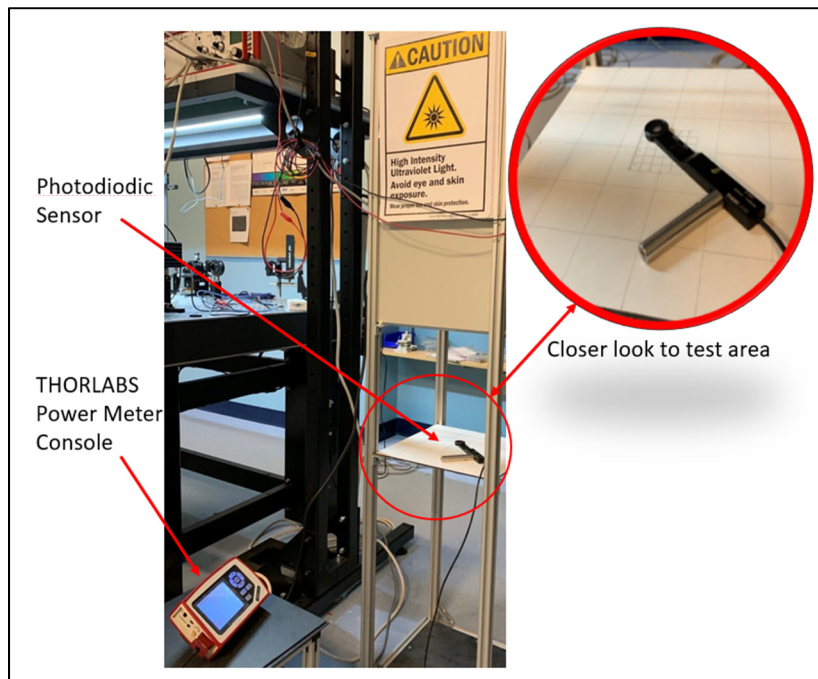
Figure 4.8 Uniformity measuring with THORLABS setup and test area

Based on the intensity measurement described in Section 4.2 and the highest light power output at a 30cm and 65cm distance from the lenses, six different uniformity evaluations were performed. Two Zones were tested for each of the three lenses configurations. Table 4.3 summarizes these tests in order.

Table 4.3 Summarized uniformity tests in order

Test Number	Lens Configuration	Tested Area
1	PD	Zone 1
2	PD	Zone 2
3	PD-PERP-PD	Zone 1
4	PD-PERP-PD	Zone 2
5	PU-PAR-PD	Zone 1
6	PU-PAR-PD	Zone 2

The results of the light power measurements are mapped and displayed in 3D and 2D plots presented in Figures 4.9, 4.10. and 4.11. The Spatial non-uniformity was calculated for each configuration based on the equation below:

$$Non-uniformity\ (\%) = \left[\frac{Max\ irradiance - Min\ irradiance}{Max\ irradiance + Min\ irradiance}\right] \times 100\ \% \qquad (4.2)$$

Figure 4.9 shows a pseudocolor image of the light uniformity result for one lens in the PD configuration at 30cm from the test plane in Zone 1 and Zone 2. The red color represents more irradiance and the blue color indicates a lower irradiance.
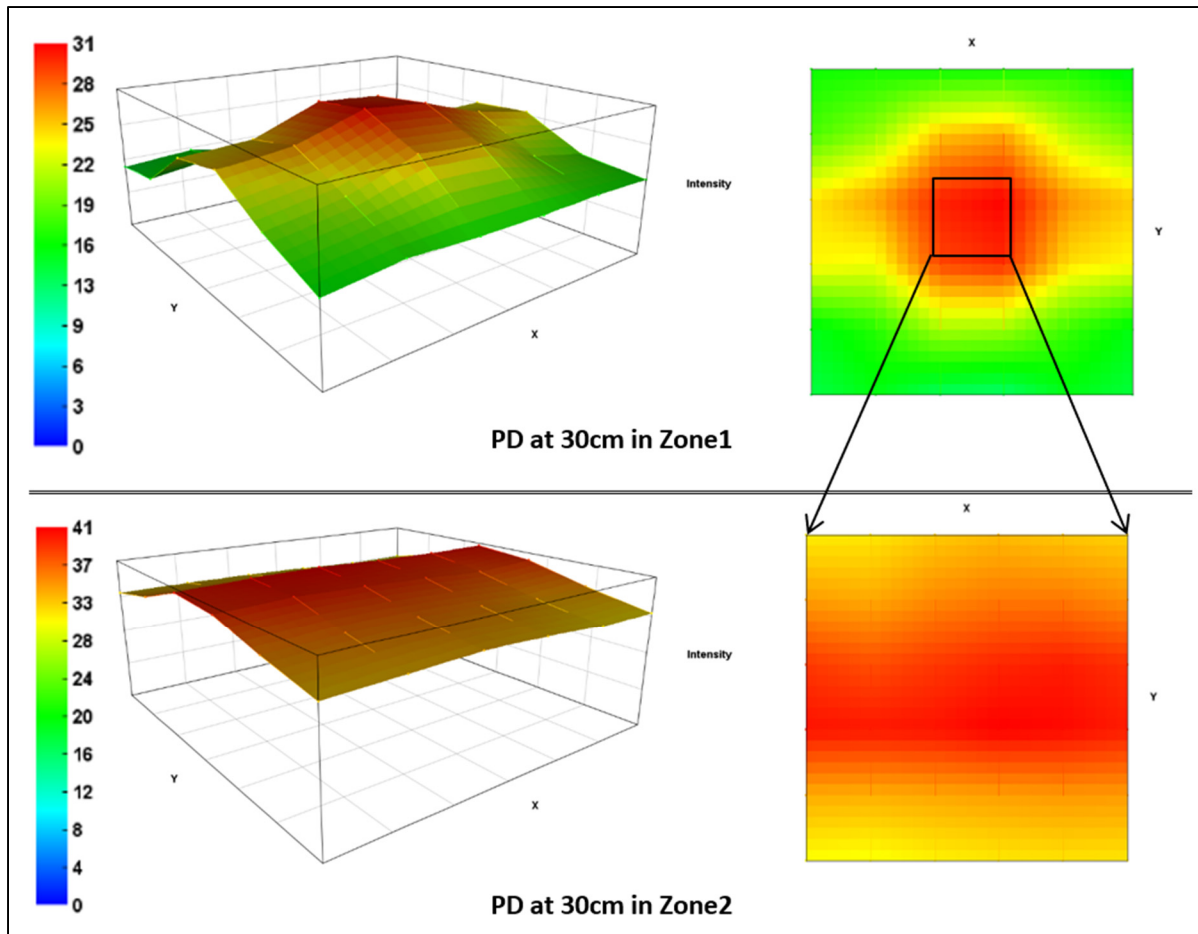
Figure 4.9 Light uniformity color map for PD lens configuration

It is obvious that the amount of light in the center is more than in other areas because of the installation of the high power 500W COB in the middle, however, the effect of the linear Fresnel lens can be seen which concentrate the lights to a line in the center. In Zone 1 we have 43.22% non-uniformity which is reduced to 15.24% in Zone 2.

By adding the second lens on top of the first one (PD) with the linear pattern-oriented perpendicularly to the first one, the PD-PERP-PD configuration setup became ready for testing, this time at 65cm away from lenses. Figure 4.10 shows the mapped results of the test in this configuration.
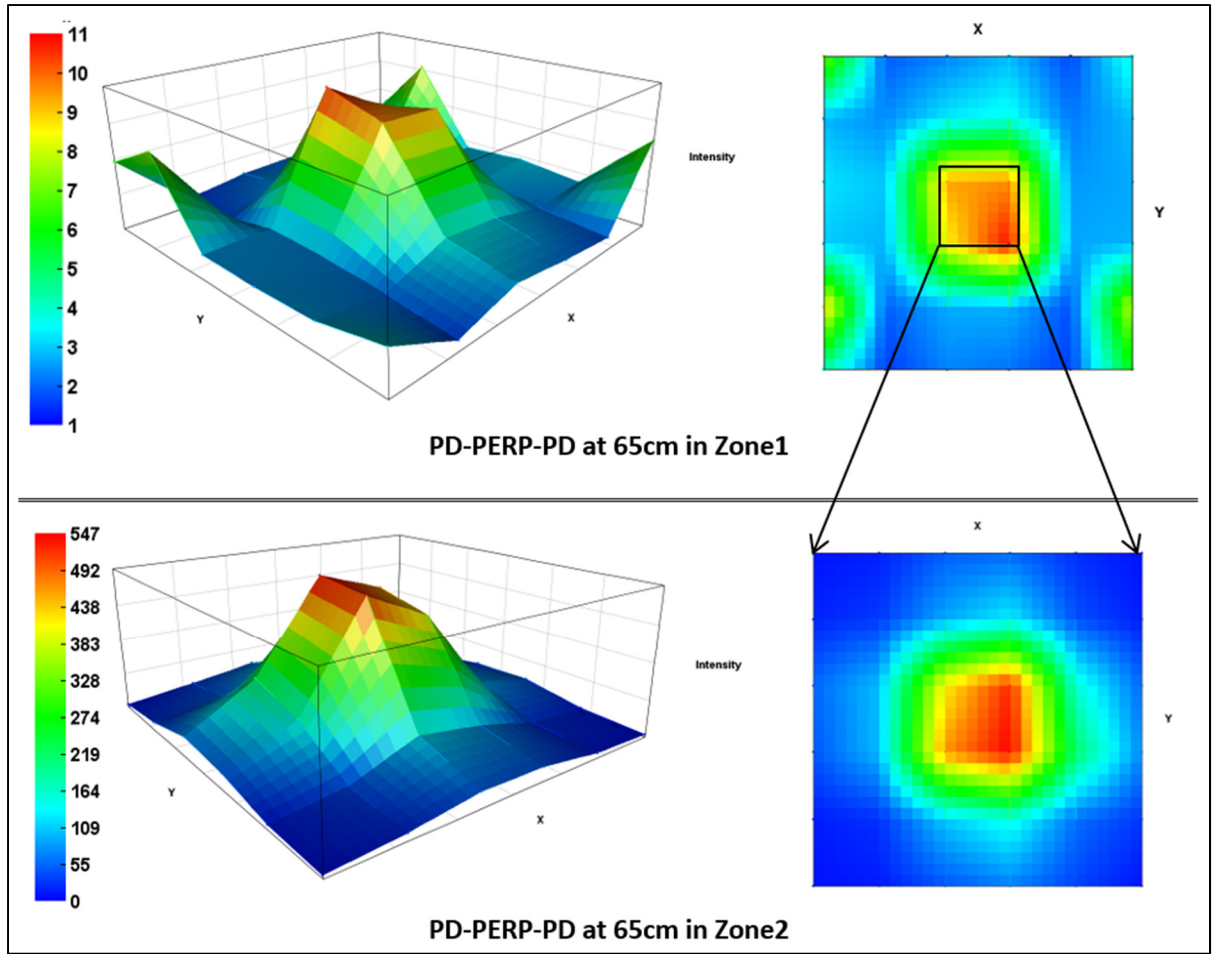
Figure 4.10 Light uniformity color map for PD-PERP-PD lens configuration at 65cm

This lens configuration concentrates as much as light was possible in a square at the center of the test plane as expected. However, since the center point has a very high-intensity value the non-uniformity percentage is more than the previous configuration, at 74.48% for Zone 1 and 96.31% for Zone 2.

In the Final lens configuration, the second lens's pattern was changed to be parallel with the first one with opposite pitch direction (upward). For PU-PAR-PD configuration the test plane was adjusted to a distance of 30cm away from the lenses as described in 4.2 to obtain the highest intensity. Figure 4.11 demonstrates the uniformity of the test plane for this lens configuration.
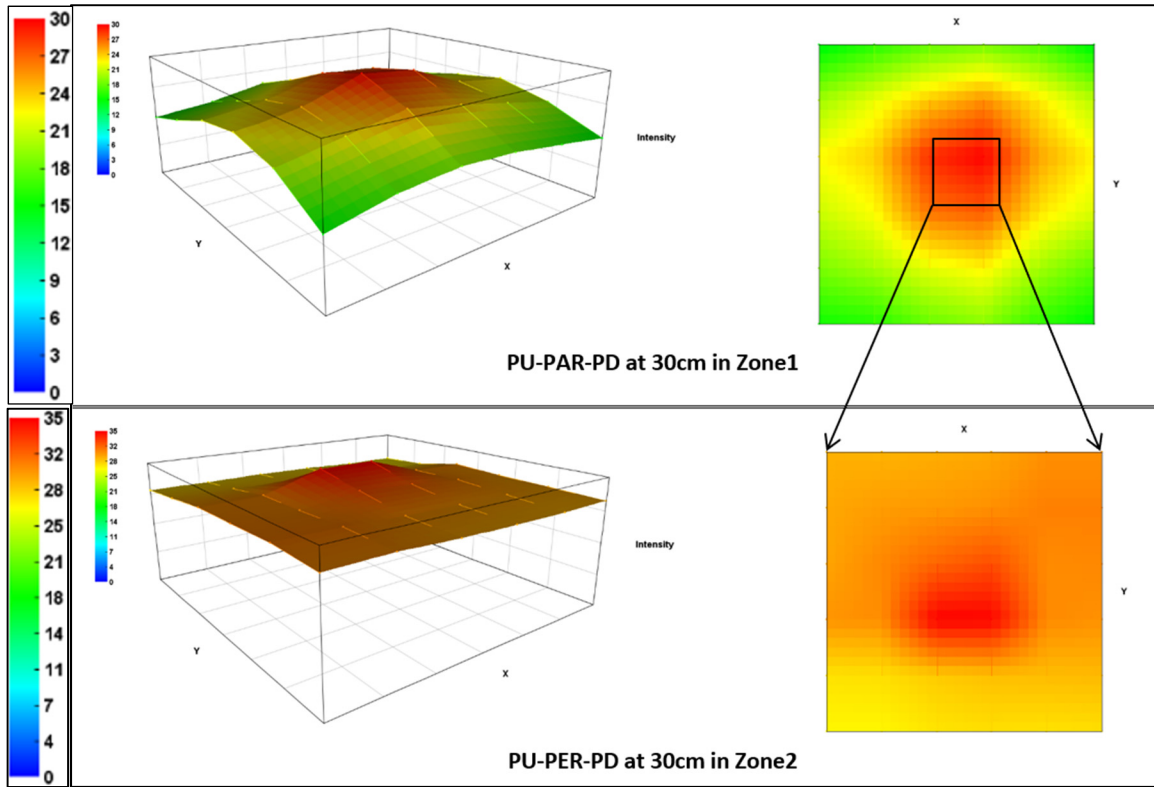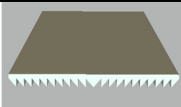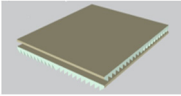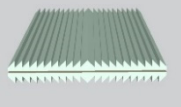
Figure 4.11 Light uniformity color map for PU-PAR-PD lens configuration

It is clearly seen that this configuration of lenses results in a better uniformity both in Zone 1 and Zone 2, which are 34.99% and 7.1% respectively. All these results and non-uniformity calculations based on equation 4.2 are summarized and reported in Table 4.4.

Table 4.4 non-uniformity of different configurations in percent

Lenses Configuration	Symbol	Test plane distance to lens	Zone 1	Zone 2
PD		30cm	43.22%	15.24%
PD-PERP-PD		65cm	74.48%	96.31%
PU-PAR-PD		30cm	34.99%	7.1%

This table shows all the results of the non-uniformity test for the three different lens configurations in the two areas named Zone 1 and Zone 2. It clearly shows that the smaller area has better uniformity, except in the PD-PERP-PD configuration which has the maximum intensity output. Based on standards, any result which is more than 10% non-uniformity is a non-classified item in solar simulators. Hence, the fabricated solar simulator obtained Class C for the PU-PAR-PD lenses configuration in Zone 2.

4.6   Temporal instability

Temporal instability of irradiance is one of the standard classifications for solar simulators. In this step, the stability of the solar simulator's light sources has been measured with an OceanOptic spectrometer, centered in the test area. These measurements were performed over a certain time interval and results were calculated based on equation 4.3 taken from ASTM E927-10 standard:

$$Temporal\ instability\ (\%) = \left[\frac{E_{max} - E_{min}}{E_{max} + E_{min}}\right] \times 100\ \% \tag{4.3}$$

E is the irradiance of the light source measured by an HR4000 fiber optic and was read by OceanView© software. The spectra irradiance of the solar simulator light engine was measured

over four different time intervals as short-term and long-term instability. Results of the measurements and classifications are summarized in Table 4.5.

Table 4.5 Measured temporal instability and classification

Measuring Time	Temporal instability	Class
30s	1.16%	A
60s	0.86%	A
3600s (1h)	0.26%	A
10800s (3h)	1.54%	A

The temporal instability for the fabricated solar simulator was classified as Class A. Irradiance changed at the start-up and affected the short-term instability at the 30 seconds time step. A slight increase in instability was also observable at the long-term (3h) time-step. This effect is due to the system warm-up which is below Class A limits. Figure 4.12 plots the stability of the solar simulator irradiance graphs over long-term stability using four different time intervals, namely 30s, 60s, 1h, and 3h.
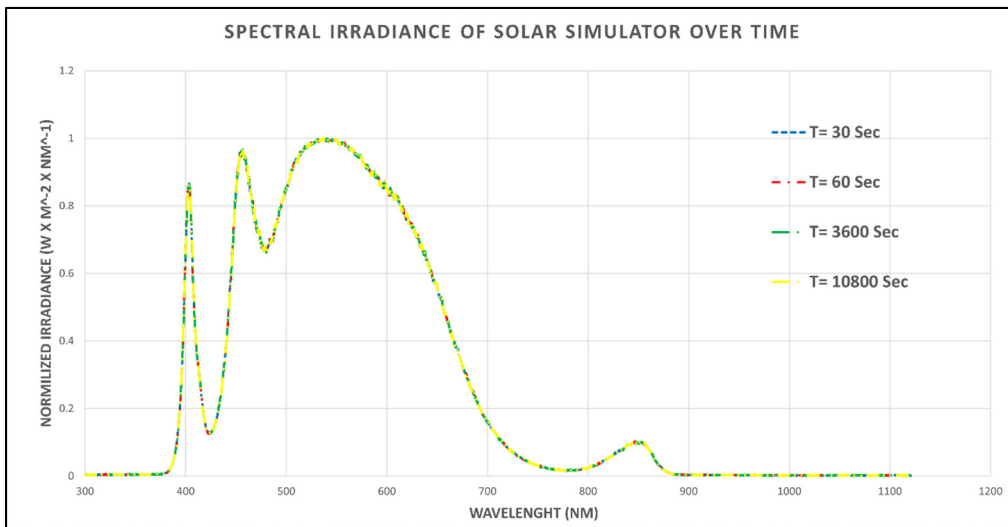
Figure 4.12 Short-term and Long-term instability response for solar simulator

This figure demonstrates that there is no drop or increase in the light intensity or change in spectral shape over the measurement period.

4.7   I-V curves comparison with standard LED-Based simulator

To compare the fabricated solar simulator light engine with a standard LED-based solar simulator we decided to test different solar cells under both devices and compare the I-V curves of each type of solar cell. We used a Newport LSH-7320 LED-based Class ABA solar simulator at UQAM university for this comparison. The LSH-7320 LED solar simulator is designed for researching the market for PVs in the field. It is certified class ABA under IEC 60906-9, specifically, A class for Temporal stability, B class for uniformity classification, and A class for the spectral match. We have chosen four types of PV cells for this test. Amorphous Silicon (a-Si), Copper Indium Gallium Selenide (CIGS), Monocrystalline (mono-Si), and Organic Photovoltaic (OPV) solar cells were used for this experiment. For a more accurate comparison between these two sets of examinations, we made the test conditions equal. Both sets of tests were performed at 25 degrees Celsius and under the same output light power of the simulator. As the UQAM solar simulator has a maximum of 1 Sunlight output, we adjusted the light output of the fabricated solar simulator to 1 Sun output by dimming the main COB to 1 Sun power output at the center of the test plane at 65 cm with PD-PERP-PD lens configuration. This lens configuration was chosen due to its higher intensity results. To measure the short-circuit current (I_{sc}), a Keithley source measure unit (SMU) model 2450 was used. Figure 4.13 shows the I-V curve test set up (A) and internal connection of SMU (B).
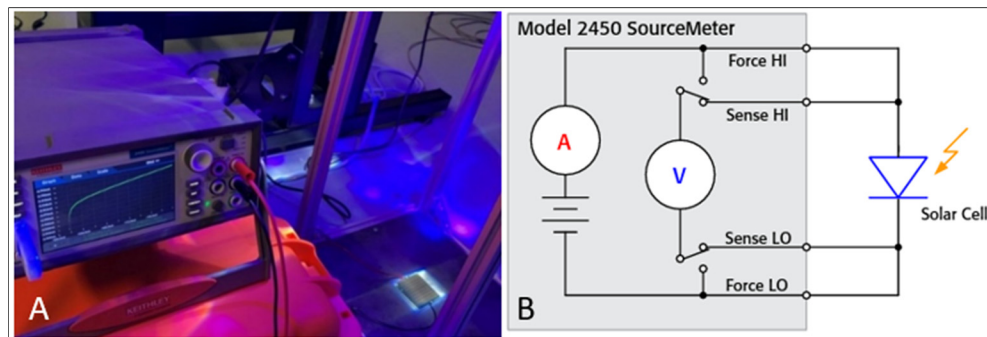
Figure 4.13 A) I–V measurement setup B) Connections of the Model 2450 to a solar cell

For each cell, the SMU was set up individually and tests were conducted. Figure 4.14 shows the results of each I-V curve for the different PV cells. Blue graphs are the result of the I-V curve measurement with the UQAM (standard) solar simulator and the Orange graphs are the results of the same cell at ETS under the fabricated solar simulator.
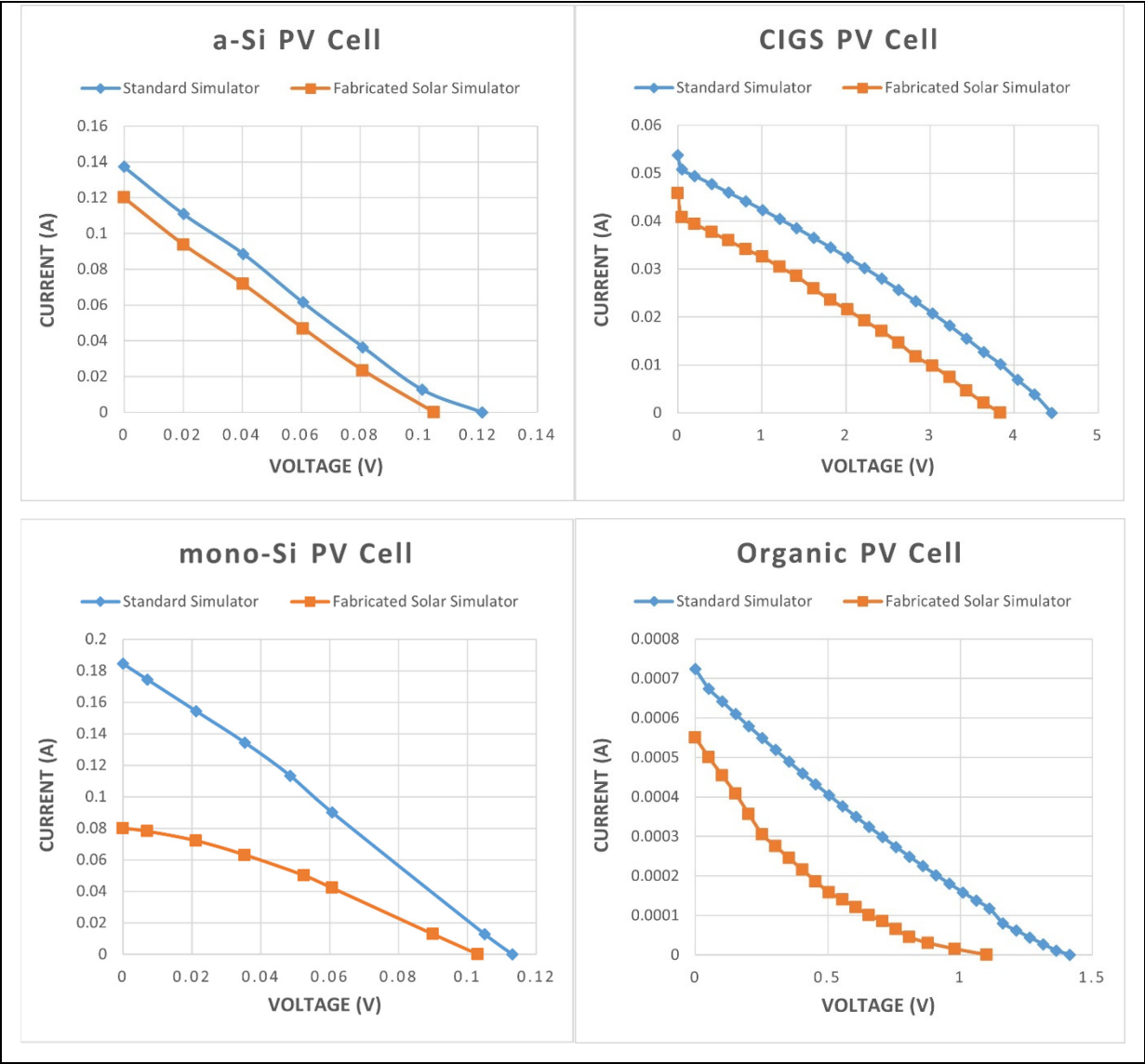
Figure 4.14 Measured electrical (I–V) characteristics of different PV cells under standard solar simulator and fabricated solar simulator

As the fabricated solar simulator does not have a full spectrum light. It could be seen that the I-V curve has a different shape from the one tested under the standard solar simulator. However, the I_{sc} has a small decrease in three of the tested cells. Also, there are not a lot of changes in voltage. But by looking at the mono-Si graph, a huge decrease in I_{sc} can be seen, which implies that there is a change in the power that this cell received. This difference in power absorption in mono-Si could be described as a lack of the RED and IR portion of the fabricated solar simulator and represents that it is not only the power that affected the I-V curve but also the wavelengths that could change the I-V curve and efficiency of the solar cell. Table 4.6 and Table 4.7 shows the result of this test and the calculated efficiency base on this equation:

$$\eta = \frac{P_{max}}{P_{in}} \qquad (4.4)$$

Where P_{max} is calculated from the results of I-V measurement and P_{in} is the input power that is selected to be $1000^{W}/m^2$, which is equal to 1 Sun power for both devices.

Table 4.6 Efficiency of different PV cells under standard solar simulators

Standard Solar Simulator Class ABA				
Solar Cell	I_{sc} (A)	V_{oc} (V)	P_{max} (W)	η (%)
a-Si	0.137	0.121	0.004	0.143
CIGS	0.054	4.445	0.068	2.607
mono-Si	0.184	0.113	0.005	0.211
OPV	0.0007	1.414	0.213×10^{-3}	0.008

Table 4.7 Efficiency of different PV cells under fabricated solar simulator

Fabricated Solar Simulator				
Solar Cell	I_{sc} (A)	V_{oc} (V)	P_{max} (W)	η (%)
a-Si	0.120	0.105	0.003	0.111
CIGS	0.046	3.836	0.043	1.668
mono-Si	0.080	0.103	0.003	0.101
OPV	0.0005	1.100	0.087×10^{-3}	0.003

As we have seen in the graphs and in these results tables. the I_{sc} under the fabricated device for all of the cells are lower than the standard solar simulator. Overall these result indicates that the used solar cells are not well functioning and the efficiency should not be considered as a reference, however, solar simulator comparison is can be made as the failure factor is constant. The lower short circuit current means that the power absorption is lower than the standard device. This happened because of the missing parts of the light spectrum in the fabricated solar simulator. This difference is more apparent when looking at the results for the mono-Si solar cell which is obvious because this type of solar cell is more sensitive to the RED and IR regions of the spectrum. There was no spec sheet available for tested solar cells, and there was no way to know the exact bandgap. However, it could be said that the a-Si, CIGS, and Organic cells usually have bigger band gaps and can absorb more photons of light and higher energy, and are less affected by the RED region of the spectrum, which could explain why there is no huge decrease in I_{sc}.

4.8   Discussion

In this chapter, the Intensity of light output, Color temperature, Spectral distribution, Spatial irradiance non-uniformity, and Temporal stability of fabricated LED-based light engine for solar simulators were investigated. Besides these characterizations, I-V curve measurements of four different types of solar cells were performed and their efficiencies were compared operated by using a standard solar simulator and fabricated solar simulator.

For the measurement of Intensity and irradiance non-uniformity of the solar simulator, we used Thorlabs S130C photodiode sensor which has a broad spectral range (from 400 nm to 1100 nm) with a relatively flat spectral response connected to the Thorlabs PM100D power meter console. This was the best and the only wide-range sensor in the laboratory where we tested our device. With its 9.7mm x 9.7mm active detector area, the measurement was taken over the 300mm x 300mm (Zone 1) test area under different distances from the Fresnel lenses and different configurations of Fresnel lenses. Three lens configuration sets were tested under the reflector box to study the best configuration in terms of uniformity and intensity. All these tests were conducted for a smaller test area of 60mm x 60mm dimensions (Zone 2) to consider as a small test area solar simulator. The optimal distance was experimentally determined as follows for each lens configuration. Irradiance measurement was taken from a distance ranging from 10cm to 80cm with the Fresnel lenses with steps of 10cm. In PD-PERP-PD lens configuration, it was observed that in the interval between 60cm and 70cm. The separate irradiance maxima in the test plane start to overlap with each other to form a single square with maximum irradiance at the center of the test plane. Then, within this distance interval, we decreased the measurement step to 5cm in order to make a more accurate evaluation of maximum intensity and the optimal distance, which was approximately 65cm from the lenses for this lens configuration. We measured a 5.47 Sun power (5.47 x 1000 W/m^2) light output at the maximum point in the center of the test plane with this lens configuration and setup. The optimal light intensity output for the other two lens configurations was measured at a 30cm distance from the lenses, which were measured as 0.35 and 0.4 Sunlight output. Due to the goal of fabricating a high flux output simulator, we decided to use these distances to fix the movable test plane and conduct the uniformity test for both large and small areas. The measurement results met the Class C Spatial non-uniformity for PU-PAR-PD in Zone 2. The fabricated solar simulator uniformity is non-classified in the other lens configurations which could be improved in future work by changing the shape of the reflector box from a rectangle to a cylindrical reflector box with flexible reflectors such as Anodized Aluminium sheets.

The color temperature of the main COB was measured with a Photo Research Spectroradiometer Model PR-670 which has a measurement range of 380nm to 780nm, to

compare with the spec sheet of a purchased COB and the reference sun color temperature. Results confirmed that the chosen COB LED for the visible spectrum portion of the solar simulator light engine almost match with sun color temperature, however, the lack of Red light in this LED light source could be seen, which could be compensated by adding a warmer light color to the main COB in the visible range.

The spectral distribution of each individual COB, as well as the combination of all COBs, was measured by means of a calibrated High-resolution fiber optic spectrometer model HR4000, in the Photonic innovation lab (phi-lab) at École de Technologie Supérieure. This device is responsive from 200-1100 nm with a 0.025 nm resolution. Results show that the experimental spectrum and theoretical spectrum of the proposed solar simulator is near to the spectrum of the sun in the majority of the visible range except for the Reddish light region. However, the experimental spectrum of the solar simulator in the infra-red range is weaker especially from 800 nm to 1100 nm, and since, the deviation from the reference spectrum is more than 4% it could not be classified on spectral match characterization. Therefore, the power of COBs in the infra-red range and some region in visible light should be increased to get the same spectrum as the sun in future work. This could be expanded to Blue light as well to cover the observable deviation of the spectrum between 400nm to 430nm.

The instability of light output was measured over four time periods using the HR4000 spectrometer and read the data via OceanView software. Due to the high-quality driver and heat management a temporal instability of <0.2% was achieved and classified Class A in temporal instability.

The last experiment was the I-V curve and efficiency measurement under the fabricated solar simulator and a standard LED-based solar simulator. We used a Newport LSH-7320 LED-based Class ABA solar simulator in UQAM university for this comparison. Because of the COVID-19 situation, there was no way to move the simulators to the same laboratory to completely match the test condition. We tried to keep the laboratory temperatures at around 25 degrees of Celsius, but the UQAM standard simulator was in a vacuum glove box making it

not possible for us to move the fabricated device to a chamber with more than 150cm height. We adjusted the light output of both devices on 1 Sun, however, we were not sure that the standard simulator was calibrated and we could not be sure that the exact light output power that the UQAM simulator gives is exactly 1 Sun, resulting in a change of the I_{sc}. Four types of PV cells were tested under both simulators with the described situation and results show that the efficiency in all of the solar cells dropped. This could be increased by improving the spectrum and test conditions in the future. The complete spectrum of the simulator is very important to have the best efficiency because the cell is highly dependent on wavelength as well as intensity.

Although we accept that the shortcomings addressed in the present framework and the structure may require improvements in design, this system has been tested and is mainly debated here as an experimental prototype approach to evaluating the feasibility of a high output (more than 1 Sun) LED-based solar simulator with a large test area. The performance properties of this solar simulator can be enhanced by using better quality materials, especially Fresnel lens and reflectors. Furthermore, the use of high-power LEDs in the UV and IR range as they become available on the market will allow for better spectral response for the whole system.

As a suggestion for future work, this prototype of a solar simulator light engine with 5 suns light output, could be developed to build a scalable High Flux Solar Simulator (HFSS). We used Dialux software to simulate the light output of an HFSS with nine light engines. Each light engine was aimed at the test plane. Figure 4.15 demonstrates the Dialux 3D output simulation of an HFSS with one light engine in the center and eight tilted light engines around it, targeted to a test plain. This is only a visual schematic that describes the future idea, more detail like the exact wavelength, focal length, and test plane distance need future research and fabrication besides measurements.
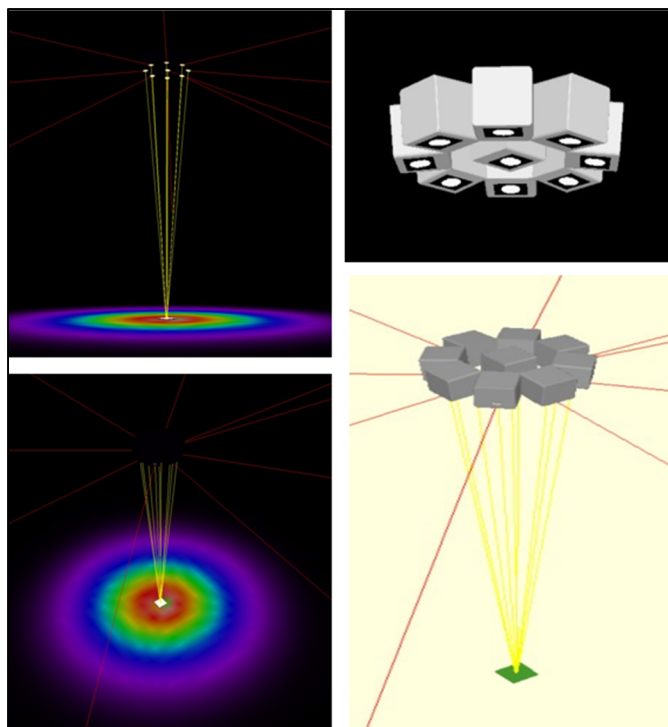
Figure 4.15 Simulated HFSS using fabricated solar simulator light engine

CONCLUSION

LED-based solar simulators have their advantages which could not be disregarded in comparison to other simulators that used non-LED light sources. With LED technology development in the industry, researchers conduct more time on LED-based solar simulators research in recent years. However, there are few full high-power LED simulators that used Cheap On Board LEDs, and only limited works are done on a high flux output simulator with a large-area uniform illumination test plane. In this work, a high-power LED-based light engine for solar simulators was designed and fabricated, using a lower quantity of LEDs integrated with Fresnel lenses to reach more than one Sunlight output at the test plane.

Firstly, a careful up-to-date literature review of existent LED-based solar simulators around the world and on the theoretical background supporting this study had been carried out. Then, the importance of solar energy and the improvement of photovoltaic cells were described. Different modes of operation of a solar simulator and different standards with classification methods of a solar simulator were then introduced. Next, we discussed the development and fabrication of a high-power light engine for large-area solar simulators (LASS) and High Flux Solar Simulators (HFSS) applications. The use of a lower quantity of LEDs is one of the advantages of this research and could be considered as a more compact light engine with a simple driving electrical system and cooling system. Also, the advantage of COB-LED is that easy to be wired and installed. Subsequently, a total of five high-power LED COBs with 1000W power consumption were installed on particular heatsinks integrated with high-speed fans and fixed symmetrically on a 30cm x 30cm dimensions metal plate with a 2mm thickness. The complete COBs and heatsinks chassis were installed on the base structure on the top of a 60cm long reflector box with no gap between reflectors, ended to 30cm x 30cm linear Fresnel lenses. A movable metal test plane was added to the structure with a span of 80cm long to adjust the distance of the test plane from the lenses. Finally, experimental results were carried out to characterize the fabricated solar simulator. Six different evaluation methods were performed: Intensity, Color temperature, Spectral match, Spatial non-uniformity, Temporal instability, and I-V curve measurement of four different types of solar cells. The intensity

measurement showed a 5.45 suns light output at the center of the test plane for one of the lens configurations, but the uniformity of the test plane in this configuration note is classified as standard. This could be improved in the future by using a cylindrical reflector box and higher quality reflectors and Fresnel lenses. However, the non-uniformity of irradiance generated from COB-LEDs in one of the lens configurations matches Class-C of the ASTM E 927-05 (2005). Spectral match measurement shows a perfect match in the visible range, but in extended wavelength bands (UV, IR) the deviation is more than the standard criteria. Especially in the Red and Infra-Red region of the spectrum, it could not be classified as standard. These mismatched spectrums were shown by measuring the I-V curve and efficiency of four different solar cells. The lack of spectrum reduces the I_{sc} of all solar cells in comparison to the result of testing the same cells under a standard LED-based solar simulator.

Given the results and potential source of the identified problems, we can develop the following recommendation for future work:

- Using more power on IR range COBs.
- Designing and fabricating a customized UV SMD board to have all ranges of the UV spectrum in one board equivalent to a COB.
- Designing a cylindrical reflector box with a round linear Fresnel lens to improve the uniformity.
- Using high-quality reflector and Fresnel lenses to improve light output flux and uniformity.

APPENDIX A

MEANWELL LED DRIVER SPEC SHEETS

TAIWAN ... **SELV IP65 IP67** ... **Type HL** ... **CB CE**

■ Features
- Constant Voltage + Constant Current mode output
- Metal housing with class I design
- Standby power consumption <0.5W at remote off
- IP67 / IP65 rating for indoor or outdoor installations
- Function options: output adjustable via potentiometer; 3 in 1 dimming (dim-to-off)
- Typical lifetime > 62000 hours
- 7 years warranty

■ Applications
- LED high-bay lighting
- Parking space lighting
- LED fishing lamp
- LED greenhouse lighting
- Type "HL" for use in Class I , Division 2 hazardous (Classified) location.

■ Description
HLG-600H series is a 600W AC/DC LED driver featuring the dual mode constant voltage and constant current output. HLG-600H operates from 90 ~ 305VAC and offers models with different rated voltage ranging between 12V and 54V. Thanks to the high efficiency up to 96%, with the fanless design, the entire series is able to operate for -40℃ ~ +90℃ case temperature under free air convection. The design of metal housing and IP67/IP65 ingress protection level allows this series to fit both indoor and outdoor applications. HLG-600H is equipped with various function options, such as dimming methodologies, so as to provide the optimal design flexibility for LED lighting system.

■ Model Encoding
HLG - 600H - 15 A

- Function options
- Rated output voltage (12V/15V/20V/24V/30V/36V/42V/48V/54V)
- Rated wattage
- Series name

Type	IP Level	Function	Note
A	IP65	Io and Vo adjustable through built-in potentiometer	In Stock
B	IP67	3 in 1 dimming function (0~10VDC, 10V PWM signal and resistance)	In Stock
AB	IP65	Io and Vo adjustable through built-in potentiometer & 3 in 1 dimming function (0~10VDC, 10V PWM signal and resistance)	In Stock
Blank	IP67	Io and Vo fixed	In Stock

Figure-A I-1 Meanwell HLG 600H

Table-A I-1 HLG 600H Specification

SPECIFICATION

MODEL		HLG-600H-12☐	HLG-600H-15☐	HLG-600H-20☐	HLG-600H-24☐	HLG-600H-30☐	HLG-600H-36☐	HLG-600H-42☐	HLG-600H-48☐	HLG-600H-54☐
OUTPUT	DC VOLTAGE	12V	15V	20V	24V	30V	36V	42V	48V	54V
	CONSTANT CURRENT REGION Note.4	6 – 12V	7.5 – 15V	10 – 20V	12 – 24V	15 – 30V	18 – 36V	21 – 42V	24 – 48V	27 – 54V
	RATED CURRENT	40A	36A	28A	25A	20A	16.7A	14.3A	12.5A	11.2A
	RATED POWER	480W	540W	560W	600W	600W	601.2W	600.6W	600W	604.8W
	RIPPLE & NOISE (max.) Note.2	150mVp-p	150mVp-p	150mVp-p	150mVp-p	150mVp-p	200mVp-p	250mVp-p	250mVp-p	350mVp-p
	VOLTAGE ADJ. RANGE	Adjustable for A-Type only (via built-in potentiometer)								
		10.2 – 12.6V	12.7 – 15.8V	17 – 21V	20.4 – 25.2V	25.5 – 31.5V	30.6 – 37.8V	35.7 – 44.1V	40.8 – 50.4V	45.9 – 56.7V
	CURRENT ADJ. RANGE	Adjustable for A-Type only (via built-in potentiometer)								
		20 – 40A	18 – 36A	14 – 28A	12.5 – 25A	10 – 20A	8.3 – 16.7A	7.1 – 14.3A	6.2 – 12.5A	5.6 – 11.2A
	VOLTAGE TOLERANCE Note.3	±3.0%	±2.0%	±1.5%	±1.0%	±1.0%	±1.0%	±1.0%	±1.0%	±1.0%
	LINE REGULATION	±0.5%	±0.5%	±0.5%	±0.5%	±0.5%	±0.5%	±0.5%	±0.5%	±0.5%
	LOAD REGULATION	±2.0%	±1.5%	±1.0%	±0.5%	±0.5%	±0.5%	±0.5%	±0.5%	±0.5%
	SETUP, RISE TIME Note.6	500ms, 80ms/ 115VAC, 230VAC								
	HOLD UP TIME (Typ.)	15ms/ 115VAC, 230VAC								
INPUT	VOLTAGE RANGE Note.5	90 – 305VAC 127 – 431VDC (Please refer to "STATIC CHARACTERISTIC" section)								
	FREQUENCY RANGE	47 – 63Hz								
	POWER FACTOR (Typ.)	PF≥0.98/115VAC, PF≥0.95/230VAC, PF≥0.93/277VAC @full load (Please refer to "POWER FACTOR (PF) CHARACTERISTIC" section)								
	TOTAL HARMONIC DISTORTION	THD< 20% (@ load≥50% /115VAC, 230VAC; @ load ≥75%/277VAC) (Please refer to "TOTAL HARMONIC DISTORTION (THD)" section)								
	EFFICIENCY (Typ.) 230VAC	92%	93.5%	94.5%	95%	95%	95.5%	96%	96%	96%
	277VAC	92.5%	93.5%	94.5%	95%	95%	95.5%	96%	96%	96%
	AC CURRENT (Typ.)	7A/ 115VAC 3.3A / 230VAC 2.9A / 277VAC								
	INRUSH CURRENT (Typ.)	COLD START 70A(twidth=1000μs measured at 50% Ipeak) at 230VAC; Per NEMA 410								
	MAX. No. of PSUs on 16A CIRCUIT BREAKER	1 unit (circuit breaker of type B) / 2 units (circuit breaker of type C) at 230VAC								
	LEAKAGE CURRENT	<0.75mA/ 277VAC								
	STANDBY POWER CONSUMPTION	<0.5W at remote off								
PROTECTION	OVER CURRENT Note.4	95 – 108%								
		Constant current limiting, recovers automatically after fault condition is removed								
	SHORT CIRCUIT	Constant current limiting, recovers automatically after fault condition is removed								
	OVER VOLTAGE	13 – 16V	16.5 – 20.5V	22 – 26V	26 – 30V	32.5 – 36.5V	39.5 – 43.5V	46 – 50V	52.5 – 56.5V	59 – 63V
		Shut down o/p voltage, re-power on to recover								
	OVER TEMPERATURE	Shut down o/p voltage, re-power on to recover								
FUNCTION	REMOTE ON/OFF CONTROL	Power on: "High" >2 – 5V or Open circuit Power off: "Low"<0 – 0.5V or Short circuit								
	5V STANDBY	5Vsb : 5V@0.5A; tolerance ±5%, ripple: 100mVp-p(max.)								
ENVIRONMENT	WORKING TEMP.	Tcase= -40 – +90℃ (Please refer to "OUTPUT LOAD vs TEMPERATURE" section)								
	MAX. CASE TEMP.	Tcase= +90℃								
	WORKING HUMIDITY	20 – 95% RH non-condensing								
	STORAGE TEMP., HUMIDITY	-40 – +85℃, 10 – 95% RH non-condensing								
	TEMP. COEFFICIENT	±0.03%/℃ (0 – 55℃)								
	VIBRATION	10 – 500Hz, 5G 12min./1cycle, period for 72min. each along X, Y, Z axes								
SAFETY & EMC (Note 10)	SAFETY STANDARDS Note.7	UL 60950-1, UL 8750(type"HL"), CSA C22.2 No. 250.13-12, ENEC EN61347-1, EN61347-2-13 independent, EN62384, IP65 or IP67, J61347-1, J61347-2-13, CCCGB4943.1, EAC TPTC 004, AS/NZS 60950.1(by CB), KC61347-1, KC61347-2-13(for 24A,36A,48A,54A only) approved								
	WITHSTAND VOLTAGE	I/P-O/P:3.75KVAC I/P-FG:2KVAC O/P-FG:1.5KVAC								
	ISOLATION RESISTANCE	I/P-O/P, I/P-FG, O/P-FG:100MOhms /500VDC /25℃/70%RH								
	EMC EMISSION Note.7	Compliance to EN55032 (CISPR32) Class B, EN55015, EN61000-3-2 Class C (@ load ≥50%) ; EN61000-3-3, EAC TPTC 020; KC KN15, KN61547(for 24A,36A,48A,54A only)								
	EMC IMMUNITY	Compliance to EN61000-4-2,3,4,5,6,8,11, EN61547, EN55024, light industry level (surge immunity Line-Earth 4KV, Line-Line 2KV), EAC TP TC020; KC KN15, KN61547 (for 24A,36A,48A,54A only)								
OTHERS	MTBF	76.9Khrs min. MIL-HDBK-217F (25℃)								
	DIMENSION	280*144*48.5mm (L*W*H)								
	PACKING	3.9Kg; 4pcs/16.6Kg/0.9CUFT								

NOTE
1. All parameters NOT specially mentioned are measured at 230VAC input, rated current and 25℃ of ambient temperature.
2. Ripple & noise are measured at 20MHz of bandwidth by using a 12" twisted pair-wire terminated with a 0.1uf & 47uf parallel capacitor.
3. Tolerance : includes set up tolerance, line regulation and load regulation.
4. Please refer to "DRIVING METHODS OF LED MODULE".
5. De-rating may be needed under low input voltages. Please refer to "STATIC CHARACTERISTIC" sections for details.
6. Length of set up time is measured at first cold start. Turning ON/OFF the driver may lead to increase of the set up time.
7. The model certified for CCC(GB19510.14, GB19510.1, GB17743 and GB17625.1) is an optional model .
8. This series meets the typical life expectancy of >62,000 hours of operation when Tcase, particularly ⒠ point (or TMP, per DLC), is about 75℃ or less.
9. Please refer to the warranty statement on MEAN WELL's website at http://www.meanwell.com
10. The driver is considered a component which will be installed into a final equipment. All the EMC tests are been executed by mounting the unit on a 360mm*360mm metal plate with 1mm of thickness. The final equipment must be re-confirmed that it still meets EMC directives. For guidance on how to perform these EMC tests, please refer to "EMI testing of component power supplies."
11. The ambient temperature derating of 3.5℃/1000m with fanless models and of 5℃/1000m with fan models for operating altitude higher than 2000m(6500ft).
12. For any application note and IP water proof function installation caution, please refer our user manual before using.

Figure-A I-2 HLG 600H Dimming Operation

OUTPUT LOAD vs TEMPERATURE

◎ If HLG-600H operates in constant current mode with the rated current, the maximum workable Ta is 55℃.

STATIC CHARACTERISTICS

※ De-rating is needed under low input voltage.

POWER FACTOR(PF) CHARACTERISTIC

※Tcase at 80℃

TOTAL HARMONIC DISTORTION (THD)

※ 48V Model, Tcase at 80℃

EFFICIENCY vs LOAD

HLG-600H series possess superior working efficiency that up to 96% can be reached in field applications.
※ 48V Model, Tcase at 80℃

Figure-A I-3 HLG 600H Output Load

■ Features
- Constant Voltage + Constant Current mode output
- Metal housing design with functional Ground
- Built-in active PFC function
- No load / Standby power consumption <0.5W
- IP67 / IP65 rating for indoor or outdoor installations
- Function options: output adjustable via potentiometer; 3 in 1 dimming (dim-to-off); Smart timer dimming; DALI; Auxiliary DC output
- Typical lifetime>50000 hours
- 5 years warranty

■ Applications
- LED street lighting
- LED architectural lighting
- LED bay lighting
- LED floodlighting
- Type "HL" for use in Class I, Division 2 hazardous (Classified) location.

■ Description

ELG-150 series is a 150W AC/DC LED driver featuring the dual mode constant voltage and constant current output. ELG-150 operates from 100~305VAC and offers models with different rated voltage ranging between 12V and 54V. Thanks to the high efficiency up to 91%, with the fanless design, the entire series is able to operate for -40℃ ~ +90℃ case temperature under free air convection. The design of metal housing and IP67/IP65 ingress protection level allows this series to fit both indoor and outdoor applications. ELG-150 is equipped with various function options, such as dimming methodologies, so as to provide the optimal design flexibility for LED lighting system

■ Model Encoding

```
ELG - 150 - 24  A  -□
```
- Input wiring type { Blank:2-wire input for standard model / 3Y:3-wire input for standard model
- Function mode option
- Rated output voltage(12/24/36/42/48/54V)
- Rated wattage
- Series name

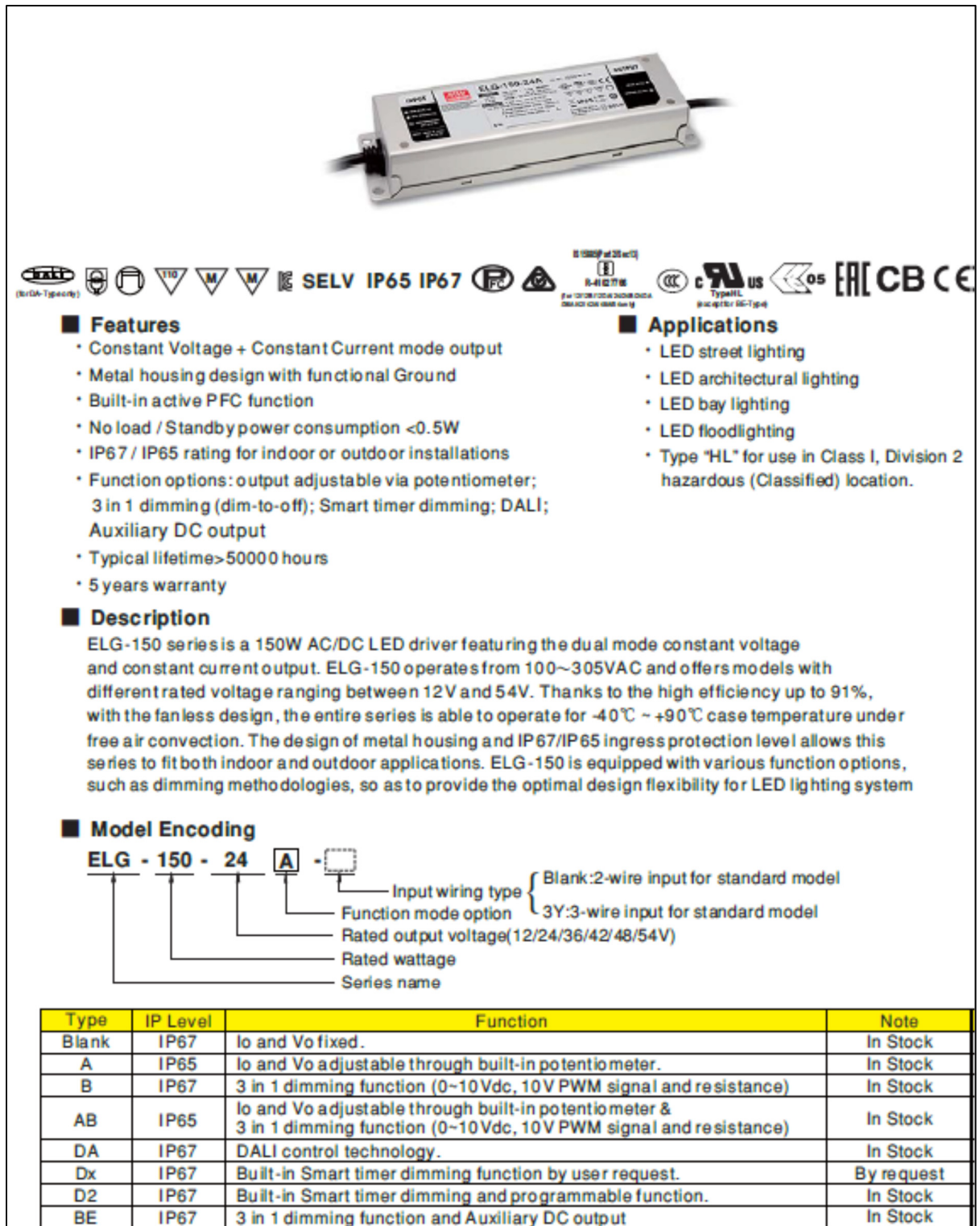| Type	IP Level	Function	Note
Blank	IP67	Io and Vo fixed.	In Stock
A	IP65	Io and Vo adjustable through built-in potentiometer.	In Stock
B	IP67	3 in 1 dimming function (0~10Vdc, 10V PWM signal and resistance)	In Stock
AB	IP65	Io and Vo adjustable through built-in potentiometer & 3 in 1 dimming function (0~10Vdc, 10V PWM signal and resistance)	In Stock
DA	IP67	DALI control technology.	In Stock
Dx	IP67	Built-in Smart timer dimming function by user request.	By request
D2	IP67	Built-in Smart timer dimming and programmable function.	In Stock
BE	IP67	3 in 1 dimming function and Auxiliary DC output	In Stock

Figure-A I-4 Meanwell ELG 150

Table-A I-2 ELG 150 Specification

SPECIFICATION

MODEL			ELG-150-12□	ELG-150-24□	ELG-150-36□	ELG-150-42□	ELG-150-48□	ELG-150-54□
OUTPUT	DC VOLTAGE		12V	24V	36V	42V	48V	54V
	CONSTANT CURRENT REGION Note2		6~12V	12~24V	18~36V	21~42V	24~48V	27~54V
	RATED CURRENT		10A	6.25A	4.17A	3.57A	3.13A	2.8A
	RATED CURRENT (for BE Type only)		8A	5.6A	3.73A	3.2A	2.8A	2.5A
	RATED POWER	For All the Types	100VAC~180VAC					
			84W	105W	105W	105W	105W	105W
		Except for BE Type	200VAC~305VAC					
			120W	150W	150.1W	150W	150.2W	151.2W
		For BE Type only	96W	134.4W	134.28W	134.4W	134.4W	135W
	RIPPLE & NOISE (max.) Note3		150mVp-p	200mVp-p	250mVp-p	250mVp-p	250mVp-p	350mVp-p
	VOLTAGE ADJ. RANGE		Adjustable for A/AB-Type only (via the built-in potentiometer)					
			10.8~13.2V	21.6~26.4V	32.4~39.6V	37.8~46.2V	43.2~52.8V	49~58V
	CURRENT ADJ. RANGE		Adjustable for A/AB-Type only (via the built-in potentiometer)					
			5~10A	3.2~6.25A	2.1~4.17A	1.8~3.57A	1.56~3.13A	1.4~2.8A
	VOLTAGE TOLERANCE Note4		±3.0%	±3.0%	±2.5%	±2.5%	±2.0%	±2.0%
	LINE REGULATION		±0.5%	±0.5%	±0.5%	±0.5%	±0.5%	±0.5%
	LOAD REGULATION		±2.0%	±1.0%	±1.0%	±0.5%	±0.5%	±0.5%
	AUXILIARY DC OUTPUT		Nominal 15V (deviation 11.5~15.5V)@0.3A for BE-Type only					
	SETUP, RISE TIME Note6		1600ms, 80ms/115VAC 500ms, 100ms/230VAC					
	HOLD UP TIME (Typ.)		10ms/115VAC, 230VAC					
INPUT	VOLTAGE RANGE Note5		100~305VAC 142~431VDC (Please refer to "STATIC CHARACTERISTIC" section)					
	FREQUENCY RANGE		47~63Hz					
	POWER FACTOR		PF≥0.97/115VAC, PF≥0.95/230VAC, PF≥0.92/277VAC@full load (Please refer to "POWER FACTOR (PF) CHARACTERISTIC" section)					
	TOTAL HARMONIC DISTORTION		THD<20% (@load≥50%/115VC; @load≥60%/230VAC; @load≥75%/277VAC) (Please refer to "TOTAL HARMONIC DISTORTION (THD)" section)					
	EFFICIENCY (Typ.)		88%	89%	90%	90%	90%	91%
	EFFICIENCY (Typ.)(for BE Type only)		86%	87%	88%	88%	88%	89%
	AC CURRENT		1.7A/115VAC 0.9A/230VAC 0.7A/277VAC					
	INRUSH CURRENT(Typ)		COLD START 65A(twidth=550μs measured at 50% peak) at 230VAC; Per NEMA 410					
	MAX. No. of PSU on 16A CIRCUIT BREAKER		3 units (circuit breaker of type B)/6 units (circuit breaker of type C) at 230VAC					
	LEAKAGE CURRENT		<0.75mA /277VAC					
	NO LOAD / STANDBY POWER CONSUMPTION		No load power consumption <0.5W for Blank/A/Dx/D2-Type; Standby power consumption <0.5W for B/AB/DA-Type					
PROTECTION	OVER CURRENT		95~108%					
			Constant current limiting, recovers automatically after fault condition is removed					
	SHORT CIRCUIT		Hiccup mode, recovers automatically after fault condition is removed					
	OVER VOLTAGE		14~18V	28~34V	41~48V	47~54V	54~62V	59~68V
			Shut down output voltage, re-power on to recover					
	OVER TEMPERATURE		Shut down output voltage, re-power on to recover					
ENVIRONMENT	WORKING TEMP.		Tcase=-40~+90℃ (Please refer to "OUTPUT LOAD vs TEMPERATURE" section)					
	MAX. CASE TEMP.		Tcase=+90℃					
	WORKING HUMIDITY		20~95% RH non-condensing					
	STORAGE TEMP., HUMIDITY		-40~+80℃, 10~95% RH					
	TEMP. COEFFICIENT		±0.03%/℃ (0~60℃)					
	VIBRATION		10~500Hz, 5G 12min./1cycle, period for 72min. each along X, Y, Z axes					
SAFETY & EMC	SAFETY STANDARDS		UL8750(type"HL")(except for BE-type), CSA C22.2 No. 250.13-12; IEC/EN/AS/NZS 61347-1,IEC/EN/AS/NZS 61347-2-13 independent, EN62384,BIS IS15885(for 12/12B/12DA/24/24B/24DA/36A/42/42A/48A/54 only), EAC TP TC 004,GB 19510.1,GB 19510.14; IP65 or IP67; KC KN61347-1,KN61347-2-13 approved					
	DALI STANDARDS		Compliance to IEC62386-101,102,207 for DA-Type only					
	WITHSTAND VOLTAGE		I/P-O/P:3.75KVAC I/P-FG:2.0KVAC O/P-FG:1.5KVAC					
	ISOLATION RESISTANCE		I/P-O/P, I/P-FG, O/P-FG:100M Ohms /500VDC /25℃/ 70%RH					
	EMC EMISSION		Compliance to EN55015,EN61000-3-2 Class C (@load≥60%); EN61000-3-3; GB17743,GB17625.1,EAC TP TC 020; KC KN15,KN61547					
	EMC IMMUNITY		Compliance to EN61000-4-2,3,4,5,6,8,11; EN61547, light industry level (surge immunity Line-Earth 6KV, Line-Line 4KV),EAC TP TC 020; KC KN15,KN61547					
OTHERS	MTBF		899.8Khrs min. Telcordia SR-332 (Bellcore) 313.66Khrs min. MIL-HDBK-217F (25℃)					
	DIMENSION		219*63*35.5mm (L*W*H)					
	PACKING		0.95Kg; 16pcs/16.0kg/0.77CUFT					

NOTE
1. All parameters NOT specially mentioned are measured at 230VAC input, rated current and 25℃ of ambient temperature.
2. Please refer to "DRIVING METHODS OF LED MODULE". For DA-Type, Constant Current region is 60%~100% of maximum voltage under rated power delivery.
3. Ripple & noise are measured at 20MHz of bandwidth by using a 12" twisted pair-wire terminated with a 0.1uf & 47uf parallel capacitor.
4. Tolerance : includes set up tolerance, line regulation and load regulation.
5. De-rating may be needed under low input voltages. Please refer to "STATIC CHARACTERISTICS" sections for details.
6. Length of set up time is measured at first cold start. Turning ON/OFF the driver may lead to increase of the set up time.
7. The driver is considered as a component that will be operated in combination with final equipment. Since EMC performance will be affected by the complete installation, the final equipment manufacturers must re-qualify EMC Directive on the complete installation again.
8. This series meets the typical life expectancy of >50,000 hours of operation when Tcase, particularly (tc) point (or TMP, per DLC), is about 80℃ or less.
9. Please refer to the warranty statement on MEAN WELL's website.
10. The ambient temperature derating of 3.5℃/1000m with fanless models and of 5℃/1000m with fan models for operating altitude higher than 2000m(6500ft).

■ DIMMING OPERATION

AC/N (Blue)
AC/L (Brown)

ELG-150

DIM+(Blue)*
DIM-(White)**
Vo-(Black)
Vo+(Red)

* DIM+ for B/AB-Type
  DA+ for DA-Type
  PROG+ for D2-Type
* *DIM- for B/AB-Type
  DA- for DA-Type
  PROG- for D2-Type

※ **3 in 1 dimming function (for B/AB-Type)**

· Output constant current level can be adjusted by applying one of the three methodologies between DIM+ and DIM-:
  0~10VDC, or 10V PWM signal or resistance.
· Direct connecting to LEDs is suggested. It is not suitable to be used with additional drivers.
· Dimming source current from power supply: 100μA (typ.)

◎ Applying additive 0 ~ 10 VDC

Vo+
Vo-
DIM+
Additive Voltage
DIM-

"DO NOT connect "DIM- to Vo-"

Output current (%)

Dimming input: Additive voltage

◎ Applying additive 10 V PWM signal (frequency range 100Hz ~ 3KHz):

Vo+
Vo-
DIM+
Additive PWM signal
DIM-

"DO NOT connect "DIM- to Vo-"

Output current (%)

Duty cycle of additive 10 V PWM signal dimming input

◎ Applying additive resistance:

Vo+
Vo-
DIM+
Additive Resistance
DIM-

"DO NOT connect "DIM- to Vo-"

Output current (%)

Short
(N= driver quantity for synchronized dimming operation)
Dimming input: Additive resistance

Note : 1. Min. dimming level is about 8% and the output current is not defined when 0%< Iout<8%.
       2. The output current could drop down to 0% when dimming input is about 0kΩ or 0Vdc, or 10V PWM signal with 0% duty cycle.

Figure-A I-5 ELG 150 Dimming Operation

■ OUTPUT LOAD vs TEMPERATURE(Note.9)

■ STATIC CHARACTERISTIC

※De-rating is needed under low input voltage.

■ POWER FACTOR (PF) CHARACTERISTIC

※ Tcase at 80℃ Constant Current Mode

- 277V(150W)
- 230V(150W)
- 115V(105W)

■ TOTAL HARMONIC DISTORTION (THD)

※ 54V Model, Tcase at 80℃

- 277VAC(150)
- 230VAC(150)
- 115VAC(105)

■ EFFICIENCY vs LOAD

ELG-150 series possess superior working efficiency that up to 91% can be reached in field applications.
※ 54V Model, Tcase at 80℃

- 277V(150W)
- 230V(150W)
- 115V(105W)
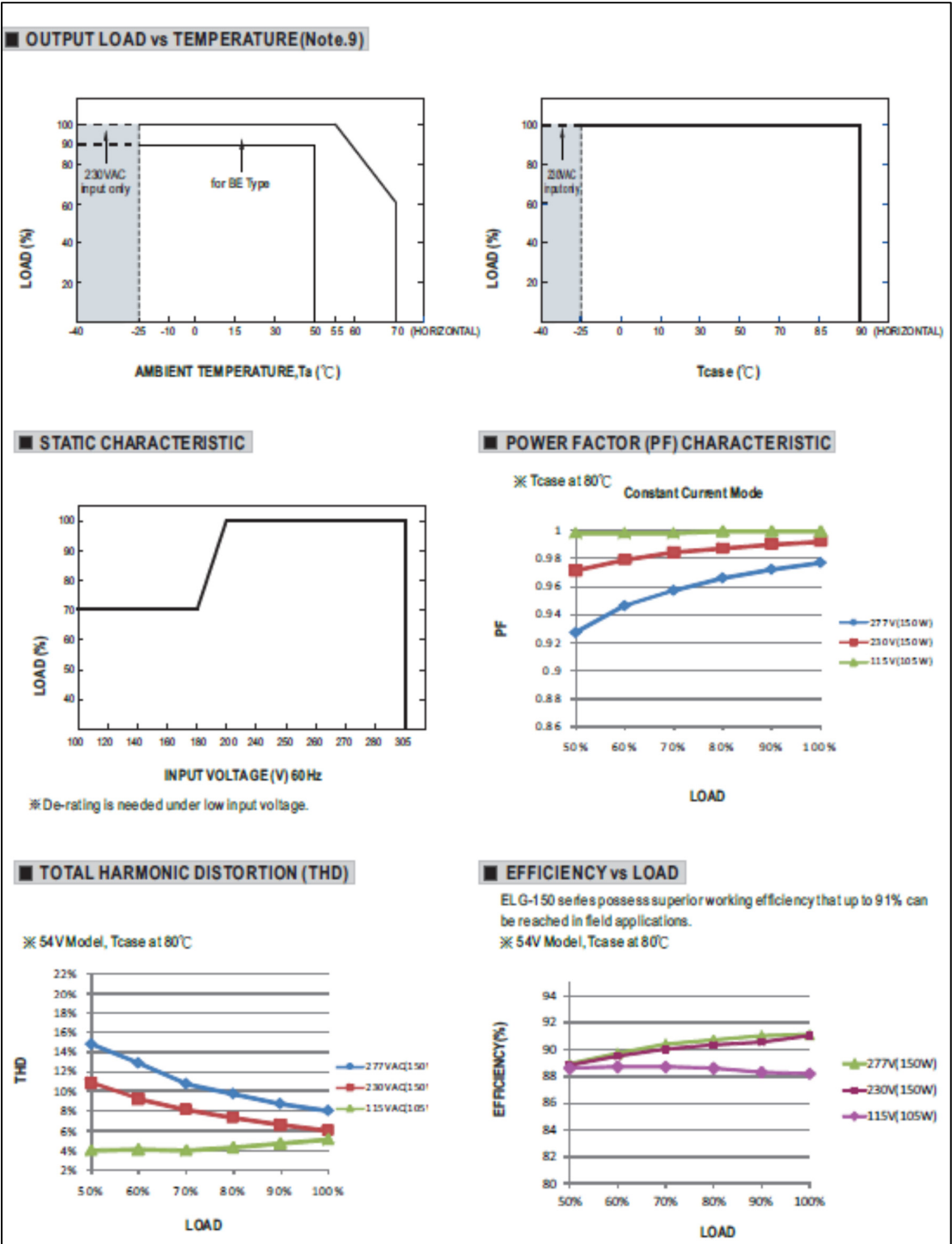
Figure-A I-6 ELG 150 Output Load

LIST OF BIBLIOGRAPHICAL REFERENCES

94063A Solar Simulator. (n.d.). Retrieved August 17, 2020, from https://www.newport.com/p/94063A#mz-expanded-view-984565495677

Ajayan, J., Nirmal, D., Mohankumar, P., Saravanan, M., Jagadesh, M., & Arivazhagan, L. (2020). A review of photovoltaic performance of organic/inorganic solar cells for future renewable and sustainable energy technologies. *Superlattices and Microstructures*, *143*(April), 106549. https://doi.org/10.1016/j.spmi.2020.106549

Alessandro, C. D., Maio, D. De, Mundo, T., Musto, M., Di, F., Monti, M., Dalena, D., Palmieri, V. G., Luca, D. De, Gennaro, E. Di, & Russo, R. (2020). *Low cost high intensity LED illumination device for high uniformity laboratory purposes*. *June*, 1–12. https://doi.org/10.20944/preprints202006.0322.v1

Allil, R. C., Manchego, A., Allil, A., Rodrigues, I., Werneck, A., Diaz, G. C., Dino, F. T., Reyes, Y., & Werneck, M. (2018). Solar tracker development based on a POF bundle and Fresnel lens applied to environment illumination and microalgae cultivation. *Solar Energy*, *174*(June), 648–659. https://doi.org/10.1016/j.solener.2018.09.061

Alxneit, I, Project, G. D.-S. F. for the E. R. A., & 2011, undefined. (n.d.). *R12. 5 solar simulator evaluation report*.

Alxneit, Ivo. (2011). Measuring temperatures in a high concentration solar simulator - Demonstration of the principle. *Solar Energy*, *85*(3), 516–522. https://doi.org/10.1016/j.solener.2010.12.016

Antón, I., Domínguez, C., Sala, G., Martínez, M., Díaz, V., Álvarez, J. L., & Alonso, J. (2005). Indoor characterization of concentrator modules: application on the production line. *In Proceedings of the 3rd International Solar Concentrator Conference for the Generation of Electricity or Hydrogen.*

Artificial light source for solar simulation (Conference) | ETDEWEB. (n.d.). Retrieved August 28, 2020, from https://www.osti.gov/etdeweb/biblio/8338370

ASTM-E927-05. (2005). *Standard Specification for Solar Simulators for Photovoltaic Testing*. *i*, 5–9. https://doi.org/10.1520/E0927-05.related

ASTM. (2013). Standard Tables for Reference Solar Spectral Irradiances : Direct Normal and. *Astm*, *03*(Reapproved), 1–21. https://doi.org/10.1520/G0173-03R12.2

ASTM E892 - 87(1992) Tables for Terrestrial Solar Spectral Irradiance at Air Mass 1.5 for a 37-Deg Tilted Surface (Withdrawn 1999). (n.d.). Retrieved August 13, 2020, from https://www.astm.org/Standards/E892.htm

Bacardit, A., & Cartoixà, X. (2020). Revisiting the role of irradiance in the determination of sunscreens' sun protection factor. *Journal of Physical Chemistry Letters*, *11*(4), 1209–1214. https://doi.org/10.1021/acs.jpclett.9b03437

Bazzi, A. M., Klein, Z., Sweeney, M., Kroeger, K. P., Shenoy, P. S., & Krein, P. T. (2012). Solid-state solar simulator. *IEEE Transactions on Industry Applications*, *48*(4), 1195–1202. https://doi.org/10.1109/TIA.2012.2199071

Beeson, E. J. G. (1978). *The CSI lamp simulation*.

Bickler, D. (1962). The simulation of solar radiation. *Solar Energy*, *6*(2), 64–68. https://doi.org/10.1016/0038-092X(62)90006-3

Bliss, M., Betts, T. R., & Gottschalg, R. (2008). ultimate "gloss" "white" spray paint oleumAdvantages in using LEDs as the main light source in solar simulators for measuring PV device characteristics. *Reliability of Photovoltaic Cells, Modules, Components, and Systems*, *7048*(September 2008), 704807. https://doi.org/10.1117/12.795428

Bliss, M., Plyta, F., Betts, T. R., & Gottschalg, R. (2014). LEDs Based Characterisation of Photovoltaic Devices. *International Conference on Energy Efficient LED Lighting and Solar PhotoVoltaic Systems Conference, Indian Institute of Technology, Kanpur, India, 27th-29th March 2014*, 1200.

Bodnár, I., Koós, D., Iski, P., & Skribanek, Á. (2020). Design and construction of a sun simulator for laboratory testing of solar cells. *Acta Polytechnica Hungarica*, *17*(3), 165–184. https://doi.org/10.12700/APH.17.3.2020.3.9

Burgin, R., & Edwards, E. F. (1970). The tungsten halogen lamp decade. *Lighting Research & Technology*, *2*(2), 95–108. https://doi.org/10.1177/14771535700020020901

Class ABA LED Solar Simulator. (n.d.). Retrieved August 17, 2020, from https://www.newport.com/f/class-aba-led-solar-simulators?q=7320:relevance:isObsolete:false:-excludeCountries:CA:npCategory:led-solar-simulators

Codd, D. S., Carlson, A., Rees, J., & Slocum, A. H. (2010). A low cost high flux solar simulator. *Solar Energy*, *84*(12), 2202–2212. https://doi.org/10.1016/j.solener.2010.08.007

Conibeer, G. (2007). Third-generation photovoltaics. In *Materials Today* (Vol. 10, Issue 11, pp. 42–50). Elsevier. https://doi.org/10.1016/S1369-7021(07)70278-X

Davis, A. (2011). Fresnel lens solar concentrator derivations and simulations. *Novel Optical Systems Design and Optimization XIV*, *8129*(September 2011), 81290J. https://doi.org/10.1117/12.892818

Davis, A., Bush, R. C., Harvey, J. C., & Foley, M. F. (2001). P-95: Fresnel Lenses in Rear Projection Displays. *SID Symposium Digest of Technical Papers*, *32*(1), 934. https://doi.org/10.1889/1.1832025

DECKER, A., & POLLACK, J. (1972). *A 400 kilowatt argon arc lamp for solar simulation(Design and performance of high powered argon arc lamp for solar simulation)*.

Dennis, T. (2014). An arbitrarily programmable solar simulator based on a liquid crystal spatial light modulator. *2014 IEEE 40th Photovoltaic Specialist Conference, PVSC 2014*, 3326–3330. https://doi.org/10.1109/PVSC.2014.6925647

Dennis, T., Fisher, B., Meitl, M., & Wilson, J. (2015, December 14). A high-concentration programmable solar simulator for testing multi-junction concentrator photovoltaics. *2015 IEEE 42nd Photovoltaic Specialist Conference, PVSC 2015*. https://doi.org/10.1109/PVSC.2015.7356196

Dennis, T., Yasanayake, C., Gerke, T., Payne, A., Eng, L., Fisher, B., & Meitl, M. (2016). A programmable solar simulator for realistic seasonal, diurnal, and air-mass testing of multi-junction concentrator photovoltaics. *Conference Record of the IEEE Photovoltaic Specialists Conference*, *2016-November*, 2327–2332. https://doi.org/10.1109/PVSC.2016.7750054

Designation: E490 − 00a Standard Solar Constant and Zero Air Mass Solar Spectral

Irradiance Tables 1. (n.d.). https://doi.org/10.1520/E0490-00AR14

Dominguez, C., Anton, I., & Sala, G. (2008). Solar simulator for indoor characterization of large area high-concentration PV modules. *Conference Record of the IEEE Photovoltaic Specialists Conference*. https://doi.org/10.1109/PVSC.2008.4922739

Domínguez, C., Antón, I., & Sala, G. (2008). Solar simulator for concentrator photovoltaic systems. *Optics Express*, *16*(19), 14894. https://doi.org/10.1364/oe.16.014894

Duarte, F. O., Mello, M. M., Masili, M., & Ventura, L. (2019). Set up for irradiation and performing spectroscopy for human lenses. *IFMBE Proceedings*, *68*(3), 299–304. https://doi.org/10.1007/978-981-10-9023-3_53

Ekman, B. M., Brooks, G., & Rhamdhani, M. A. (2015). *Development of High)lux Solar Simulators for Solar Thermal Research*.

Gallo, A., Marzo, A., Fuentealba, E., & Alonso, E. (2017). High flux solar simulators for concentrated solar thermal research: A review. In *Renewable and Sustainable Energy Reviews* (Vol. 77, pp. 1385–1402). Elsevier Ltd. https://doi.org/10.1016/j.rser.2017.01.056

Gangopadhyay, U., Jana, S., & Das, S. (2013). State of Art of Solar Photovoltaic Technology. *Conference Papers in Energy*, *2013*, 1–9. https://doi.org/10.1155/2013/764132

Gevorgyan, S. A., Eggert Carlé, J., Søndergaard, R., Trofod Larsen-Olsen, T., Jørgensen, M., & Krebs, F. C. (2013). Accurate characterization of OPVs: Device masking and different solar simulators. *Solar Energy Materials and Solar Cells*, *110*, 24–35. https://doi.org/10.1016/j.solmat.2012.11.020

Giller H. F. (2000). A review of UV lamps. *Water Environment Federation*.

Girish, T. E. (2006). Some suggestions for photovoltaic power generation using artificial light illumination. *Solar Energy Materials and Solar Cells*, *90*(15), 2569–2571. https://doi.org/10.1016/j.solmat.2006.03.026

González, M. I. (2017). An LED solar simulator for student labs. *Physics Education*, *52*(3), 035002. https://doi.org/10.1088/1361-6552/aa5f86

Goranson, G. G. (1965). *N A T I O N A L A E R O N A U T I C S A N D S P A C E A D M I N I S T R A T I O N Comments on the Operation of the JPL 25-ft Space Simulator 43 I C A L I F O R N I A I N S T I T U T E O F T E C H N O L O G Y P A S A D E N A. C A L I F O R N I A*. https://ntrs.nasa.gov/search.jsp?R=19660010341

Grandi, G., Ienina, A., & Bardhi, M. (2014). Effective low-cost hybrid LED-halogen solar simulator. *IEEE Transactions on Industry Applications*, *50*(5), 3055–3064. https://doi.org/10.1109/TIA.2014.2330003

Green, M. A. (2009). The path to 25% silicon solar cell efficiency: History of silicon cell evolution. *Progress in Photovoltaics: Research and Applications*, *17*(3), 183–189. https://doi.org/10.1002/pip.892

Green, M. A. (2002). Third generation photovoltaics: Solar cells for 2020 and beyond. *Physica E: Low-Dimensional Systems and Nanostructures*, *14*(1–2), 65–70. https://doi.org/10.1016/S1386-9477(02)00361-2

Hamadani, B. H., Chua, K., Roller, J., Bennahmias, M. J., Campbell, B., Yoon, H. W., & Dougherty, B. (2012). Towards realization of a large-area light-emitting diode-based solar simulator. *Progress in Photovoltaics: Research and Applications*, *21*(4), n/a-n/a. https://doi.org/10.1002/pip.1231

Hamadani, Behrang H., Roller, J., Dougherty, B., & Yoon, H. W. (2013). Fast and reliable

spectral response measurements of PV cells using light emitting diodes. *Conference Record of the IEEE Photovoltaic Specialists Conference*, 73–75. https://doi.org/10.1109/PVSC.2013.6744102

Han, Y. M., Wang, R. Z., Dai, Y. J., & Xiong, A. H. (2007). Experimental studies on highly concentrated solar radiation by using fresnel lens group. *ISES Solar World Congress 2007, ISES 2007*, *1*, 698–701. https://doi.org/10.1007/978-3-540-75997-3_130

Hirsch, D., Zedtwitz, P. V., Osinga, T., Kinamore, J., & Steinfeld, A. (2003). A new 75 kW high-flux solar simulator for high-temperature thermal and thermochemical research. *Journal of Solar Energy Engineering, Transactions of the ASME*, *125*(1), 117–120. https://doi.org/10.1115/1.1528922

History | CITIZEN ELECTRONICS CO.,LTD. (n.d.). Retrieved December 12, 2020, from http://ce.citizen.co.jp/e/company/history.php

Holter, M., NUDELMAN, S., & York, G. S. (1962). *Fundamentals of Infrared Technology*.

Humphries, W. (1978). *Use of the Marshall Space Flight Center solar simulator in collector performance evaluation*. https://www.osti.gov/servlets/purl/12213605

Hussain, F., Othman, M. Y. H., Yatim, B., Ruslan, H., Sopian, K., Anuar, Z., & Khairuddin, S. (2011). Fabrication and irradiance mapping of a low cost solar simulator for indoor testing of solar collector. *Journal of Solar Energy Engineering, Transactions of the ASME*, *133*(4), 4–7. https://doi.org/10.1115/1.4004548

IEC. (2008). *Standard, IEC 60904–3, Photovoltaic Devices—Part 3: Measurement Principles for Terrestrial Photovoltaic (PV) Solar Devices with Reference Spectral ….*

IEC 60904-9. (2006). IEC 60904-9 Photovoltaic devices – Part 9: Solar simulator performance requirements Dispositifs. In *61010-1 © Iec:2001*. https://standards.globalspec.com/std/1030690/iec-60904-9

Irwan, Y. M., Leow, W. Z., Irwanto, M., Fareq, M., Amelia, A. R., Gomesh, N., & Safwati, I. (2015). Indoor Test Performance of PV Panel through Water Cooling Method. In *Energy Procedia* (Vol. 79). Elsevier B.V. https://doi.org/10.1016/j.egypro.2015.11.540

Jang, S. H., & Shin, M. W. (2010). Fabrication and thermal optimization of LED solar cell simulator. *Current Applied Physics*, *10*(SUPPL. 3), S537–S539. https://doi.org/10.1016/j.cap.2010.02.035

Jinglong Du, Xiang Huang, D. (2013). ICMREE 2013 - Proceedings: 2013 International Conference on Materials for Renewable Energy and Environment. In *ICMREE 2013 - Proceedings: 2013 International Conference on Materials for Renewable Energy and Environment* (Vol. 1).

JIS C 8912. (1998). *Japanese Industrial Standard - Solar simulators for crystalline solar cells and modules - JIS C 8912*.

Kalogirou, S. A. (2014a). Solar Energy Engineering: Processes and Systems: Second Edition. In *Solar Energy Engineering: Processes and Systems: Second Edition*. Elsevier Inc. https://doi.org/10.1016/C2011-0-07038-2

Kalogirou, S. A. (2014b). Performance of Solar Collectors. In *Solar Energy Engineering* (pp. 221–256). Elsevier. https://doi.org/10.1016/b978-0-12-397270-5.00004-2

Kejlová, K., Bendová, H., Chrz, J., Dvořáková, M., Svobodová, L., Vlková, A., Kubáč, L., Kořínková, R., Černý, J., Očadlíková, D., Rucki, M., Heinonen, T., Jírová, D., Letašiová, S., Kandarova, H., & Kolářová, H. (2020). Toxicological testing of a photoactive phthalocyanine-based antimicrobial substance. *Regulatory Toxicology and*

Pharmacology, *115*, 104685. https://doi.org/10.1016/j.yrtph.2020.104685

Kim, K. A., Dostart, N., Huynh, J., & Krein, P. T. (2014). Low-cost solar simulator design for multi-junction solar cells in space applications. *2014 IEEE Power and Energy Conference at Illinois, PECI 2014*. https://doi.org/10.1109/PECI.2014.6804544

Kockott, D., & Schoenlein, A. (n.d.). *Test method To what extent does the radiation of a solar simulator meet a "reference sun"? A quantitative approach*. https://doi.org/10.1016/j.polymertesting.2012.04.005

Kohraku, S., & Kurokawa, K. (2003). New methods for solar cells measurement by LED solar simulator. *Proceedings of the 3rd World Conference on Photovoltaic Energy Conversion*, *B*, 1977–1980.

Kohraku, S., & Kurokawa, K. (2006). A fundamental experiment for discrete-wavelength LED solar simulator. *Solar Energy Materials and Solar Cells*, *90*(18–19), 3364–3370. https://doi.org/10.1016/j.solmat.2005.09.024

Kolberg, D., Schubert, F., Lontke, N., Zwigart, A., & Spinner, D. M. (2011). Development of tunable close match LED solar simulator with extended spectral range to UV and IR. *Energy Procedia*, *8*, 100–105. https://doi.org/10.1016/j.egypro.2011.06.109

Kongtragool, B., & Wongwises, S. (2008). A four power-piston low-temperature differential Stirling engine using simulated solar energy as a heat source. *Solar Energy*, *82*(6), 493–500. https://doi.org/10.1016/j.solener.2007.12.005

Krusi, P., & Schmid, R. (1983a). The CSI 1000 W lamp as a source for solar radiation simulation. *Solar Energy*, *30*(5), 455–462. https://doi.org/10.1016/0038-092X(83)90116-0

Krusi, P., & Schmid, R. (1983b). The CSI 1000 W lamp as a source for solar radiation simulation. *Solar Energy*, *30*(5), 455–462. https://doi.org/10.1016/0038-092X(83)90116-0

Kuhn, P., & Hunt, A. (1991). A new solar simulator to study high temperature solid-state reactions with highly concentrated radiation. *Solar Energy Materials*, *24*(1–4), 742–750. https://doi.org/10.1016/0165-1633(91)90107-V

Landrock, C., Omrane, B., Aristizabal, J., Kaminska, B., & Menon, C. (2011). An improved light source using filtered tungsten lamps as an affordable solar simulator for testing of photovoltaic cells. *Proceedings - 2011 IEEE 17th International Mixed-Signals, Sensors and Systems Test Workshop, IMS3TW 2011*, 153–158. https://doi.org/10.1109/IMS3TW.2011.25

LED Light Pulses Enter the Nano Realm to Keep Pace with High-Speed Imaging - ProQuest. (n.d.). Retrieved August 14, 2020, from https://search.proquest.com/docview/2409320396/fulltextPDF/7CA734CE3B814732PQ/1?accountid=27231

Lewis, N. S., & Francisco, S. (2007). *Powering the Planet*. www.undp.org/seed/eap/activities/wea

Li, Y., Yang, Y., Zheng, H., Yu, F., Liang, Q., Yang, H., Yi, X., Wang, J., & Li, J. (2019). Review of high power phosphor-converted light-emitting diodes. *2019 16th China International Forum on Solid State Lighting and 2019 International Forum on Wide Bandgap Semiconductors China, SSLChina: IFWS 2019*, 111–115. https://doi.org/10.1109/SSLChinaIFWS49075.2019.9019776

Linden, K. J., Neal, W. R., & Serreze, H. B. (2014). Adjustable spectrum LED solar simulator.

Light-Emitting Diodes: Materials, Devices, and Applications for Solid State Lighting XVIII, *9003*(February 2014), 900317. https://doi.org/10.1117/12.2035649

Lisbona, E. F. (2013). Calibration, Testing, and Monitoring of Space Solar Cells. In *Solar Cells* (pp. 501–529). Elsevier Ltd. https://doi.org/10.1016/B978-0-12-386964-7.00016-0

Manke, E. (2010). *Standards For Simulators Can Vary Widely* . https://www.newport.com/medias/sys_master/images/images/h74/h27/8797264412702/Solar-Industry-Solar-Simulation.pdf

Meng, Q., Wang, Y., & Zhang, L. (2011). Irradiance characteristics and optimization design of a large-scale solar simulator. *Solar Energy*, *85*(9), 1758–1767. https://doi.org/10.1016/j.solener.2011.04.014

MIRTICH, M. (1976, November 14). *Thermal-environmental testing of a 30-cm engineering model thruster*. https://doi.org/10.2514/6.1976-1034

Mohan, M. V. A., Pavithran, J., Osten, K. L., Jinumon, A., & Mrinalini, C. P. (2014). Simulation of spectral match and spatial non-uniformity for LED solar simulator. *2014 IEEE Global Humanitarian Technology Conference - South Asia Satellite, GHTC-SAS 2014*, 111–117. https://doi.org/10.1109/GHTC-SAS.2014.6967568

Multijunction, C., & Cells, S. (2000). *Jianzeng Xu and James*. 1324–1327.

Mundus, M., Dasa, K., Wang, X., Hohl-Ebinger, J., & Warta, W. (2015). SPECTRALLY SHAPED SUPERCONTINUUM FOR ADVANCED SOLAR CELL CHARACTERIZATION. In *ise.fraunhofer.de*. https://www.ise.fraunhofer.de/content/dam/ise/de/documents/publications/conference-paper/31-eupvsec-2015/Mundus_2DO46.pdf

Novickovas, A., Baguckis, A., Mekys, A., & Tamosiunas, V. (2015). Compact light-emitting diode-based AAA class solar simulator: Design and application peculiarities. *IEEE Journal of Photovoltaics*, *5*(4), 1137–1142. https://doi.org/10.1109/JPHOTOV.2015.2430013

Nushra Oishi, A., Shadman Shafkat Tanjim, M., & Tanseer Ali, M. (2020). *Efficiency Improvement Analysis for Recent High-Efficient Solar Cells*.

Our Energy Needs: World Energy Consumption & Demand | CAPP. (2020). https://www.capp.ca/energy/world-energy-needs/

Öztürk, Emre; Aktaş, Mehmet; Şenyüz, T. (2020). *SUN LOAD ANALYSIS AND TESTING ON AUTOMOTIVE FRONT LIGHTING PRODUCTS*. Light & Engineering. http://web.b.ebscohost.com/abstract?site=ehost&scope=site&jrnl=02362945&AN=143271810&h=cCg9aXxdKZY29mYYOAX1UrzKnHMv5dLCJKydGBK5AmBp%2BExRo%2BMoWP8bwzBR0UREaQw9AV7mQRVQD%2FHnJ9aZsw%3D%3D&crl=c&resultLocal=ErrCrlNoResults&resultNs=Ehost&crlhashurl=login.asp

Pernpeintner, J., Happich, C., Lüpfert, E., Schiricke, B., Lichtenthäler, N., & Weinhausen, J. (2015). Linear Focus Solar Simulator Test Bench for Non-destructive Optical Efficiency Testing of Parabolic Trough Receivers. *Energy Procedia*, *69*, 518–522. https://doi.org/10.1016/j.egypro.2015.03.060

Petrasch, J., Coray, P., Meier, A., Brack, M., Häberling, P., Wuillemin, D., & Steinfeld, A. (2007a). A novel 50 kW 11,000 suns high-flux solar simulator based on an array of xenon arc lamps. *Journal of Solar Energy Engineering, Transactions of the ASME*, *129*(4), 405–411. https://doi.org/10.1115/1.2769701

Petrasch, J., Coray, P., Meier, A., Brack, M., Häberling, P., Wuillemin, D., & Steinfeld, A.

(2007b). A novel 50 kW 11,000 suns high-flux solar simulator based on an array of xenon arc lamps. *Journal of Solar Energy Engineering, Transactions of the ASME*, *129*(4), 405–411. https://doi.org/10.1115/1.2769701

Petrasch, J., & Steinfeld, A. (2005). A novel high-flux solar simulator based on an array of xenon arc lamps - Optimization of the ellipsoidal reflector and optical configuration. *International Solar Energy Conference*, 175–180. https://doi.org/10.1115/ISEC2005-76009

Ren, X., Liu, S., Zhang, X., & Chen, X. (2007). Fabrication of holographic Fresnel lens used as a solar concentrator. *Holography and Diffractive Optics III*, *6832*(January 2008), 68321N. https://doi.org/10.1117/12.754929

Reynolds, K. (2015, March). *LED-Based Sun-Simulator Design*. Prophotonix. https://www.prophotonix.com/wp-content/uploads/2017/12/March_2015_LED_Solar_Simulator_ArticlePS.pdf

Ross B, B. D. (1963). *Solar energy measurement techniques*.

Sarikh, S., Raoufi, M., Bennouna, A., Benlarabi, A., & Ikken, B. (2020). Implementation of a plug and play I-V curve tracer dedicated to characterization and diagnosis of PV modules under real operating conditions. *Energy Conversion and Management*, *209*(October 2019), 112613. https://doi.org/10.1016/j.enconman.2020.112613

Schembri, M. (n.d.). *An Introduction to Solar Simulator Devices*.

Sellami, N. (2013). *Design and characterisation of a novel translucent solar concentrator*. *June*, 1–57.

Sellami, N., & Mallick, T. K. (2013). Optical efficiency study of PV Crossed Compound Parabolic Concentrator. *Applied Energy*, *102*, 868–876. https://doi.org/10.1016/j.apenergy.2012.08.052

Solar Energy Conversion: The Solar Cell - R.C. Neville - Google Books. (n.d.). Retrieved August 12, 2020, from https://books.google.ca/books?id=B1Gbvn0uhdYC&dq=incoming+energy+to+a+solar+cell&lr=&source=gbs_navlinks_s

Stuckelberger, M., Perruche, B., Bonnet-Eymard, M., Riesen, Y., Despeisse, M., Haug, F. J., & Ballif, C. (2014). Class AAA LED-based solar simulator for steady-state measurements and light soaking. *IEEE Journal of Photovoltaics*, *4*(5), 1282–1287. https://doi.org/10.1109/JPHOTOV.2014.2335738

Sun Fact Sheet. (2018). https://nssdc.gsfc.nasa.gov/planetary/factsheet/sunfact.html

Tavakoli, M., Jahantigh, F., & Zarookian, H. (2020). Adjustable high-power-LED solar simulator with extended spectrum in UV region. *Solar Energy*, *May*, 0–1. https://doi.org/10.1016/j.solener.2020.05.081

Tito-haykestep, J., Tito, J. B., Madany, H. T. E.-, El-metwally, K., & Zahran, M. (2020). Design and Implementation of LED Solar Simulator. *Wseas Transactions on Power Systems*, *15*, 68–78. https://doi.org/10.37394/232016.2020.15.8

Trenberth, K. E., Fasullo, J. T., & Kiehl, J. (2009). Earth's global energy budget. *Bulletin of the American Meteorological Society*, *90*(3), 311–323. https://doi.org/10.1175/2008BAMS2634.1

Tsao, J. U., Lewis, N., & Crabtree Argonne, G. (n.d.). *Solar FAQs*.

Ucal, M., & Xydis, G. (2020). Multidirectional Relationship between Energy Resources, Climate Changes and Sustainable Development: Technoeconomic Analysis. *Sustainable*

Cities and Society, *60*(March), 102210. https://doi.org/10.1016/j.scs.2020.102210

US3248590A - High pressure sodium vapor lamp - Google Patents. (n.d.). Retrieved September 1, 2020, from https://patents.google.com/patent/US3248590A/en

van Vliet, J. A. J. M., & de Groot, J. J. (1981). HIGH-PRESSURE SODIUM DISCHARGE LAMPS. *IEE Proceedings A: Physical Science. Measurement and Instrumentation. Management and Education. Reviews*, *128*(6), 415–441. https://doi.org/10.1049/ip-a-1.1981.0066

Vu, H., Kieu, N. M., Gam, D. T., Shin, S., Tien, T. Q., & Vu, N. H. (2020). Design and evaluation of uniform LED illumination based on double linear fresnel lenses. *Applied Sciences (Switzerland)*, *10*(9). https://doi.org/10.3390/app10093257

Wang, W., Aichmayer, L., Laumert, B., & Fransson, T. (2014). Design and validation of a low-cost high-flux solar simulator using Fresnel lens concentrators. *Energy Procedia*, *49*, 2221–2230. https://doi.org/10.1016/j.egypro.2014.03.235

What Are "COB" LEDs and Why Do They Matter? (n.d.). Retrieved August 14, 2020, from https://siliconlightworks.com/resoures/what-are-cob-leds

William P. Hirshman, Garret Hering, and M. S. (2008). Market Survey: Cell & Module Production. *Photon International*.

Winston, R., Miñano, J., & Benitez, P. (2005). *Nonimaging optics*. https://books.google.ca/books?hl=en&lr=&id=aa9iLJGbWJUC&oi=fnd&pg=PP1&dq=R.+Winston,+J.+C.+Miñano,+P.+Benítez,+Nonimaging+Optics,+Elsevier+Academic+Press,+2005.&ots=lP-KhknSsD&sig=WcD0WeYX3NemsXHaTnTVSaGQo3k

Xie, W. T., Dai, Y. J., Wang, R. Z., & Sumathy, K. (2011). Concentrated solar energy applications using Fresnel lenses: A review. In *Renewable and Sustainable Energy Reviews* (Vol. 15, Issue 6, pp. 2588–2606). Pergamon. https://doi.org/10.1016/j.rser.2011.03.031

Yass, K., & Curtis, H. B. (n.d.). *NASA TM X-3059 eo CASE FILE LOW-COST, AIR MASS 2 SOLAR SIMULATOR*. https://ntrs.nasa.gov/search.jsp?R=19740019606

Zacharopoulos, A., Mondol, J. D., Smyth, M., Hyde, T., & O'Brien, V. (2009). *State of the art solar simulator with flexible mounting* (pp. 854–863). International Solar Energy Society. https://pure.ulster.ac.uk/en/publications/state-of-the-art-solar-simulator-with-flexible-mounting-3